表　　題　ミトコンドリア心筋症患者由来 iPS 細胞を用いた病態解明

論 文 の 区 分　　博士課程

著　　者　　名　Razan Elfadi Ahmed Abbas

担当指導教員氏名　花園　豊　　教授

所　　属　自治医科大学大学院医学研究科
専攻　　人間生物学系
専攻分野　　生体分子医学
専攻科　　再生医科学

２０24 年１月 10 日申請の学位論文

DISEASE MODELING OF MITOCHONDRIAL CARDIOMYOPATHY USING PATIENT-DERIVED INDUCED PLURIPOTENT STEM CELLS

ミトコンドリア心筋症患者由来 iPS 細胞を用いた病態解明

Razan Elfadil Ahmed, MBBS

A Thesis Submitted in Fulfillment of the Requirements for the Degree of Doctor of Philosophy

Division of Regenerative Medicine, Center for Molecular Medicine
Jichi Medical University

Academic Year 2023

Abstract

Introduction

Mitochondrial cardiomyopathy (MCM) represents the most severe manifestation of mitochondrial diseases, currently lacking specific treatment options. The recent rise of human induced pluripotent stem cell-derived cardiomyocytes (iPSC-CMs) provides promising patient-specific tools for cardiac disease modeling and allows for a deeper understanding of disease pathophysiology and investigating more targeted treatment options.

Aims

iPSC-CMs derived from MCM patients can provide much needed platforms for MCM research and drug development. Therefore, my primary aim was to establish the largest MCM-iPSC library to date to evaluate MCM-iPSC-CM phenotypes. Nevertheless, there were problems facing their wide use, namely purification and *in vitro* contractility analysis. Therefore, I aimed to:

Aim 1. Production of AAV-based PSC-CM purification and sarcomere function analysis methods

Despite that PSCs can be efficiently differentiated into cardiomyocytes, there was a lack of quick and efficient methods for PSC-CM purification and contractile function assessment *in vitro*, which hindered their usage for disease modeling. Thus, I aimed to establish PSC-CM purification and sarcomere function analysis methods that allow for the generation of more precise MCM-iPSC-CM disease models. To this end, I had two sub-aims to investigate:

Sub-aim 1. Development of purification method for PSC-CMs

Currently used PSC-CM purification methods produce highly purified PSC-CMs (>90%). Nevertheless, these methods are time-consuming or require good functioning mitochondria lacking in MCM-iPSC-CMs. Thus, I aimed to generate an efficient adeno-associated virus (AAV)-based, antibiotic resistance purification method suitable for MCM-iPSC-CMs.

Sub-aim 2. Establishment of contractility assessment method of PSC-CMs *in vitro*

Because of the immature and disorganized sarcomeres of PSC-CMs, their contractile function cannot be efficiently measured using the conventional method for adult cardiomyocytes. To that end, I aimed to develop AAV-based fluorescent tags to visualize sarcomeres and assess contractile function accurately in PSC-CMs.

Aim 2. Establishment of MCM-iPSC-CM disease model library

After addressing the purification and sarcomere function analysis, I aimed to produce the largest MCM-iPSC library for MCM disease modeling. I established iPSCs from 23 MCM patients and four healthy donors and examined MCM-iPSC-CM morphology, physiology, and metabolism to ask how much they recapitulated those of MCM. This library will allow for a deeper understanding of the molecular mechanisms and identification of treatment options for MCM patients.

Results

First, I generated an AAV-based cardiomyocyte purification tool in which a blasticidin resistance gene is expressed under the control of the cardiac troponin T (cTnT) promoter. Using this method, I obtained > 90% PSC-CM purity, solving the problem of a suitable purification method for MCM disease modeling.

Second, I developed an AAV-based sarcomere visualization method for sarcomere contractile function analysis. PSC-CMs display underdeveloped and disorganized sarcomeres compared to adult cardiomyocytes, which makes it difficult to assess their contractility via conventional methods. To tackle this issue, I attempted an AAV-based approach as well. I constructed vectors to express GFP fused Z-line proteins (Tcap, Pdlim3, and Csrp) under the control of cTnT promoter. Tcap and Pdlim3 successfully localized to the Z-line, enabling effective live-imaging and precise measurement of PSC-CM sarcomere function *in vitro*.

With both problems addressed, I started the MCM-iPSC-CM disease modeling study. First, I established iPSCs from fibroblasts of 23 MCM patients and four healthy donors. Then, I differentiated them into MCM-iPSC-CMs and purified the cardiomyocytes using my novel AAV-based method. Finally, I examined their morphology, physiology, and metabolism. MCM-iPSC-CMs had disturbed mitochondrial function as expected. Moreover, they exhibited hypertrophic phenotype as early as day 21 of cardiac differentiation, recapitulating the hypertrophic cardiomyopathy observed in MCM patients. The sarcomere morphology along with Ca^{2+} handling properties were disrupted as well.

Conclusion

I generated AAV-based tools for PSC-CM purification and sarcomere function study. Then, I used these methods to establish the largest library of MCM-iPSC-CM disease models to date, which can be used for drug discovery and basic research to understand MCM. Current results of MCM-iPSC-CMs are promising to recapitulate MCM phenotypes in a dish.

Keywords
Induced pluripotent stem cell-derived cardiomyocytes (iPSC-CMs), Cardiomyocytes Mitochondrial cardiomyopathy (MCM), Adeno-associated virus (AAV)

This thesis is dedicated to my family, teachers, and friends, who supported me through this journey.

Table of Contents

ABSTRACT ..... **- 4 -**

CHAPTER 1 ..... **- 12 -**

INTRODUCTION AND AIM OVERVIEW ..... **- 12 -**

1.1) Introduction ..... - 12 -
1.2) Aim Overview ..... - 15 -
Aim 1. Production of AAV-based PSC-CMs purification and sarcomere function analysis methods - *15* -
Sub-aim 1-2: Establishment of contractility assessment method of PSC-CMs in vitro ..... - *15* -
Aim 2. Establishment of MCM-iPSC-CM disease models library ..... - *15* -

CHAPTER 2 ..... **- 16 -**

MATERIALS AND METHODS ..... **- 16 -**

2.1) Mouse embryonic stem cell (mESC) maintenance ..... - 16 -
2.2) Human PSC (hPSC) maintenance ..... - 17 -
2.3) Cardiac differentiation of mESCs ..... - 17 -
2.4) Cardiac differentiation of iPSC-CMs ..... - 18 -
2.5) Generation of AAV-shuttle vectors ..... - *20* -
2.6) AAV production method ..... - 21 -
2.7) Real-time PCR for AAV quantification ..... - 22 -
2.8) Generation of iPSCs from MCM patients ..... - 23 -
2.9) Flowcytometry ..... - 26 -
2.10) Immunostaining ..... - 27 -
2.11) Ca^{2+} transients ..... - 28 -
2.12) Contractility assessment ..... - 28 -
2.13) Mitochondrial respiratory function analysis ..... - 29 -
2.14) ATP and H_2O_2 assay ..... - 30 -
2.15) RNA-sequencing ..... - 30 -
2.16) Statistics ..... - 30 -

CHAPTER 3 ..... **- 31 -**

AAV-BASED MODIFICATION OF PSC-CMS ..... **- 31 -**

3.1) Introduction ..... - 31 -
3.1.1) Background ..... - *31* -
3.1.2) Comparison between ESCs and iPSCs ..... - *32* -
Table 10 .Overview of the key distinctions between ESCs and iPSCs ..... - *32* -
3.1.3) Cardiac differentiation of hPSCs ..... - *33* -
3.1.4) Challenges of hPSC cardiac differentiation ..... - *34* -
3.1.5) AAV-mediated gene delivery ..... - *38* -
3.2) Results ..... - 40 -
3.2.1) Cardiac differentiation of mPSC-CMs ..... - *40* -
3.2.2) Cardiac differentiation of hPSC-CMs ..... - *41* -
3.2.3) Generation of PSC-CM purification method without the need for drug-resistance knock-in - *42* -

3.2.4) Establishing a method to assess PSC-CM sarcomere function in vitro ..... *- 44 -*
3.3) Discussion ..... - 50 -

CHAPTER 4 ..... **- 52 -**

MCM DISEASE MODELING WITH IPSC-CMS ..... **- 52 -**

4.1) Introduction ..... - 52 -
4.1.1) Mitochondrial diseases ..... *- 52 -*
4.1.2) MCM: A complex spectrum of mitochondrial diseases ..... *- 53 -*
4.1.3) Current approaches to study MCM ..... *- 54 -*
4.1.4) Current treatment options of MCM ..... *- 56 -*
4.2) Results ..... - 58 -
4.2.1) Production and quality check of iPSC cell lines from MCM patient-derived fibroblasts ..... *- 58 -*
4.2.2) MCM-iPSCs showed reduced proliferation ..... *- 59 -*
4.2.3) MCM-iPSC differentiation capacity ..... *- 62 -*
4.2.4) MCM-iPSC-CMs mitochondrial function ..... *- 63 -*
4.2.5) MCM-iPSC-CMs exhibited hypertrophy compared to control iPSC-CMs ..... *- 66 -*
4.2.6) MCM-iPSC-CMs exhibited abnormal sarcomere formation ..... *- 69 -*
4.2.7) MCM-iPSC-CMs showed abnormal mitochondrial morphology ..... *- 71 -*
4.2.8) MCM-iPSC-CMs showed abnormal Ca^{2+} handling ..... *- 73 -*
4.3) Discussion ..... - 75 -

CHAPTER 5 ..... **- 78 -**

OVERALL DISCUSSION AND CONCLUSION ..... **- 78 -**

Discussion ..... - 78 -
Conclusion ..... - 80 -
Acknowledgments ..... - 80 -
Funding support ..... - 80 -

REFERENCES ..... **- 81 -**

List of Figures

Figure 1. Mitochondrial diseases are caused by mutations of mitochondrial or nuclear DNA ..... - 12 -
Figure 2. iPSCs production and possible usage ..... - 14 -
Figure 3. Timeline of the main events in the history of stem cell research ..... - 31 -
Figure 4. Cardiac differentiation of hPSCs ..... - 33 -
Figure 5. Currently employed PSC-CMs purification methods ..... - 36 -
Figure 6. Schematic overview of the maturation approaches of PSC-CMs ..... - 37 -
Figure 7. mPSC differentiation and puromycin purification. ..... - 40 -
Figure 8. hPSC differentiation and puromycin purification. ..... - 41 -
Figure 9. Blasticidin purification of human PSC-CMs without knock-in. ..... - 43 -
Figure 10. Lifeact sarcomere labelling vs. knock in sarcomere tags. ..... - 45 -
Figure 11. Sarcomere Z line proteins. Muscle LIM protein, Actin-associated LIM protein, and Telethonin were chosen for subsequent AAV packaging. ..... - 46 -
Figure 12. Z line protein fluorescent AAV6 construction and transduction. ..... - 48 -
Figure 13. Sarcomere visualization and function analysis using Tcap-GFP and Pdlim3-GFP. ..... - 49 -
Figure 14. Genes implicated in MCM and their respective functions, related to MCM-iPSCs cohort in this study. ..... - 53 -
Figure 15. Pluripotency gene expression ..... - 58 -
Figure 16. Cumulative cell number at day 14. ..... - 61 -
Figure 17. MCM-iPSC cardiac differentiation. ..... - 62 -
Figure 18. Gene expression of some MCM-related genes by age. ..... - 64 -
Figure 19. MCM-iPSC-CMs ATP and H_2O_2 levels. ..... - 65 -
Figure 20. MCM-iPSC-CMs exhibited significant hypertrophy. ..... - 69 -
Figure 21. MCM-iPSC-CMs exhibited disrupted sarcomere structure. ..... - 70 -
Figure 22. Representative images of MCM-iPSC-CMs mitochondrial structure. ..... - 72 -
Figure 23. Representative averaged profiles of cytosolic Ca^{2+} transients of MCM-iPSC-CMs. ..... - 74 -

List of Tables

Table 1. 2i medium preparation for mESC-CMs maintenance ..... - 16 -
Table 2. SFD medium for cardiac differentiation and maintenance of mESC-CMs ..... - 18 -
Table 3. RPMI+B27-Ins medium composition ..... - 19 -
Table 4. RPMI+B27+Ins medium composition ..... - 19 -
Table 5. Primers used for the amplification of Tcap, Pdlim3, and Csrp from mouse cDNA ..... - 20 -
Table 6. Reagents required for AAV serotype 6 (AAV6) packaging ..... - 22 -
Table 7. Conditions for real-time PCR ..... - 23 -
Table 8. Summary of the data of MCM patients ..... - 25 -
Table 9. Tyrode's solution preparation ..... - 28 -
Table 10 .Overview of the key distinctions between ESCs and iPSCs ..... - 32 -
Table 11. Advantages and disadvantages of using AAVs in gene delivery ..... - 38 -
Table 12. Z-line proteins. ..... - 47 -
Table 13. Overview of some MCM mice models. ..... - 55 -
Table 14 . Summary of iPSC-CMs MCM disease models ..... - 56 -
Table 15. Summary of the observed morphological and functional changes of MCM-iPSC-CMs ..... - 76 -

Chapter 1
Introduction and Aim Overview

1.1) Introduction

Mitochondrial diseases are multisystemic disorders caused by mutations in the mitochondrial or nuclear DNA (mtDNA and nDNA, respectively), resulting in decreased mitochondrial function. It has extremely heterogeneous phenotypes, depending on the tissue involved, the gene mutation, and mitochondrial heteroplasmy level[1]. Heteroplasmy rate is the co-expression of wild-type inherited polymorphisms and somatic mutations within the mtDNA genomes[2]. It is one of the most important determinants of mitochondrial disease severity. The threshold that determines a disease state is 50% to 100% mutant mtDNA; however, clinical disease states have been reported with levels as low as 10%[3]. Mitochondrial disease usually affects tissues with high energy demands, such as the cardiovascular, nervous, muscular, and endocrine systems (**Figure 1**).

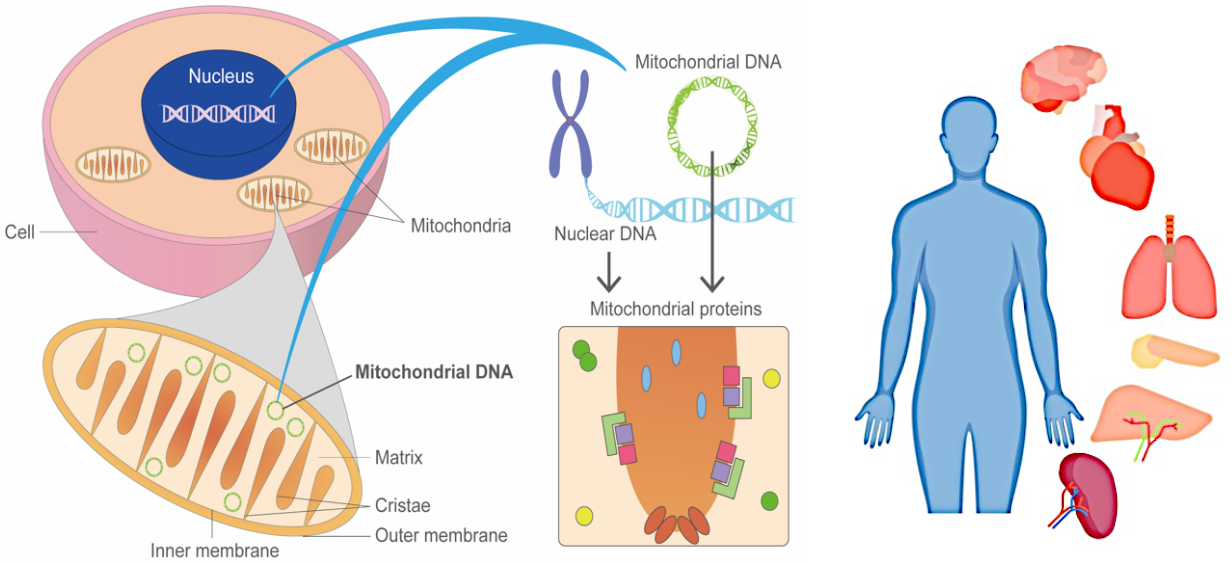

Figure 1. Mitochondrial diseases are caused by mutations of mitochondrial or nuclear DNA.

Muti-organ involvement cause heterogenous phenotypes of mitochondrial disease, Modified from Tokuyama et al[4] .

The heart is one of the first and most severely affected organs due to its high energy requirements. Approximately 40% and 30% of affected children and adults, respectively, develop mitochondrial cardiomyopathy (MCM) that reduces the 5-year survival by less than half[5,6]. More than 350 genes (in the mitochondrial and nuclear DNA) are reported to cause MCM[7]. MCM presents in various manifestations ranging from hypertrophic or dilated cardiomyopathy (HCM or DCM) to arrhythmia and sudden cardiac death. The variety in the mutated genes and disease manifestation necessitates a convergent approach to study MCM and consolidate the most significant alterations of MCM. This will facilitate the development of wide-scope treatments. Conventionally, MCM research relied mainly on doner fibroblasts and knock-out mice models. Nevertheless, these fail to recapitulate the individualized pathophysiology of the patients. Thus, a more specific way is needed.

The quick leap of iPSC research has completely changed the way to study diseases. iPSCs can be differentiated to various cell types, including cardiomyocytes, providing patient-specific tools for basic research and therapy development (**Figure 2**). Since their generation, iPSC-CMs were utilized to unravel the complexities of various cardiac disorders like long QT syndrome[8], arrhythmogenic right ventricular cardiomyopathy[9], HCM[10], DCM[11], and atrial fibrillation[12].

Nevertheless, the wide use of iPSC technology in MCM disease research is limited by many reasons. Among them are the lack of suitable tools to efficiently purify PSC-CMs and study their contractile function *in vitro*. Establishing such methods will bring us closer to realizing the full potential of iPSCs in MCM research.

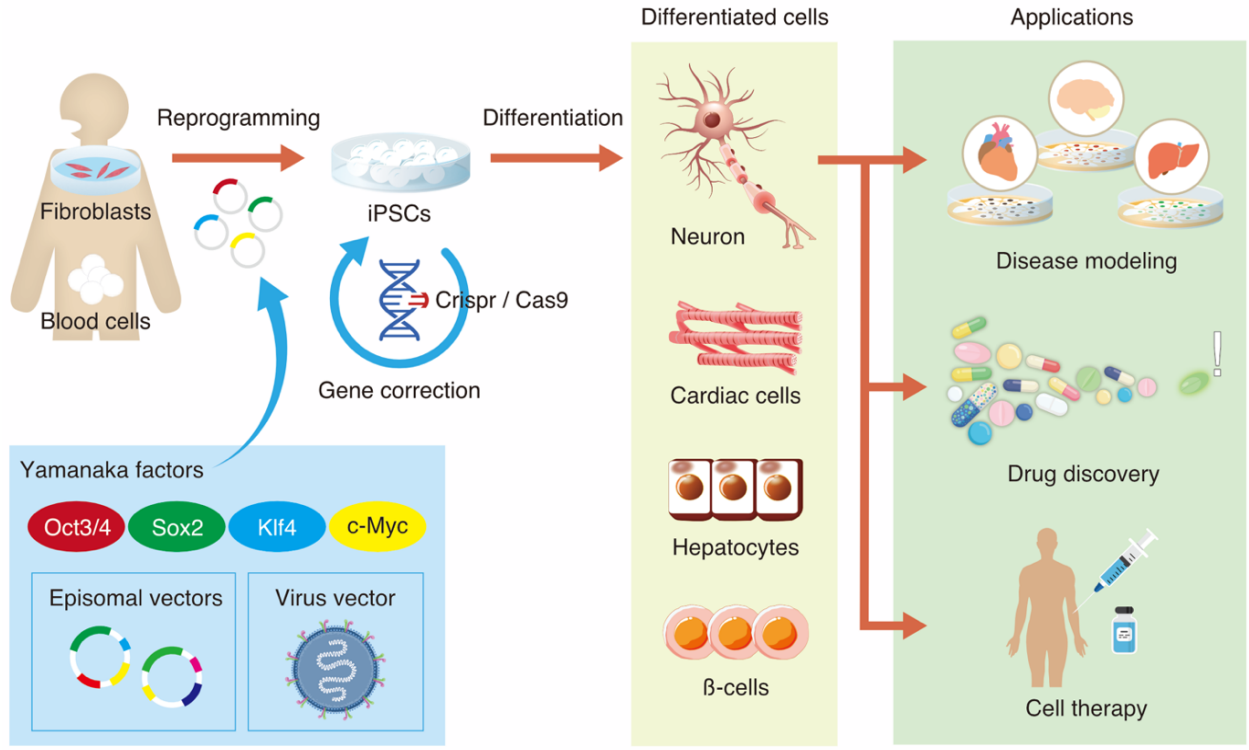

Figure 2. iPSCs production and possible usage.

iPSCs are produced by introducing Yamanaka factors into somatic cells. Those cells can be differentiated into various cell types and have the potential for further clinical applications. Modified from 徳山, 小児内科, 2022.

1.2) Aim Overview

Aim 1. Production of AAV-based PSC-CMs purification and sarcomere function analysis methods

Sub-aim 1-1. Development of purification method for PSC-CMs

Currently employed PSC-CM purification techniques are either characterized by prolonged durations (such as fluorescence-based cell sorting, cell surface marker-based cell sorting, or genetically encoded antibiotic selection) or depend on optimal mitochondrial function (metabolic-based selection)[13]. The latter may not be suitable for diseased cardiomyocytes because many cardiac diseases exhibit some degree of mitochondrial impairment. Therefore, I aimed to develop a new method to deliver an antibiotic-resistance gene regulated by a cardiac promoter to PSC-CMs using adeno-associated virus (AAV) for antibiotic selection.

Sub-aim 1-2: Establishment of contractility assessment method of PSC-CMs *in vitro*

Current methods to study the contractile function of adult cardiomyocytes are not suitable for PSC-CMs because of the immature and disorganized sarcomeres that PSC-CMs have. We initially generated fluorescent-tag knock-in to sarcomere genes in mouse and human PSCs to visualize sarcomeres in PSC-CMs and measure contractile function[14,15]. Nevertheless, this method requires knock-in, a time-consuming procedure, and is not suitable for iPSC-CMs derived from many patients. Therefore, instead of knock-in, I aimed to develop AAV-based delivery of fluorescent tags to assess sarcomere function in PSC-CMs. Small Z-line (part of the sarcomere) proteins were selected as the fusion partners of GFP to be packaged into AAV vectors.

Aim 2. Establishment of MCM-iPSC-CM disease models library

MCM patients usually manifest with HCM or DCM due to compromised mitochondria. Thus, it is expected that both structures (cell morphology, sarcomere arrangement, mitochondrial morphology, and localization) and functions (contractility, Ca^{2+} handling, and mitochondrial function) of MCM-iPSC-CMs must be altered to resemble MCM phenotypes. To establish the MCM-iPSC-CM disease model, I first generated iPSCs from MCM patients' fibroblasts and differentiated them into MCM-iPSC-CMs. Next, I evaluated the morphology, physiology, and metabolism of MCM-iPSC-CMs to ask if MCM-iPSC-CMs recapitulate MCM phenotypes.

Chapter 2
Materials and Methods

2.1) Mouse embryonic stem cell (mESC) maintenance

mESCs used in this research were SMM18, a fluorescence reporter line previously generated by our group[14], in which TagRFP was knocked into the Myom2 locus. Cells were cultured in 0.1% (w/v) gelatin-coated tissue culture dish without feeders in 2i medium containing the components described in **Table 1**. Cells were cultured at 37 °C humidified air with 5% CO2 and passaged every 2-3 days.

Table 1. 2i medium preparation for mESC-CMs maintenance

Component	Company	Concentration/ Amount
Glasgow minimum essential medium (GMEM)	Sigma-Aldrich	450 ml
Fetal bovine serum (FBS)	Moregate	10% (50 ml)
Leukemia inhibitory factor (LIF)	Fujifilm	1,000 U/ml
2-mercaptoethanol (55mM)	Thermo Fisher Scientific	0.1 mM
CHIR99021	Cayman	3 μM
PD0325901	Stemgent	1 μM
L-alanine-L-glutamine (GlutaMAX Supplement, 200mM)	Thermo Fisher Scientific	2 mM
Sodium pyruvate (100 mM)	Thermo Fisher Scientific	1 mM
MEM non-essential amino acids solution (100x)	Thermo Fisher Scientific	Diluted to 1x

2.2) Human PSC (hPSC) maintenance

Cells were cultured in 6-well tissue culture plates. Seeding density was 75,000-125,000 cells in one well of 6-well plate with 2 mL in AK02N medium (StemFit) containing 0.5 μg/mL of iMatrix-511 (Takara) and 10 μM of ROCK inhibitor Y27632. On the following day, the medium was changed to AK02N only. Cells were cultured at 37 °C humidified air with 5% CO2 and passaged twice a week. For cardiac differentiation or MCM-iPSCs, iMatrix-511 precoating was performed (2.5-5 μg iMatrix-511 diluted in 1.5-2 mL PBS) for at least 30 minutes before cell seeding.

2.3) Cardiac differentiation of mESCs

Cardiac differentiation was performed following our previous report[15]. Briefly, serum-free differentiation medium (SFD) was used as the basal medium. SFD preparation is explained in **Table 2**. mESCs were suspended in SFD to form embryoid bodies. Two days later, the culture medium was changed to SFD supplemented with Activin-A (5 ng/ml, R&D System), Bone morphogenetic protein 4 (BMP4, 1.9 ng/ml, R&D System), and vascular endothelial growth factor (VEGF, 5 ng/ml, Wako) for two days to prime cells toward mesoderm. At day four, cells were dissociated and plated on a 0.1% gelatin-coated dish in SFD medium supplemented with VEGF (5 ng/ml), basic fibroblast growth factor (bFGF, 10 ng/ml, R&D System), and fibroblast growth factor 10 (FGF10, 25 ng/ml, R&D System) for three days to induce cardiac lineage differentiation. Beating cells can be observed at day seven. From day seven onwards, cells were cultured in SFD medium with puromycin (2 μg/ml) to enrich the purity of cardiomyocytes. To determine the purity of cardiomyocytes, cells were immunolabeled with the cardiac marker cTnT and then flowcytometry was performed as explained in **Method 2.9**. Using this method, we can obtain more than 90% purity.

Table 2. SFD medium for cardiac differentiation and maintenance of mESC-CMs

Component	Company	Concentration /Amount
Iscove's modified Dulbecco's medium (IMDM)	Thermo Fisher Scientific	375 ml
Ham's F-12 medium	Thermo Fisher Scientific	125 ml
B27 supplement (50X), minus Vitamin A	Thermo Fisher Scientific	Diluted to 0.5X
N2 supplement (100x)	Thermo Fisher Scientific	Diluted to 0.5X
Bovine Serum Albumin	Sigma-Aldrich	0.05% (w/v)
L-alanine-L-glutamine (GlutaMAX Supplement, 200mM)	Thermo Fisher Scientific	2 mM
Ascorbic acid	Wako	0.05 mg/ml
1-thioglycerol	Sigma-Aldrich	450 µM

2.4) Cardiac differentiation of iPSC-CMs

Human iPSCs were replated on iMatrix-coated plates in the passaging medium described in 3.2, four days before starting the differentiation process (day -4). On day -3 and day -1, the medium was changed with AK02N. On day 0, the medium was changed with RPMI+B27-Ins (as described in **Table 3**) supplemented with GSK3 inhibitor CHIR99021 (final concentration 6 µM) to induce mesodermal lineage differentiation. To induce cardiac differentiation, the medium was changed with RPMI+B27-Ins supplemented with Wnt inhibitor (WntC59) on day 2. On day 4, the medium was changed with RPMI+B27-Ins alone. From day 7, iPSC-CMs were maintained in RPMI+B27+Ins (as described in **Table 4**) for further experiments. For purification of the TIP1-11 line, puromycin (final concentration 10 µg/mL) was added from day 7 to day 10 to selectively culture cardiomyocytes.

For AAV-based purification, blasticidin (final concentration 2.5-5 μg/mL) was added from day 7 to 9 or day 11 to 15 (for MCM-iPSC-CMs). For further experiments with MCM-iPSC-CMs, cells were replated with RPMI+B27+Ins supplemented with Y27632 on 0.1% gelatin and iMatrix (2 μg/mL) at day 15. From day 16, cells were cultured in RPMI+B27+Ins supplemented with 1% Chemically Defined Lipid Concentrate (Thermo fisher) or Lipid Mixture (Sigma Aldrich).

Table 3. RPMI+B27-Ins medium composition

Component	Company	Amount
RPMI 1640	Thermo Fisher Scientific	500 ml
B27 supplement, minus insulin	Thermo Fisher Scientific	10 ml
L-alanine-L-glutamine (GlutaMAX Supplement, 200mM)	Thermo Fisher Scientific	5 ml

Table 4. RPMI+B27+Ins medium composition

Component	Company	Amount
RPMI 1640	Thermo Fisher Scientific	500 ml
B-27 Supplement (50X), serum free	Thermo Fisher Scientific	10 ml
L-alanine-L-glutamine (GlutaMAX Supplement, 200mM)	Thermo Fisher Scientific	5 ml

2.5) Generation of AAV-shuttle vectors

For PSC-CM purification, an AAV shuttle vector, in which cTNT promoter drives a blasticidin-resistance gene, was constructed. First, plasmid construction was done via inserting a blasticidin resistance cassette from a previously generated plasmid into pAAV-cTnT backbone using restriction enzymes, transformed into *E. coli* competent cells (DH5-α strain) and plasmid DNA was isolated via miniprep kit (Qiagen).

For sarcomere visualization, Telethonin (TCAP), PDZ and LIM domain protein 3 (PDLIM3), and Cysteine and glycine-rich protein 1 (CSRP) were amplified from mouse heart cDNA and inserted into an AAV-shuttle vector that contains EGFP under the control of cTnT promoter (pAAV-cTnT-mEGFPn3), primers are listed in **Table 5**. The transformation and plasmid DNA isolation were conducted. After the plasmid construction and sequence confirmation, the shuttle vectors were used for AAV production as described in **Methods 2.6**.

Table 5. Primers used for the amplification of Tcap, Pdlim3, and Csrp from mouse cDNA

Name	Direction	Sequence (5' to 3')
Tcap F1	Forward	5' ACATAGCAGAGGGAGCAATCAG 3'
Tcap R1	Reverse	5' TTGTCCTAGCCAGGAAGTGC 3'
Pdlim F1	Forward	5' CTGGACCCACTCGAGGGAAG 3'
Pdlim R1	Reverse	5' TGAGTGTTCTTGTCTGCAAAGG 3'
Csrp F1	Forward	5' CCAGAGTCTTCACCATGCCA 3'
Csrp R1	Reverse	5' TAGGGCTGTGAGAAAGCAGG 3'

2.6) AAV production method

The detailed protocol was previously published[15]. Briefly, HEK293T cells were cultured in DMEM supplemented with FBS (final concentration 10%) until reaching 70-80% confluency. Then 3.5 μg of the shuttle vector, 26 μg of pHelper (a vector coding E2A, E4, and VA of adenovirus), 16.5 μg of pRC6 (a vector coding AAV2 Rep and AAV6 Cap genes), and 1 mL of DMEM without sodium pyruvate (DMEM-Pyr) were mixed into tube (1). Next, 224 μL of polyethylenimine (PEI) and 776 μL of DMEM-Pyr were mixed separately then added into the tube (1), vortexed, incubated for 30 minutes at room temperature, then added to the culture medium. 24 hours later, the medium was changed with DMEM-Pyr. 5 days later, the medium was centrifuged, filtered through 45-μm filter syringe, and then centrifuged using an ultrafiltration unit (100 kDa molecular weight cut-off [MWCO]) precoated with 5 ml of 1% BSA, until AAV amount became 0.5-1 mL. For larger scale production, the medium after filtration through 45-μm filter was purified and concentrated through a tangential flow filtration system (300 kDa MWCO) to approximately 20 mL, then further concentrated with an ultrafiltration unit.

For AAV quantification, 5 μL of AAV was mixed with 195 μL of DMEM-Pyr and 10 U of benzonase and incubated at 37 °C for 1 h. Next, 200 μL of proteinase K buffer (0.02 M Tris HCl and 1% SDS) and 5 μL of proteinase K (20 mg/mL) were added and incubated at 37 °C for 1 h. Then, 400 μL of 25:24:1 Phenol/chloroform/isoamyl alcohol solution were added, vortexed, and centrifuged. 200 μL of the aqueous phase was transferred to a new tube, 1μl of Dr. GenTLE Glycogen (20 mg/mL) and 20 μL of 3 M CH_3COONa (pH 5.2) were added, and vortexed. 250 μL of 2-Propanol and 100 μL of 100% ethanol were added and vortexed. The mixture was incubated at -80 °C for 15 min, centrifuged, and the supernatant was aspirated. Then 70% ethanol was added, centrifuged, aspirated and air dried. Finally, 200 μL of Tris-EDTA (TE; pH 8.0) was added to resolve the AAV genomes. A List of the used reagents is provided in **Table 6**.

Table 6. Reagents required for AAV serotype 6 (AAV6) packaging

Component	Company
Dulbecco's Modified Eagle's Medium (DMEM) – high glucose	Sigma-Aldrich
Dulbecco's Modified Eagle's Medium (DMEM) – high glucose, without sodium pyruvate	Sigma-Aldrich
AAVproR Helper Free System (AAV6) (vectors; pHelper, pRC6)	Takara
polyethylenimine MAX (MW. 40,000)	Polyscience
Millex-HV Syringe Filter Unit, 0.45 μm, PVDF (0.45-μm filter)	Merck Millipore
Centrifugal ultrafiltration unit (100k MWCO), Vivaspin-20	Sartorius
Bovine Serum Albumin	Sigma-Aldrich
Benzonase (25 U/μL)	Merck Millipore
Proteinase K	Takara
Dr. GenTLE Precipitation Carrier (20mg/mL Glycogen, 3 M Sodium Acetate (pH 5.2))	Takara
Ethanol (99.5)	Fujifilm wako
2-Propanol	Fujifilm wako
Tris-Ethylenediaminetetraacetic acid	Nippon Gene

2.7) Real-time PCR for AAV quantification

AAV sample obtained from **Method 2.6** was diluted 100-fold using TE buffer. A standard solution of pAAV-CMV-Vector at 6.5 ng/μL was prepared using TE buffer to obtain 10^9 vector genomes/μL (vg/μL). Then, a series of 10-fold dilution was made from 10^4 to 10^8 with TE buffer.

To calculate the AAV titer,1 μL of the sample DNA (or the standards) was mixed with 0.4 μL of 5 μM ITR primers (5′-GGAACCCCTAGTGATGGAGTT-3′ and 5′-CGGCCTCAGTGAGCGA-3′), 3.6 μL of distilled water, and 5 μL of SYBR Green master mix. Real-time PCR was performed using the conditions in **Table 7**. Based on the standards and Ct values, real-time PCR machine provides the copy number of vector genome in 1 μL of a sample. Original AAV titer was calculated using the following equation: a copy number provided by real-time PCR (vg/μL) x 8 x 10^3 x 2, wherein 8 x 10^3 as a dilution factor during AAV genome isolation, and 2 as the difference factor of AAV (single strand) and plasmid (double strand).

Table 7. Conditions for real-time PCR

Component	Temperature	Time
Initial denature	95 °C	60 seconds
denaturing	95 °C	15 seconds
Annealing and extension	60 °C	30 seconds
40 cycles of denaturing, annealing and extension followed by melting curve		

2.8) Generation of iPSCs from MCM patients

Fibroblasts of 26 patients suffering from MCM patients and four healthy donors were obtained from Dr. Kei Murayama of Chiba Children's Hospital, Prof. Hitoshi Osaka, or RIKEN Bioresource Research Center. **Table 8** shows the mutations and cardiac involvement of each patient.

To generate iPSCs from MCM patient-derived fibroblasts, SRV-iPSC-1 vector (Tokiwa bio) was used to express the four reprogramming factors (OCT4, SOX2, KLF4, and c-MYC) along with EGFP in one vector following the manufacturer's instructions. This allowed for the reprogramming genes to be introduced into cells at the same time and in the same ratio. Stable gene expression is maintained by SRV's own RNA-dependent RNA polymerase (RdRp). SRV elimination was carried out by interfering with viral transcription/replication using siRNA following the manufacturer's instructions. After single clones (minimum of 12 clones per patient) were expanded, GFP-negative clones with a higher fraction of SSEA4 and TRA1-60 positive cells were selected for further validation. Reverse transcription-quantitative PCR (RT-qPCR) was performed to confirm the successful elimination of SRV by siRNA. The top three clones expressing endogenous NANOG per patient were further evaluated, including cardiac differentiation and the expressions of pluripotency markers, SOX2, OCT3/4,

and NANOG. For iPSC lines with mitochondrial DNA mutations (lines #13, 14, 15, 16, 19, and 27), the heteroplasmy rates of respective mutations were confirmed along with cardiac differentiation and pluripotency markers. The top three lines with the highest heteroplasmy rates were selected for further study. At least one line per patient with the highest cardiac differentiation was selected for the disease modeling study.

Not all lines were successfully generated, maintained or differentiated: Line #14 was very unstable to maintain; line #20, none of the clones expressed mutant genes due to X chromosome inactivation; and no iPSC line was obtained from #23.

Table 8. Summary of the data of MCM patients

Abbreviations: HCM, hypertrophic cardiomyopathy; DCM, dilated cardiomyopathy; LVH, left ventricular hypertrophy; WPW, Wolff–Parkinson–White syndrome; VF, ventricular fibrillation; PSVT, paroxysmal supraventricular tachycardia

No.	Gene mutation	Sex	Onset	Patient status	Cardiac manifistation
1	QRSL1 c.[398G>T]:[398G>T]	F	2 days	Dead (5m)	HCM
2	ATAD3 deletion	M	0 days	Dead (7m1d)	HCM
3	TOP3A c.[527C>T]: [1072_1073dup]	F	10 years	Alive (17y)	DCM
4	*COQ4 c.[718C>T]:[421C>T]*	F	0 days	Dead (1d)	HCM
5	ECHS1 c.[176A>G]:[476A>G]	F	0 days	Dead (1d)	HCM
6	BOLA3 c.[287A>G]:[287A>G]	F	2 months	Dead (5m)	HCM
7	BOLA3 c.[287A>G]:[287A>G]	F	3 months	Dead (10m)	HCM
8	BOLA3 c.[287A>G]:[287A>G]	M	4 months	Dead (4m)	HCM
9	KARS c.[1343T>A]:[953T>C]	M	4 months	Dead (4y)	HCM
10	TMEM70 c.[138delG]:[316+1G>A]	M	1 day	Alive (1y)	Noncompaction Mild LVH
11	SLC25A26 c.[305C>T]:[657delG]	M	Neonate		DCM
12	TAZ c.[589G>A]	M	4 months	Alive (5m)	DCM
13	MT-ATP6/8 m.8528T>C	F	2 days	Dead (2m)	HCM
14	MT-ATP6/8 m.8528T>C	M	6 months	Alive (8m)	HCM
15	MT-ND5	F	3	Dead	HCM

	m.13513G>A		months	(1y1m)	
16	MT-ND5 m.13513G>A	F	0 days	Dead (1m)	HCM
17	WT				
18	ACAD9 c.811T>G:p.C271G	F	2 days	Dead (1y1m)	HCM
19	m.3243A>G (MT-TL1)	F	0 days	Alive (1y4m)	DCM
20	NDUFB11 c.158_177del(p.T53fs)	F	0 months	Alive (2y4m)	WPW syndrome Left ventricular noncompaction
21	ATAD3 duplication	M	0 days	Dead (0y2m)	Heart failure
22	ATAD3 duplication	M	0 days	Dead (32day)	Cardiac tamponade
23	BOLA3 (c.287A>G(p.H96R)) homo	F	24 days	Dead (11m)	HCM
24	BOLA3 (c.287A>G:p.His96Arg /c.136C>T: p.Arg46Ter)	M	5 months	Dead (6m)	Cardiomyopathy
25	ACAD9 (c.1150G>A(p.V384M /c.1817T>A(p.L606H)	F	14 days	Alive (5m)	HCM
26	TAZ c.367C>T(p.Arg123X)	M	6 months	Dead (8m)	Heart failure, VF
27	tRNA-Leu1 m.3243 A>G	F	7 months	Dead (3y6m)	DCM, PSVT, WPW syndrome
28	WT	M			
29	WT	F			
30	WT	M			

2.9) Flowcytometry

Cardiac differentiation or purification efficiency was examined by the percentage of $cTnT^+$ cells after cardiac differentiation of mESC-CMs and hPSC-CMs for 10-14 days (**Method 2.3** and **2.4**). Cells were dissociated to single cells by treatment with TrypLE (Thermo Fisher Scientific) for 10 minutes at 37 °C, IMDM containing 10% FBS was added and centrifuged. Next, cells were resuspended in

LIFE/DEAD staining (1 μl/ml of PBS, Thermo Fisher Scientific, LOT: 2464965) at room temperature for 30 minutes. Then, cells were centrifuged and fixed in 4% (w/v) paraformaldehyde (PFA, Wako). Next, cells were permeabilized and blocked using 0.2% Triton X-100 containing 5% of FBS in PBS twice. Then, cells were stained in Cardiac Troponin T Monoclonal Antibody (1:500 of PBS, Thermo Fisher Scientific, 13-11) for 30 minutes at room temperature. Then, cells were washed twice in 0.2% Triton X-100 containing 5% of FBS in PBS. Next, cells were stained with secondary antibody staining using anti-mouse IgG conjugated with Alexa Fluor 488 (1:500, Thermo Fisher Scientific) for 30 minutes at room temperature. Finally, cells were washed twice in 0.2% Triton X-100 containing 5% of FBS in PBS. % of $cTnT^+$ cells were measured using Accuri C6 (BD) or SH800 (SONY).

2.10) Immunostaining

MCM-PSC-CMs were cultured in 24-well plates (ibidi) precoated with 0.1% gelatin and iMatrix-511 (2 μg/ml) until day 21.

For the cell wall staining, first, cells were washed in PBS twice, and then wheat germ agglutinin (WGA) conjugated with Alexa Fluor 647 dye (5 μg/ml of PBS, Thermo Fisher Scientific) was added. Cells were incubated at 37 °C for 10 minutes, then washed in PBS three times. Next, cells were fixed with 4% PFA (Wako) overnight. Then, cells were washed with PBS and permeabilized using 0.2% Triton X-100 in PBS for 15 minutes at room temperature. Then, to stain the sarcomere and mitochondria, cells were blocked with 2% FBS in PBS followed by incubation with mouse monoclonal anti-α-actinin antibody (1:500, Sigma-Aldrich, Clone: EA-53) and anti TOM20 rabbit poly-AP (1:500, Proteintech, cat number: 11802-1-AP) overnight at 4 °C. Next, cells were washed and stained with secondary antibodies, anti-mouse IgG (1:500, Thermo Fisher Scientific) and anti-rabbit IgG (1:500, Thermo Fisher Scientific), conjugated with Alexa Fluor 488 and 555, respectively. Cells were incubated at room temperature for 2 hours, then washed with PBS three times. Nuclei were stained with DAPI solution (1:1000, Dojindo). Immunofluorescent images were collected by a confocal laser scanning microscope (Olympus FluoView FV1200), an inverted fluorescence microscope (Olympus IX83 with ORCA-Flash 4.0 v3 camera), or a spinning-disk confocal microscope (CSU-W1, Yokogawa; with ORCA-Flash 4.0 v3 camera). Cell size, sarcomere structure, nuclei number, and mitochondrial morphology were analyzed by ImageJ software.

2.11) Ca^{2+} transients

To determine intracellular Ca^{2+} transients, MCM-iPSC-CMs were cultured in a 24-well plate (Falcon) until the desired day to run the experiment (day 24-25). Then, cells were washed with PBS and loaded with the intracellular Ca^{2+}-sensitive dye, Calbryte 520-AM (AAT Bioquest) in freshly prepared Tyrode's solution (**Table 9**) that had been pre-wormed for 10 minutes at 37 °C. Cells were incubated for 30 minutes at 37 °C. Evaluation of intracellular Ca^{2+} transients was carried out using live-cell imaging analysis. Cells were evoked by electrical field stimulation at 1 Hz (C-Pace, IonOptics). Intracellular Ca^{2+} transients were recorded with a 40x objective lens, 10 msec exposure, and 20 msec intervals by an inverted fluorescence microscope (Olympus IX83 with ORCA-Flash4.0 V3). ImageJ was used to quantify intracellular Ca^{2+} transients as described in the previous study[16].

Table 9. Tyrode's solution preparation

Component	Company	Concentration
NaCl	Wako	140 mM
KCl	Wako	5.4 mM
MgCl2	Wako	0.5 mM
CaCl2	Wako	2 mM
NaH2PO4	Wako	0.33 mM
D-Glucose	Wako	11 mM
HEPES	Dojindo	5 mM
pH adjusted to 7.4 using NaOH		

2.12) Contractility assessment

For sarcomere shortening, mPSC-CMs were replated in glass-bottom 24 well plates precoated with 0.1% gelatin and iMatrix-511 (2 μg/ml). AAV was transduced at the titer of 1 x 10^4 to 1 x 10^6 viral genome/cell (vg/cell). The required amount differed depending on the cell line and experimental conditions. mPSC-CMs were cultured in an AAV-containing medium for 3 days. Then, the medium was changed to a culture medium without AAV. Live-cell imaging was conducted seven days post-transduction.

Cell contraction was recorded continuously with time-lapse videos for live-cell imaging. The time-lapse recordings were then analyzed by SarcOptiM plugin of ImageJ. Detailed transduction and sarcomere shortening methods are explained in our previous study[92].

2.13) Mitochondrial respiratory function analysis

Mitochondrial function was analyzed with Seahorse XF96 extracellular flux analyzer (Seahorse Bioscience). with a Seahorse XF Cell Mito Stress Test Kit (Seahorse Bioscience) according to the manufacturer's instructions.

For MCM-iPSCs. Approximately 4 hours prior to analysis, precoated XF96 microplates were seeded at a density of 2 x 10^4 cells per well. One hour before starting the assay, the existing medium was replaced with Seahorse assay medium (XF DMEM 103575-503, Agilent, USA) supplemented with 2 mM L-glutamine, 1 mM pyruvate and 10 mM glucose for oxygen consumption rate (OCR) assessment. Oxygen consumption rate (OCR) was measured with sequential injections of 1 μM oligomycin, 0.5 μM FCCP and each 0.5 μM of rotenone/antimycin A. After completion of the assay, the number of cells in each well was confirmed by Hoechst 33342 DNA staining, and images were captured and quantified using a multi-imager (Cytation1, BioTek Instruments, USA). OCR and extracellular acidification rate (ECAR) were normalized by the corresponding cell numbers and subsequently calculated.

For MCM-iPSC-CMs, seahorse XF96 microplate was coated with 0.1% gelatin and iMatrix. At day 25 of cardiac differentiation, MCM-iPSC-CMs were seeded onto the plate with a density of 50,000 cells/well. The cells were cultured until day 30 before starting the assay. The culture medium was changed for base medium (Seahorse XF RPMI medium supplemented with 1 mM pyruvate, 2 mM glutamine, and 25 mM glucose) for 1 hour before running assay and during measurement. Selective inhibitors were sequentially injected during the measurements at the final concentrations of 3 μM oligomycin (an inhibitor for complex V [ATPase] of mitochondrial electron transport chain [ETC]), 0.5 μM carbonyl cyanide-p-trifluoromethoxy phenylhydrazone (FCCP, as a mitochondrial oxidative phosphorylation uncoupler), and 3 μM rotenone (an inhibitor for complex I of ETC) and antimycin A (an inhibitor for complex III of ETC). Basal respiration was represented by oxygen consumption rate (OCR) before applying oligomycin. ATP-linked respiration was represented by the oligomycin-sensitivity respiration rate, while proton leak was calculated by the difference between oligomycin and rotenone/antimycin A rates. Maximal mitochondrial respiration was the response to FCCP.

2.14) ATP and H_2O_2 assay

The CellTiter-Glo® 2.0 Cell Viability Assay kit (Promega, USA) was used to assess intracellular ATP content. CellTiter-Glo reagent (100 μl) was added directly to each well and the plate was read using an EG&G Berthold MicroLumat Plus LB 96V (Berthold Technologies, Germany). H_2O_2 levels were measured using the ROS-Glo H_2O_2 Assay (Promega). All assays were performed according to the manufacturer's protocol. To normalize the results, protein levels were quantified using the Pierce 660 nm protein assay (Thermo Fisher Scientific, USA) in 96-well plates seeded under the same conditions as the assay. After solubilization, absorbance was measured using Benchmark Plus (BioRad, USA).

2.15) RNA-sequencing

To perform RNA-sequencing, RNA was isolated from undifferentiated MCM-iPSCs using Direct-zol RNA 96 Kit. 500 ng total RNA was applied to QuantSeq 3' mRNA-seq Library Prep Kit (Lexogen). The libraries were pooled and sequenced at 2.3 pM with Next-seq 500/550 High Output kit (single end, 75 Cycles, Illumina). Fastq files were mapped to human genome (GRCh38) with STAR aligner, and transcripts were annotated with subread (gencode v28 annotation). Gene expression was examined as transcripts per million reads (TPM).

2.16) Statistics

Data are presented as mean ± standard deviation (SD) for at least three replicate samples. Student's t-test or Wilcoxon rank sum test was used to determine whether any statistically significant difference exists among independent groups, as described in legends. Statistical analysis was performed using GraphPad PRISM version 10 (GraphPad Software, Inc.) and R Studio software.

A p-value of less than 0.05 was considered to have statistical significance.

Chapter 3
AAV-based Modification of PSC-CMs

3.1) Introduction

3.1.1) Background

Cardiovascular diseases continue to impose a substantial global health burden. Despite progress in conventional treatments, there is a persistent need for innovative strategies to address the complex nature of cardiac disorders. The emergence and rapid development of stem cell research provided novel techniques to study cardiac disease. The beginnings of stem cell research were in the early 60s by the discovery of progenitor cells that can repopulate blood cells. This was followed by the discovery of mice and human ESCs in 1981 and 1998 respectively[17,18]. These efforts were crowned by the discovery of the generation of mouse iPSCs from fetal and adult fibroblasts[19], followed by human iPSCs in 2007[20,21]. This breakthrough discovery opened the door for a new era in stem cell research, and many groups started to generate patient-derived iPSCs to use in basic research and clinical trials[22]. A brief summary of the main events in stem cell research is in **Figure 3**.

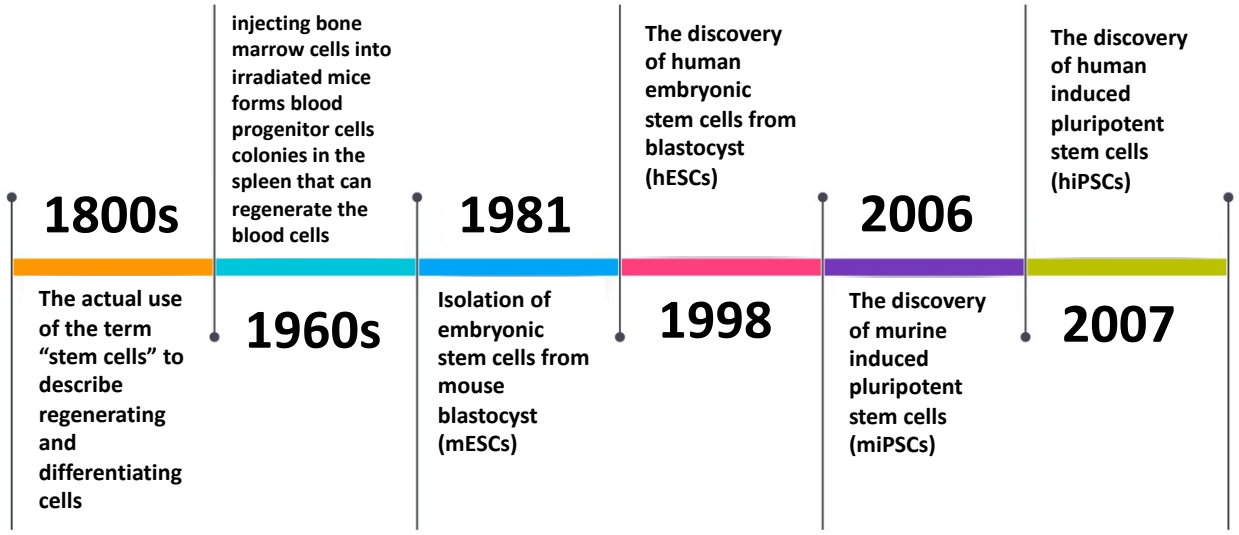

Figure 3. Timeline of the main events in the history of stem cell research.

3.1.2) Comparison between ESCs and iPSCs

PSCs are characterized by unique abilities— (1) self-renewal; the capacity to divide indefinitely, producing unaltered cell progeny that maintains the same properties of the progenitor cell, and (2) pluripotency; the ability to exit from a self-renewal state and differentiate into specialized cell types from any of the three germ layers (ectoderm, endoderm, and mesoderm) under specific signals. There are two primary types of PSCs—ESCs and iPSCs. ESCs are derived from the inner cell mass of early-stage embryos, typically at the blastocyst stage, which necessitates the destruction of the embryo. They were first isolated from mice (mESCs), then in humans (hESCs) from blastocysts[23,24]. iPSCs, on the other hand, were invented in 2006. Somatic cells can be reprogrammed into a pluripotent state by introducing specific genes, namely the Yamanaka factors (Oct4, Sox2,Klf4, and c-Myc)[19,20].

Comparatively, while both ESCs and iPSCs share pluripotency, iPSCs offer ethical advantage as they avoid embryo destruction. Also, there is a lower risk of potential immune rejection as they are derived from the patient's cells if they are used for autologous transplantation. More importantly, only iPSCs can be used for disease modeling as they have the exact same patients' genomes. The main differences between iPSC and ESCs are summarized in **Table 10**.

Table 10 .Overview of the key distinctions between ESCs and iPSCs

Characteristic	ESCs	iPSCs
Source	Inner cell mass of embryos	Somatic cells
Pluripotency	Inherently pluripotent	Reprogrammed to become pluripotent
Cost	Higher cost	Lower cost
Major Ethical Considerations	Necessitate embryo destruction	No embryo destruction
Immune Compatibility	Higher risk of immune rejection	Reduced risk of immune rejection
Tissue Matching	Limited donor availability	Potential for autologous transplantation
Genetic Stability	Stable genetic profile	Higher genetic and epigenetic variations
Epigenetic Memory	Largely absent	Retains some epigenetic memory of donor cell

3.1.3) Cardiac differentiation of hPSCs

hPSCs include both hESCs and hiPSCs. The differentiation of hPSCs into hPSC-CMs is being heavily researched since cardiovascular diseases are the number one cause of death worldwide and the fact that adult cardiac cells can't regenerate after injury[25]. Many efficient hPSC-CM differentiation protocols have emerged[26].

Recapitulating embryonic development leads to hPSC differentiation methods. Cardiac development can be divided into two stages. **(1) Development of cardiac mesoderm:** The induction of cardiac mesoderm is primarily controlled by three families of extracellular signaling molecules: wingless integrated (WNT), fibroblast growth factor (FGF), and transforming growth factor β (TGF-β). These signals induce the expression of early mesoderm markers; Brachyury (or T) and EOMES, followed by temporary activation of the transcription factor mesoderm posterior protein 1 (MESP1), which indicates entering the stage of cardiac mesoderm development. **(2) Cardiac development**: WNT inhibition leads the commitment of cardiac mesodermal progenitors to cardiac cells, which is followed by myofibrillogenesis, heart morphogenesis, and trabeculation[27,28,29].

For hPSC differentiation into hPSC-CMs, early protocols developed used Activin-A and BMP4. Nevertheless, hPSC-CM yield was low (30%). With the subsequent discovery that Activin/BMP4 differentiation depended on the endogenous Wnt/β-catenin signaling, the later was used to drive hPSC-CM differentiation. Stimulation of Wnt/β-catenin signaling in the beginning of differentiation (for example using GSK3-inhibitor CHIR99021) and then inhibition of it after the formation of cardiac mesoderm was found to be sufficient to consistently generate hPSC-CMs. Moreover, insulin was found to suppress cardiac differentiation during the first five days. After insulin was removed in the first stages of differentiation, more consistent results were obtained[29,30]. Various hPSC cardiac differentiation protocols with comparable efficiencies have been reported. Timeline of the main events of differentiation is in **Figure 4**.

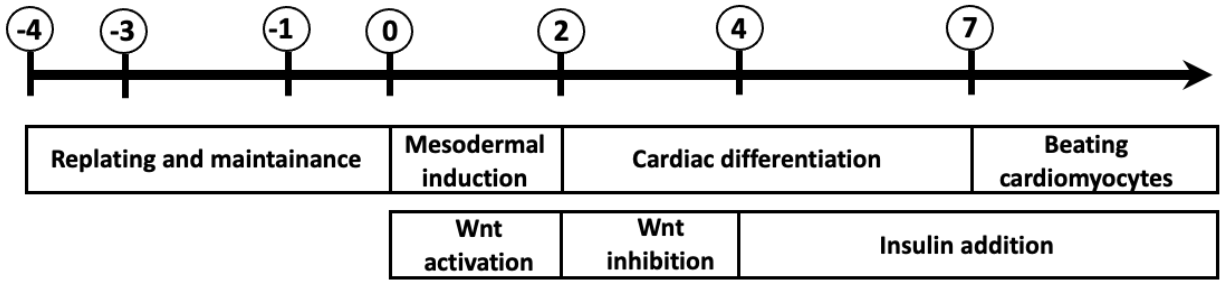

Figure 4. Cardiac differentiation of hPSCs

Wnt activation followed by Wnt inhibition is used to drive cardiac differentiation of hPSCs.

3.1.4) Challenges of hPSC cardiac differentiation

While the potential of hPSC-CMs is immense, many challenges persist in their efficient generation and purification. These challenges must be in consideration when designing or interpreting experiments that use hPSC-CMs. Continued efforts are made to optimize the *in vitro* culture environment and create pure, mature, and homogenous hPSC-CMs that can be used for cardiac disease research. Below is an overview of some challenges that face hPSC cardiac differentiation process. A schematic summary is in **Figure 5**.

3.1.4.1) Purification of hPSC-CMs

The cardiac differentiation efficiency of hPSCs varies with different cell lines and culture conditions. The culture is usually contaminated with non-cardiac cells. To use hPSC-CMs clinically, we must purify cardiomyocytes to prevent any non-specific growth or tumors. Currently used methods to purify hPSC-CMs include:

Genetic modification: This is based on the expression of a drug-resistant gene or a fluorescent reporter gene under the control of cardiac specific promoter. In the case of drug resistance (such as puromycin or neomycin), hPSC-CM purity can reach > 95%[30,31]. Fluorescent reporter gene-based selection on the other hand requires Fluorescence-activated cell sorting (FACS) to isolate fluorescent cells. Both methods are widely used, nevertheless, the gene modification process can be time-consuming especially when handling many cell lines at the same time. Another downside is that reporter genes insertion into the host genome can induce mutations[13].

Cell surface markers: Immunolabeling of cell surface cell proteins specifically expressed in hPSC-CMs can be used to sort cells by FACS or magnetic-activated cell sorting (MACS). Cell sorting targeting SIRPα was reported to enrich cardiac precursors and hPSC-CMs up to 98% purity[32]. Another study showed that 95–98% of vascular cell adhesion molecule 1 (VCAM1)-positive cells were positive for TNNT2[33]. $CD166^{+}$ cells sorted during cardiac differentiation were found to form cardiomyocytes[34]. Despite the high sensitivity of this method, its specificity remains questionable since these markers can also be expressed in other cell types[13]. Another issue is the need for FACS or MACS to sort hPSC-CMs which can be time-consuming and harmful for cell viability.

Mitochondrial dye: Another non-genetic method for isolating hPSC-CMs is based on the use of the mitochondrial dye tetramethyl rhodamine methyl ester perchlorate (TMRM)[35]. Since cardiomyocytes have higher mitochondrial activity, the

signal intensity of TMRM is greater. It was reported that hPSC-CMs can be purified using FACS up to 99% based on the TMRM signals[35]. TMRM does not affect cell viability and fades from the cells within 24 hrs. Nevertheless, since TMRM-based selection only functions in cardiomyocytes with high mitochondrial density and activity, this method cannot efficiently purify the less mature, fetal-like hPSC-CMs[13]. Further, it cannot be used when studying diseased hPSC-CMs since decreased mitochondrial activity is a common feature of many cardiac diseases.

Lactate-based culture: Cardiomyocytes efficiently produce energy from several substrates including glucose, fatty acids (preferred in adult cardiomyocytes), and lactate (preferred in fetal cardiomyocytes), while non-cardiomyocytes rely on glycolysis. Using a glucose-depleted, lactate culture medium was reported to inhibit the growth of non-cardiomyocytes and increase cardiomyocytes purity up to 99%[36]. Further depletion of glutamine in the culture medium enriched cardiomyocytes > 99%[37]. This is a simple, easy method that does not require FACS and can be used on a large scale. Nevertheless, prolonged culture in glucose- and glutamine-depleted media may have functional impairment since cardiomyocytes with mature mitochondria couldn't survive without glucose and glutamine[37]. Another downside is the inability to use this method with hPSC-CMs with compromised mitochondria such as MCM-iPSC-CMs.

mRNA-based purification: This method labels cardiac-specific mRNAs using nano-sized probes called molecular beacons. Despite the high sensitivity and specificity of this method, intracellular delivery of molecular beacons via nucleofection decreases cell viability[38,13].

microRNA-based purification: In this method, synthetic mRNA sequences recognize miRNA sequences and an open reading frame that codes a regulatory gene. When miRNA recognition sequence binds to miRNA expressed in the desired cells, the expression of the regulatory protein is suppressed, thus distinguishing miRNA-containing and non-containing cells[39]. Despite the flexibility and wide applicability of this method, the process of specific miRNA identification and verification of their specificity in target cells is a major hurdle of this cell enrichment method[13].

Physical: Physical methods like Percoll density centrifugation and fishnet-like microstructure purification can purify cardiomyocytes up to 70% and 80%, respectively[40,41]. Nevertheless, these methods have problems with decreased cardiomyocyte purity and scalability.

However, these methods are not suitable to use in large scale cardiac disease modeling studies with suspected mitochondrial dysfunction as in the case of MCM. Thus, a new method that can be used in large-scale studies on hPSC-CMs with possible compromised mitochondrial function was needed.

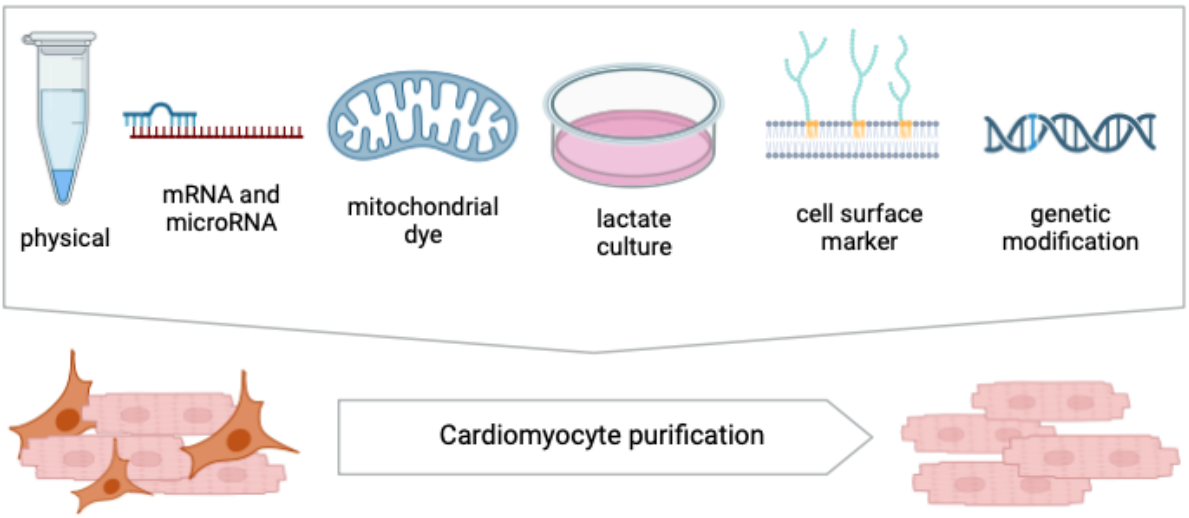

Figure 5. Currently employed PSC-CMs purification methods.

Suitable method is selected according to the experimental settings. However, large scale cardiac disease modeling studies lack appropriate purification method.

3.1.4.2) Maturity

The immature phenotype of hPSC-CMs is a major limitation for metabolic studies and clinical usage, as they may lead to an incomplete understanding of *in vivo* biophysical interactions. The currently used protocols produce hPSC-CMs that have a fetal-like phenotype[42,43].

Several methods were developed to enhance hPSC-CM maturity including prolonged culture, biochemical cues, mechanical and electrical stimulation. More recently, three-dimensional (3D) culture strategies have been used to recapitulate the native myocardial environment[42,44]. The combination of these approaches has shown promising results in enhancing the maturity and hence the utility of hPSC-CMs as disease modeling platforms.

hPSC-CM maturity is of critical importance when considering clinical application. In animal studies, non-fatal ventricular arrhythmias were observed when transplanting hPSC-CMs into pigs and monkeys. This could be a result of

transplanting immature hPSC-CMs that have automaticity[45,46].

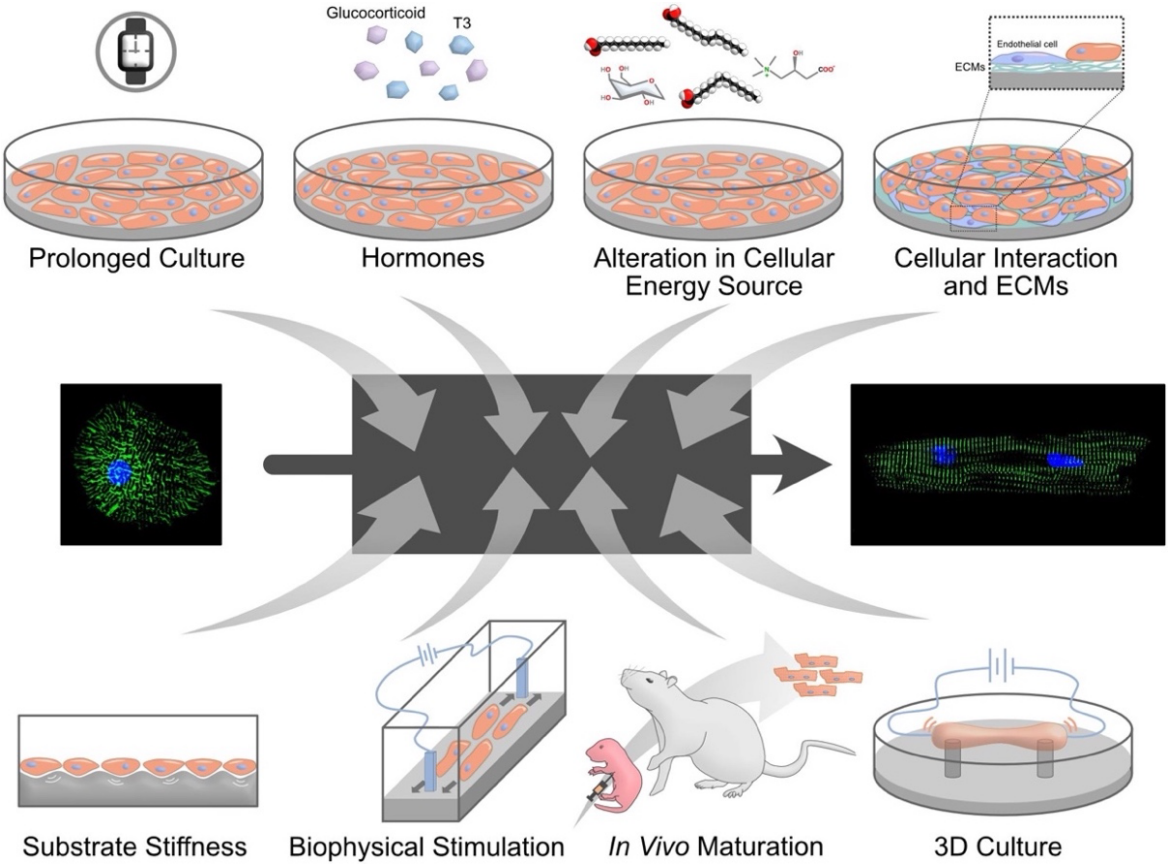

Figure 6. Schematic overview of the maturation approaches of PSC-CMs.

However, no single protocol to drive full PSC-CMs maturation is currently available. The black box in the middle symbolizes the unelucidated mechanism. Image is from our published paper[42].

3.1.4.3) Heterogeneity and sub-type homogeneity

The heterogeneity of morphology, growth curve, gene expression, and differentiation capacity were observed in different iPSC lines. Thus, producing cardiac cell type-specific homogenous PSC-CMs culture will be of critical importance when considering disease modeling and drug testing[47,48].

3.1.5) AAV-mediated gene delivery

3.1.5.1) Background

AAV is a small, non-enveloped virus that has gained prominence in gene therapy research and applications. AAV has non-pathogenic nature, low immunogenicity, and ability to transduce both dividing and non-dividing cells, which makes it an ideal candidate for applications that require sustained and targeted gene expression[49]. Moreover, its ability to persist episomally allows for stable and controlled expression. Thirteen natural AAV serotypes with various tissue tropism exist. Moreover, novel recombinant capsids of AAV are continuously generated to enhance transduction, modulate immunogenicity, or limit tropism[50]. However, considerations of transgene size, optimal vector dosages, timing of transduction, and potential off-target effects necessitate careful optimization for each experimental setup[51,52,53]. Advantages and disadvantages of using AAVs for gene delivery are listed in **Table 11**.

Table 11. Advantages and disadvantages of using AAVs in gene delivery

Advantage	Disadvantage
Injectable, easy *in vivo* delivery	Pre-developed immune tolerance which limits targeted patient populations
High transduction/gene delivery rates	Single payload dose because of development of immunity
Broad tissue tropism due to numerous optimized viral serotypes	Transgene dilution because of single payload and virus non-replication
Low immune response compared to other gene delivery strategies	Mutagenicity of delivered transgene over time
Non-replicative viral vector	Small single-stranded DNA vector limits viral load capacity

3.1.5.2) AAV vectors for gene therapy and research

The safety profile, sustained gene expression, and ability to target specific tissues or organs make AAV an attractive and versatile tool. One of the most notable applications is in the treatment of genetic disorders. AAV serves as a vector for delivering therapeutic genes into target cells, addressing the root cause of certain inherited diseases[54]. It is considered to be the safest and most effective delivery vehicle[55]. Clinical trials have demonstrated success in using AAV-based gene therapies for conditions such as inherited blindness, hemophilia, and certain neuromuscular disorders[56]. Besides gene therapy, AAV vectors are extensively

utilized in research settings to study gene function, regulation, and expression[57]. Expressing fluorescent proteins or other markers with AAV can be used for labeling and tracking specific cell types *in vivo*[2].

Ongoing advancements in AAV technology, including the exploration of novel serotypes and optimization of delivery strategies, continue to broaden the scope of its applications in gene therapy and biomedical research.

3.1.5.3) AAV in the context of PSC-CMs research

AAV proved to be an effective gene delivery method for PSC-CMs. The choice of AAV serotype is pivotal for achieving optimal transduction efficiency in PSC-CMs. Serotypes such as AAV6 and AAV9 have demonstrated superior transduction capabilities in cardiac cells *in vitro* and *in vivo*, respectively[59].

Researchers have explored the use of AAV for targeted overexpression or knockdown of specific genes, enabling them to study the impact of these genetic manipulations on cardiomyocyte development and maturation[60]. They can also be used to develop potential therapeutic interventions for cardiovascular disorders[61,62,63]. Thus, AAV is a crucial tool in advancing our understanding of cardiac biology and developing potential gene therapies targeting various cardiac conditions.

Here, I hypothesized that delivering antibiotic resistance and fluorescent sarcomere proteins into PSC-CMs by AAV may bypass some of the challenges imposed by the conventional methods of purification and functional analysis.

3.2) Results

3.2.1) Cardiac differentiation of mPSC-CMs

Many protocols could efficiently differentiate mPSCs into cardiomyocytes. The protocol I used was described in **Method 2.3** and a schematic protocol is shown in **Figure 7A** below. Briefly, I used mPSCs with Myom2-RFP reporter (SMM18). After 2 days in SFD suspension medium, mesodermal induction was driven for 2 days with activin-A, BMP4, and VEGF. From day 4 to 7, bFGF, FGF10, and VEGF were used to guide cardiac lineage development. By day 10, beating cells "mPSC-CMs" were observed.

Since SMM18 cell line has puromycin resistance cassette under the control of Na^+ - Ca^{2+} exchanger 1 (NCX1) promoter that is only active in cardiomyocytes, I added puromycin 2 μg/ml from day 7 to 10 to selectively culture cardiomyocytes. To determine the fraction of PSC-CMs, cells were immunolabeled with cTnT antibody and flow cytometry was performed at day 10 to evaluate the fraction of cTnT positive cells (**Figure 7B, Method 2.10 and 2.11**). Using this protocol, I could produce on average 90% cardiomyocytes.

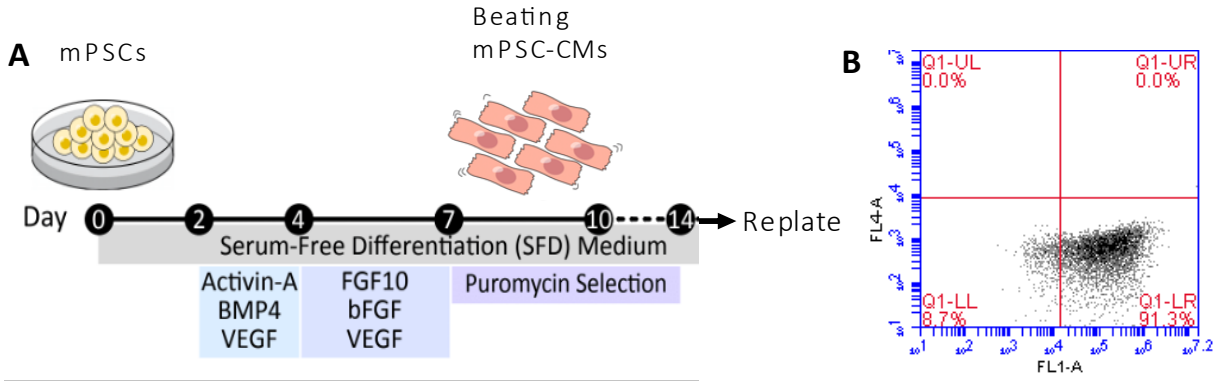

Figure 7. mPSC differentiation and puromycin purification.

A. Timeline of mPSC cardiac differentiation and puromycin purification. Puromycin was added from day 7 to select cardiomyocytes.

B. % of $cTnT^+$ mPSC-CMs with puromycin purification. Stained cells were gated in FL1A (alexa fluor, 488 nm) to detect $cTnT^+$ cells. FL1-A, fluorescence channel 1-A; FL4A, fluorescence channel 4A.

3.2.2) Cardiac differentiation of hPSC-CMs

Differentiation of hPSCs into cardiomyocytes provides a promising tool for cardiac disease research and treatment development. Many differentiation protocols were reported. The protocol I used was described in **Method 2.4,** and a schematic representation is shown in **Figure 8A.** Briefly, I used TIP11-1 cell line. hPSCs were replated in basal medium on day -4. On days -3 and -1 medium was changed. On day 0, GSK3 inhibitor was used to induce mesodermal lineage. Cardiac differentiation was prompted on day 2 using WNT inhibitor. From day 4 onward, hPSC-CMs were maintained in insulin-supplemented medium. Beating cardiomyocytes were observed from day 7.

Since TIP11-1 cell line has puromycin resistance cassette knocked-in in the 3' UTR region of *TNNT2* that is only active in cardiomyocytes, I added puromycin 20 µg/ml from day 7 to day 10 to enrich PSC-CMs in the culture. On day 10, I immunolabeled cells with anti-cTnT antibody and performed flow cytometry to evaluate the percentage of cardiac (cTnT+) cells (**Figure 8B, Method 2.10 and 2.11**). Using this protocol, I could produce on average 90% cardiomyocytes.

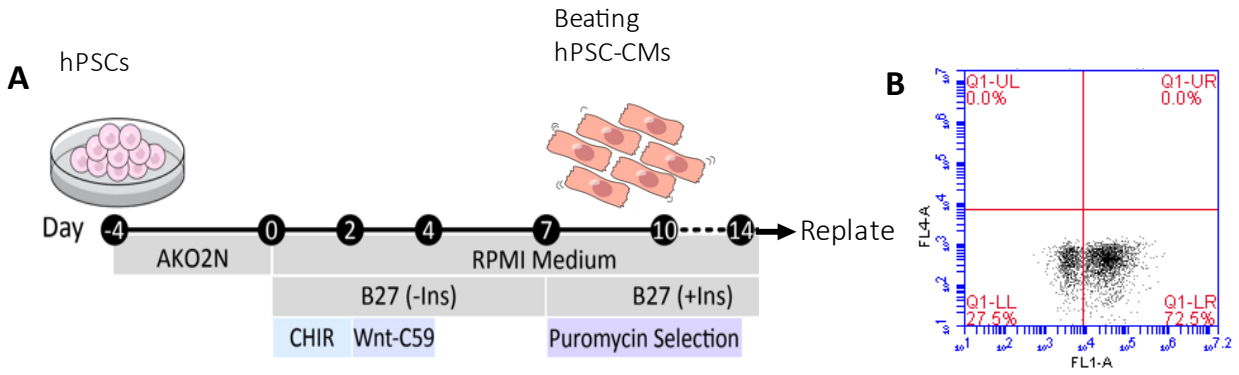

Figure 8. hPSC differentiation and puromycin purification.

A. Timeline of hPSC cardiac differentiation and puromycin purification. Puromycin was added from day 7 to select cardiomyocytes.

B. % of $cTnT^+$ hPSC-CMs with puromycin purification. Stained cells were gated in FL1A (alexa fluor 488 nm) to detect $cTnT^+$ cells. FL1-A, fluorescence channel 1-A; FL4A, fluorescence channel 4A.

3.2.3) Generation of PSC-CM purification method without the need for drug-resistance knock-in

To purify PSC-CMs, there are several methods available, most of them necessitate knock-in or transgenic reporters. These methods are time-consuming especially when simultaneously handling many cell lines. Other metabolic-based method relies on the mitochondrial function of PSC-CMs, thus not suitable to use MCM-iPSC-CMs as their mitochondrial function is expected to be disrupted.

Therefore, I aimed to establish a better antibiotics-selection method for PSC-CMs using an AAV vector. In contrast to the knock-in method, the AAV-based approach provides a scalable tool for handling many cell lines. Moreover, cardiomyocyte selection can be ensured using cardiac-specific promoters, such as wildly used cTnT promoter.

First, I designed the AAV shuttle vector (pAAV-cTnT-Blast) as explained in **Methods 2.5**. The vector map is shown in **Figure 9A**. Briefly, blasticidin-resistance gene is expressed under the control of cTnT promoter that is only expressed in cardiomyocytes. Next, I produced and quantified AAV via real-time PCR as explained in **Methods 2.6** and **2.7**. To test the purification efficiency of this method, I transduced AAV into differentiating hPSC-CMs (TIP11-1) on day 4. On days 7 and 9, I changed the medium to one containing blasticidin. On day 10, I immunolabeled cells with cTnT antibody and performed flow cytometry to evaluate the percentage of cardiac ($cTnT^+$) cells (**Methods 2.10 and 2.11, Figure 9B**). To establish the right balance between AAV and blasticidin that doesn't negatively affect the hPSC-CMs viability, I tested several combinations at different time points. I found that AAV dose of 10^5 vg/cell and a blasticidin concentration of 2.5 μg/ml was sufficient to result in 92% PSC-CMs **(Figure 9C),** a percentage higher than the minimum required to conduct disease modeling studies (~90%).

I used this method to purify MCM-iPSC-CMs for the upcoming morphological and physiological studies.

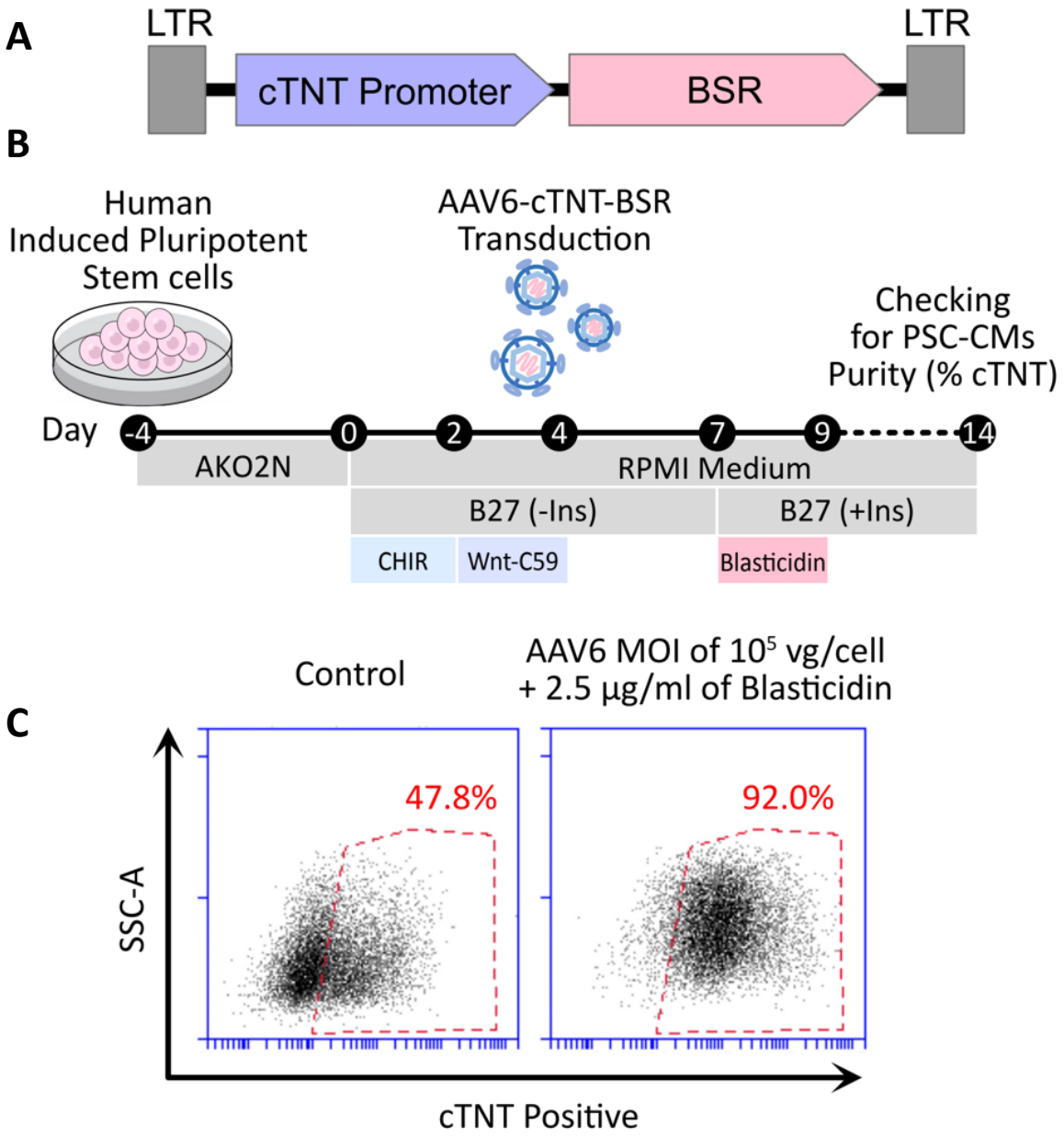

Figure 9. Blasticidin purification of human PSC-CMs without knock-in.

A. Schematic vector map of AAV, in which a blasticidin-resistance gene cassette (BSR) is inserted downstream to cTNT promoter.

B. The timeline of human PSC-CMs differentiation, AAV transduction, and blasticidin selection.

C. Representative data showing percentage of cTNT^{+} cells in human PSC-CMs (transduced 10^5 vg/cell AAV6 on day 4 then treated with 2.5 μg/mL blasticidin on days 7 and 9).

3.2.4) Establishing a method to assess PSC-CM sarcomere function *in vitro*

Assessment of the sarcomere contractile function is an essential part of PSC-CM functional analysis. Nevertheless, hPSC-CMs cultured *in vitro* display underdeveloped and disorganized sarcomeres compared to adult cardiomyocytes, which makes it difficult to assess their contractility via the conventional method that is based on phase contrast (*e.g.*, IonOptix system). With the rising number of cardiomyopathy patient-derived iPSC-CMs, the need for an accurate tool that uniformly measures sarcomere function is increasing. This can be achieved by fluorescently tagging sarcomere proteins to allow for live-imaging and analysis. To that end one group has recently developed a method for sarcomere live-imaging, lifeact-GFP[64,65], a small (17 amino acids) sarcomere fluorescent tag that labels F-actin but is excluded from Z-lines. Thus, it negatively stains the Z-line which makes it less accurate to study PSC-CM sarcomere function (**Figure 10A**).

To more acurrately study PSC-CM function *in vitro*, my colleague developed a knock-in reporter line in mPSC-CMs, namely Myom2-RFP. In which TagRFP is inserted into *Myom2* (sarcomere M-line protein) genomic locus using CRISPR/Cas9 system. The M-line of the sarcomere can be visualized with a fluorescence microscopy when mPSC-CMs reach a certain level of maturity[14] (**Figure 10B**). To test the same method using human PSC-CMs, another colleague generated an α-actinin-RFP knock-in reporter cell line which accurately visualized the Z-line of hPSC-CMs (**Figure 10C**)[15].

These fluorescent reporter lines allow us to analyze *in vitro* sarcomere contractile function, Nevertheless, they require knock-in, a time-consuming method that is not suitable when studying many PSC-CM cell lines at the same time.

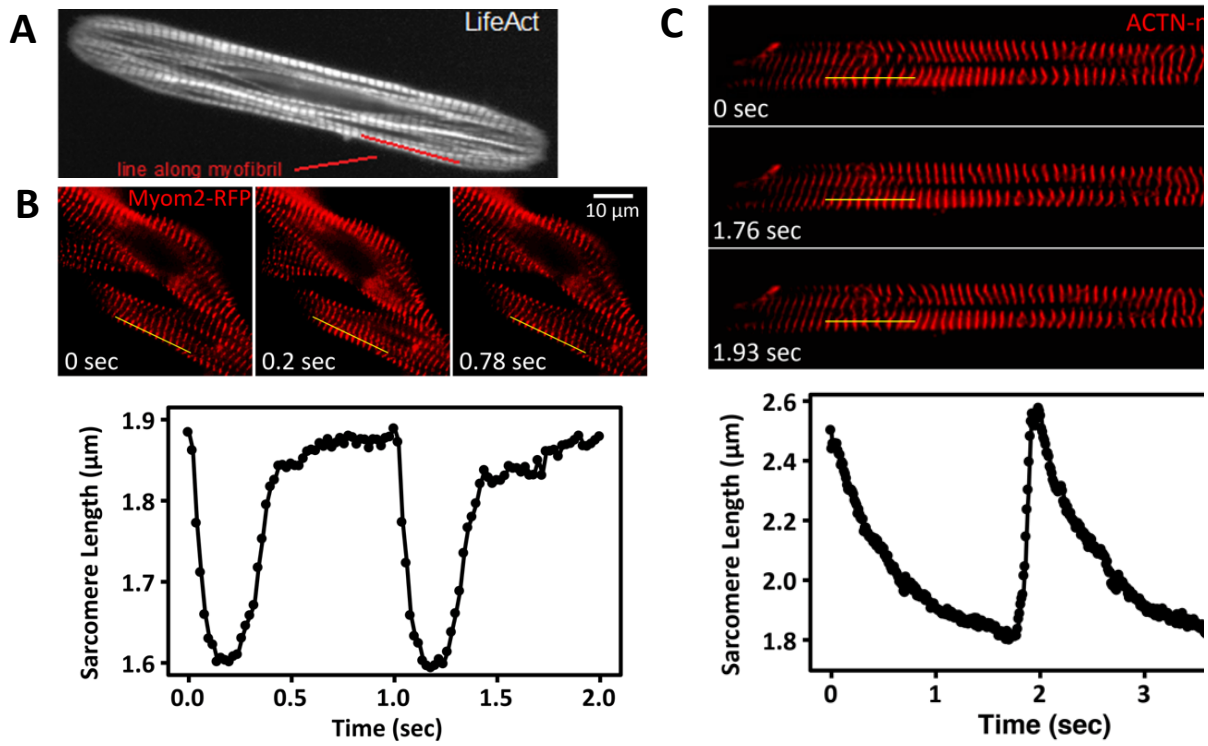

Figure 10. Lifeact sarcomere labelling vs. knock in sarcomere tags.

A. Lifeact F-actin negatively stains Z-line of the sarcomere.

B. Myom-RFP representative time-lapse imaging and sarcomere length profile during contraction of the cardiomyocytes that was electrically stimulated at 1 Hz.

C. ACTN-mCherry representative time-lapse imaging and sarcomere length profile during contraction of the cardiomyocytes that was electrically stimulated at 0.5 Hz.

To bypass producing knock-in lines, I aimed to generate sarcomere protein fluorescent tags to accurately study PSC-CMs sarcomere function *in vitro* using an AAV-based gene delivery method. I chose proteins in the Z-line, a narrow part that defines the boundaries of the sarcomeres. The Z-line contains a lot of interacting proteins that can be targeted for fluorescent labeling. Of those, I crafted a list of small Z-line proteins that can be packaged into AAV vectors (**Table 12**). From that list, I chose 3 candidates with varying sizes: Telethoni (TCAP), PDZ and LIM domain protein 3 (PDLIM3), and Cysteine and glycine-rich protein 1 (CSRP) (**Figure 11**).

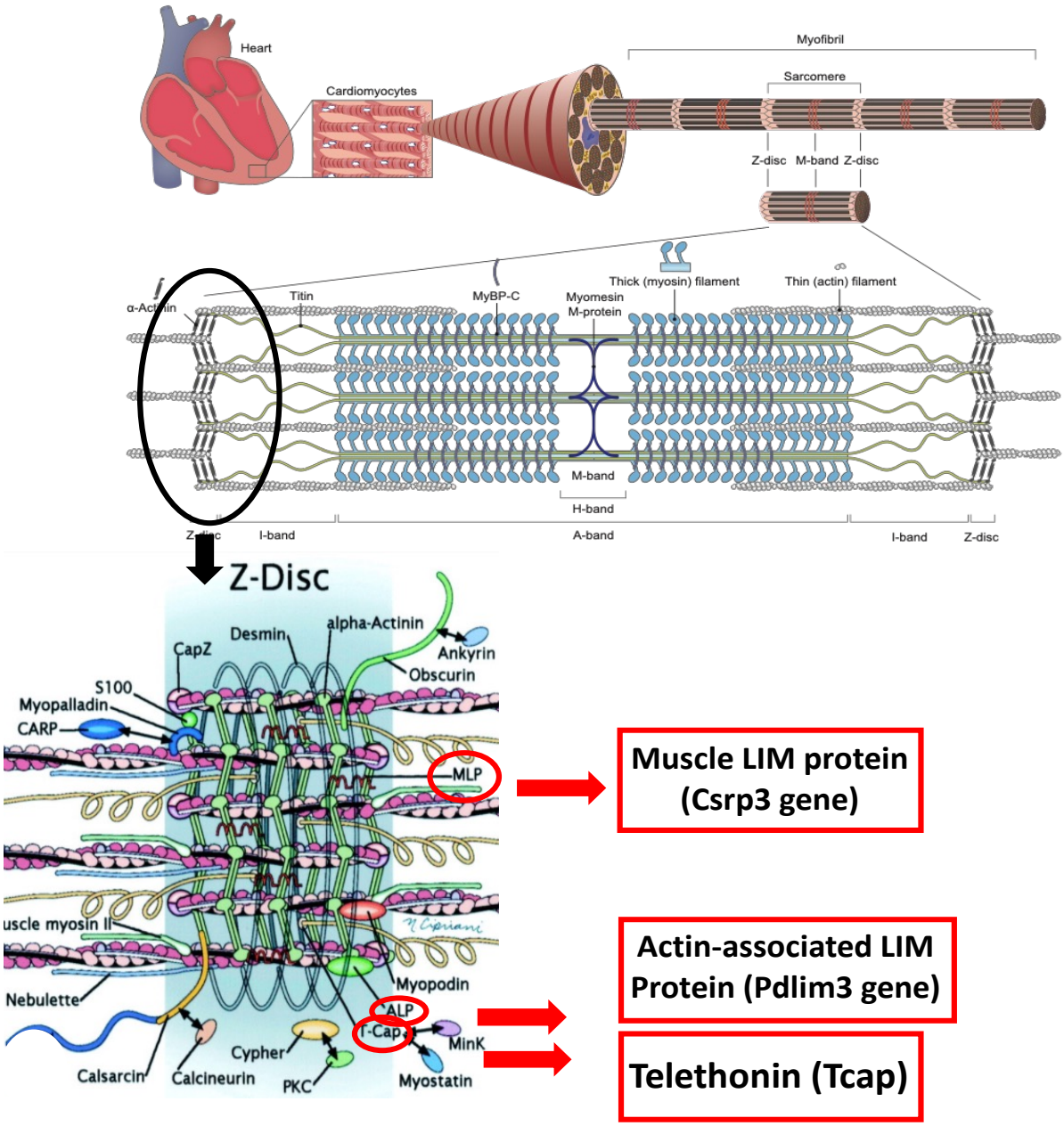

Figure 11. Sarcomere Z line proteins. Muscle LIM protein, Actin-associated LIM protein, and Telethonin were chosen for subsequent AAV packaging.

Figure is modified from our published paper[66] and from[67].

Table 12. Z-line proteins.

Protein	Gene	Size
Telethonin	Tcap	167 AA
Alpha crystallin-B	Cryab	175 AA
Muscle LIM protein	Csrp3	194 AA
Myozenin 1	Myoz1	296 AA
Myozenin 2	Myoz2	264 AA
Myozenin 3	Myoz3	245 AA
CAPZα1	Capza1	286 AA
CAPZα2	Capza2	286 AA
CAPZβ	Capzβ	277 AA
Actinin-ass LIM protein	Pdlim3	316 AA
Melusin	Itgb1bp2	350 AA
MURF 1	Trim63	350 AA
Atrogin 1	Fbxo32	355 AA
Desmin	Des	469 AA
Myotilin	Myot	496 AA
Zasp	Ldb3	679 AA

Note: Red text indicates proteins chosen for this study. AA, Amino Acid.

I constructed TCAP-GFP, PDLIM3-GFP, and CSRP-GFP AAV shuttle vectors as explained in **Methods 2.5.** Briefly, the sarcomere protein gene of interest fused with GFP was expressed under the control of the cTnT promoter (**Figure 12**). Next, I packaged them into AAV6 capsid and quantified AAV vector genome by real-time PCR as shown in **Methods 2.6** and **2.7**. Then, I transduced AAV into day 14 mPSC-CMs (SMM18 line). Seven days after transduction, I conducted live-cell imaging to confirm that GFP-fused proteins correctly localized to sarcomeres and recorded time-lapse videos from which I analyzed their sarcomere function using ImageJ software. The viral concentration required to properly transduce cells varied based on experimental conditions and the time at which mPSC-CMs were transduced. Generally, concentrations of 1×10^4 to 1×10^6 vg/cell were sufficient to transduce cells.

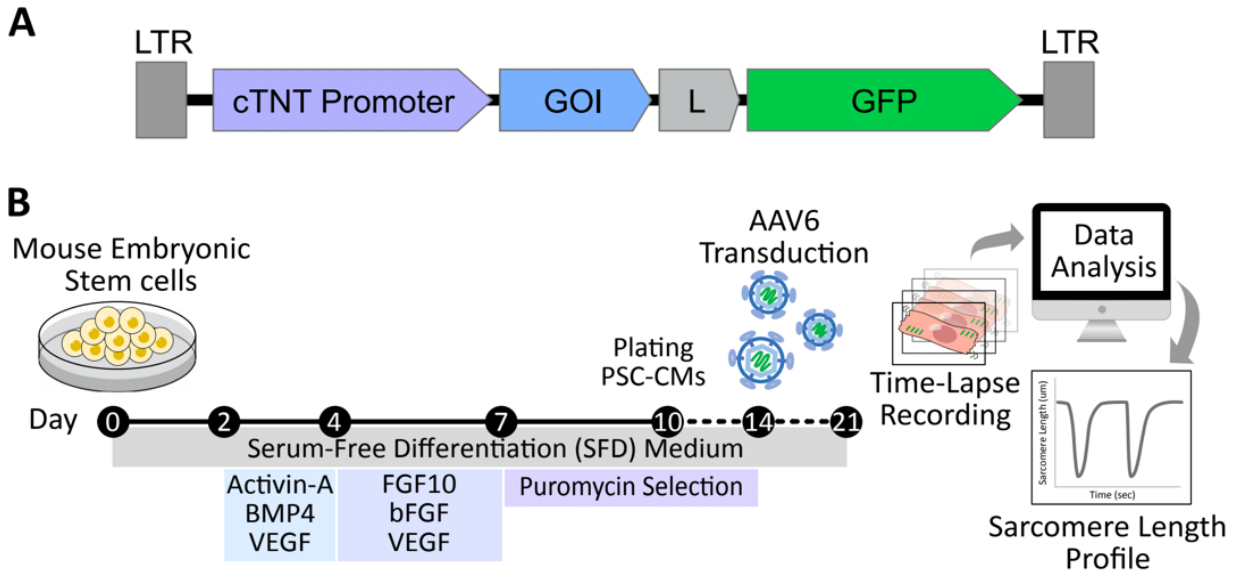

Figure 12. Z line protein fluorescent AAV6 construction and transduction.

A. Schematic vector map of AAV for sarcomere labelling, a sarcomere protein (gene of interest, GOI) is linked to GFP with a Gly-Gly-Gly-Ser linker (L) and expressed under the control of cardiac troponin T (cTNT) promoter.
B. The timeline for mouse PSC-CM differentiation and AAV transduction.
These figures are modified from data published in Journal of Visualized Experiments[15].

Both TCAP-GFP and PDLIM3-GFP localized well to the Z-line, while CSRP-GFP failed to localize to Z-line. Next, I tried to shorten the length of these proteins to make the fluorescent tags as short as possible to minimize any possible interference with normal sarcomere function. To that end, I was able to truncate TCAP protein into the first 80 amino acids. This $TCAP^{1-80}$-GFP localized well to the Z-line. Further truncated TCAP-GFP failed to localize well to the Z-line (**Figure 13**).

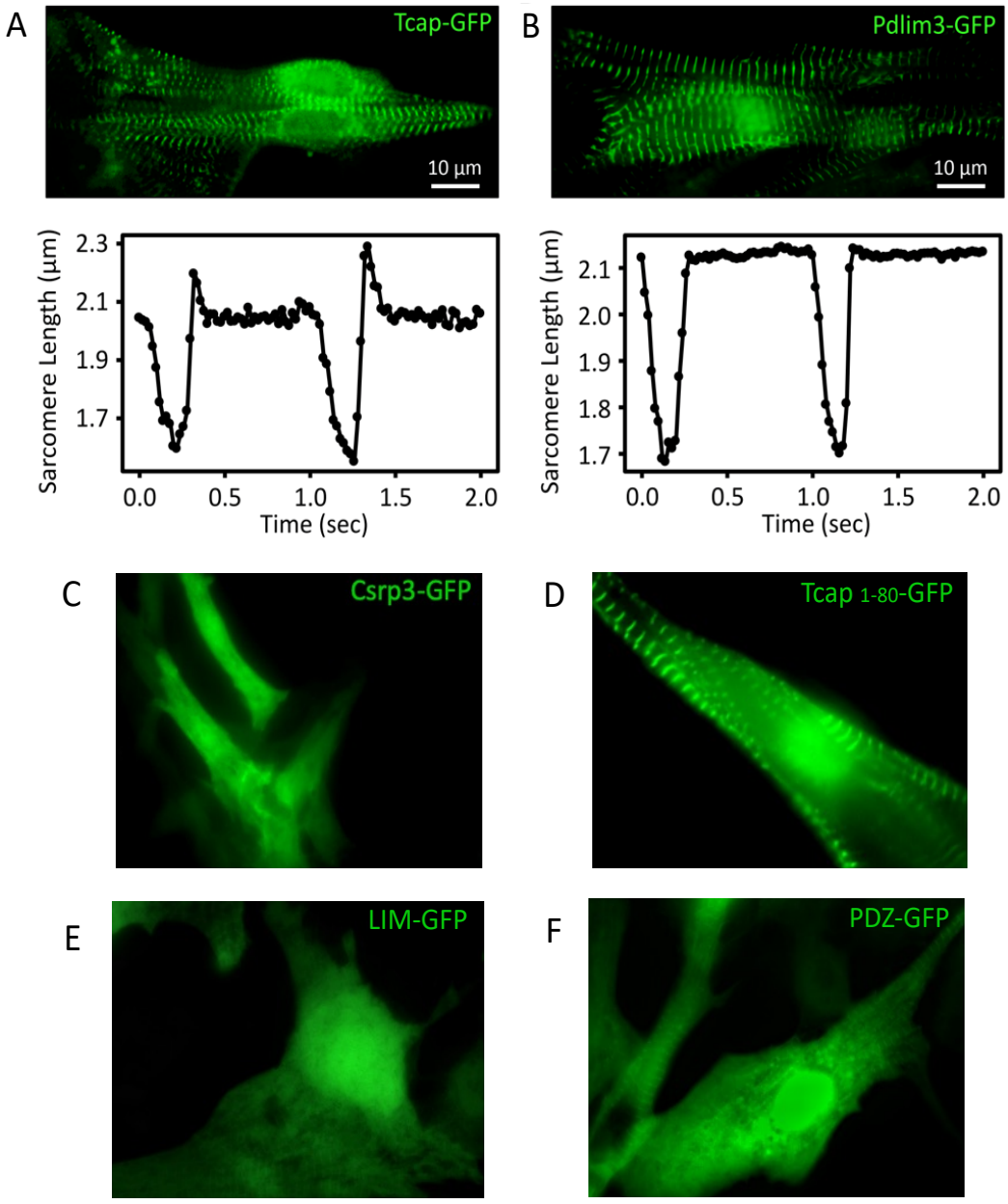

Figure 13. Sarcomere visualization and function analysis using Tcap-GFP and Pdlim3-GFP.

A and B. Representative images showing clear sarcomere localization and the corresponding sarcomere length profile of TCAP-GFP (A) and PDLIM3-GFP (B) after 3 days of transduction into PSC-CMs. That were electrically stimulated at 1 Hz.

C. Csrp-GFP failed to localize to the sarcomere.

D. The truncated version of Tcap-GFP ($Tcap^{1-80}$-GFP) successfully localized to the sarcomere.

E and F. Truncated versions of Pdlim3 (PDZ and LIM) failed to localize to the sarcomere.

A and B are from data published in Journal of Visualized Experiments[15].

3.3) Discussion

The progression from ESCs to iPSCs marked a significant shift in stem cell research. iPSCs provide patient-specific stem cell sources, minimizing the risk of immune rejection and ethical dilemmas associated with ESCs and enabling more accurate disease modeling studies. In cardiac disease modeling research, the use of PSC-CMs is hindered by the lack of suitable methods for PSC-CM purification and contractile function analysis. Here, I established an efficient, AAV-based PSC-CM purification and sarcomere function analysis method. This will open new avenues for advancing cardiac research and offering potential solutions.

Various methods currently employed for purifying PSC-CMs face limitations due to time constraints and potential mitochondrial dysfunction, hindering their use in disease modeling studies. To overcome these issues, I developed an innovative AAV-based antibiotic selection method. This involved inserting a blasticidin-resistance gene under the control of the cTnT promoter into an AAV vector, successfully enriching PSC-CMs without the need for knock-in or transgenic reporter lines. This method achieved purity of >90% PSC-CMs, enough for cardiac disease modeling studies. Replacing the promoter with more cell type-specific ones (e.g., MYL3 for ventricular cardiomyocytes) may further specify target cells for disease models. Moreover, this approach can be employed in any cell type if the specific promoter is available.

Another critical challenge in working with PSC-CMs is the lack of a standardized method to assess their contractile functions *in vitro*. Unlike adult cardiomyocytes, PSC-CMs exhibit underdeveloped and disorganized sarcomeres, the function of which cannot be measured using conventional methods. To address this, I created an alternative AAV-based method to examine sarcomere shortening in PSC-CMs using fluorescent-tagged sarcomere proteins. The study demonstrated successful localization of fluorescent-tagged Z-line proteins (TCAP-GFP and PDLIM3-GFP) in the sarcomere, allowing for live-cell imaging and sarcomere shortening analysis. To minimize any possible functional interactions, I attempted to shorten the protein sequence. The truncated version of TCAP-GFP ($TCAP^{1-80}$-GFP) exhibited sarcomere localization. However, subsequent attempts at further truncation proved unsuccessful. The careful selection of proteins and the direction of GFP fusion is critical, illustrated by the cytoplasmic distribution of CSRP-GFP, another Z-line protein, which failed to localize to the sarcomere when fused with GFP.

In conclusion, the AAV-based modifications introduced in this study contribute novel tools to PSC-CM research. The newly devised purification method and the innovative approach for analyzing sarcomere function improve the practicality and efficiency of studying PSC-CM disease models. These advancements bring us one step closer to unlocking the full potential of PSC-CMs in both research and clinical applications. Future refinements and applications of these methods hold promise for further advancing our understanding not only of cardiac biology but of other systems, as these methods can be modified and applied to other PSC models (e.g., neurons).

Chapter 4
MCM Disease Modeling with iPSC-CMs

4.1) Introduction

4.1.1) Mitochondrial diseases

Mitochondria have indispensable roles in various cellular processes, such as oxidative phosphorylation, the Krebs cycle, the urea cycle, fatty acid degradation, gluconeogenesis, and ketone production[68]. The mitochondria are the only organelle that has their own DNA, the mitochondrial DNA (mtDNA) that constitutes a circular molecule spanning 16 kilobases and housing 37 genes that encode 13 subunits of Complexes I, III, IV, and V of the electron transport chain.

The electron transport chain, composed of five enzyme complexes within the inner mitochondrial membrane, facilitates the transfer of electrons, utilizing the released energy to pump protons across the membrane, establishing an electrochemical gradient. This gradient's potential energy serves various functions, including mitochondrial ion transport, protein import, Ca^{2+} buffering, and ATP generation.[69] The latter is essential for fueling muscle contraction, neurotransmission, DNA and RNA synthesis among other functions that are required to sustain life[70]. The collaborative functioning of mitochondrial enzyme complexes is essential for maintaining this electrochemical gradient[71].

Additionally, the mitochondria contain 22 transfer RNAs and two ribosomal RNAs, crucial for facilitating mitochondrial translation machinery. Mutations affecting mitochondrial genes, presenting in both the nuclear (nDNA) and mtDNA genomes, disrupt mitochondrial function and cause various diseases such as neuropathy, hepatopathy, nephropathy, diabetes, and cardiovascular disorders, collectively known as mitochondrial diseases[72]. These conditions constitute a significant category of inherited metabolic disorders, affecting a minimum of 1 in 5000 individuals. To date, more than 350 genes associated with mitochondrial diseases have been identified, and no specific treatment exist[4,73].

4.1.2) MCM: A complex spectrum of mitochondrial diseases

The heart is one of the most severely affected organs in mitochondrial diseases due to its heavy reliance on oxidative metabolism, much like muscles and the brain[4]. MCM is defined as a myocardial condition depicted by abnormal cardiomyocyte structure, function, or both, caused by mitochondrial dysfunction, in the absence of concomitant vascular, congenital, or valvular heart disease. It occurs in approximately 20-40% of pediatric patients with mitochondrial diseases, often associated with higher mortality rates[74]. The intricacies of MCM arise from the diverse genetic landscape, with various mutations impacting mitochondrial morphology, function, and, consequently, cardiac health. MCM is frequently due to defective ETC complex subunits and their assembly factors, mtDNA maintenance, mtRNAs, rRNAs, ribosomal proteins, translation factors, or CoQ10 synthesis[75]. Some of the MCM-causing mutations and their functions are illustrated in **Figure 14**. Common clinical features in MCM patients include HCM and DCM, left ventricular myocardial noncompaction, arrhythmia, and sudden cardiac death[3]. Patients with neonatal onset, chromosomal abnormalities, or left ventricular hypertrophy, tend to have less favorable outcomes. To diagnose MCM, detailed histopathological studies, biochemical screening, cardiac investigations, genetic counseling, and detection are required[76]. In adults, MCM presents a broader and more complex range of symptoms compared to children, encompassing conduction system abnormalities, atrial fibrillation, ventricular immaturity, and ventricular preexcitation symptoms in addition to myocardial manifestations.

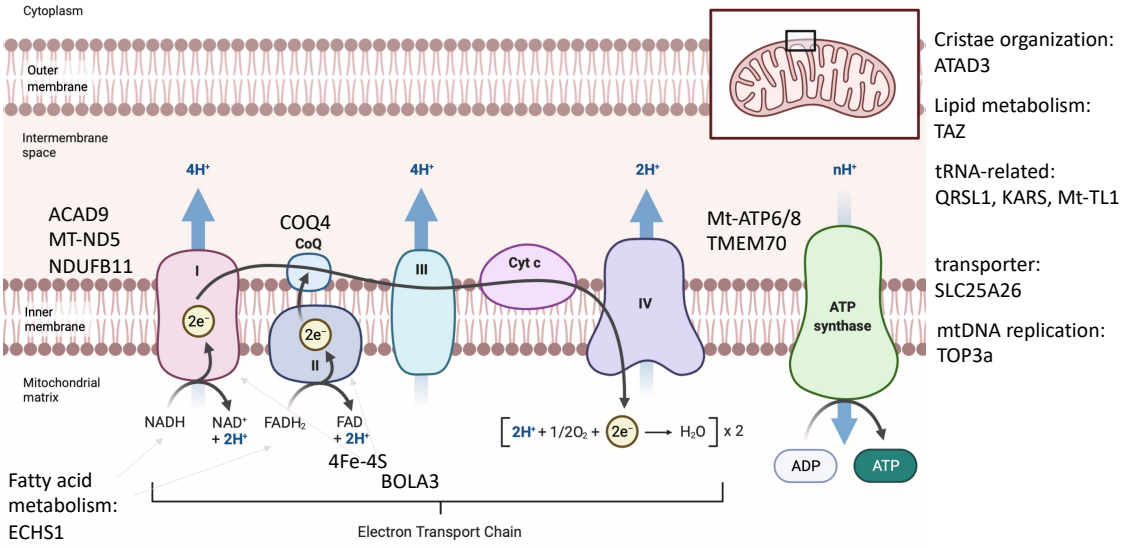

Figure 14. Genes implicated in MCM and their respective functions, related to MCM-iPSCs cohort in this study.

4.1.3) Current approaches to study MCM

Traditionally, MCM research relied on donor fibroblasts and animal models to understand disease progression and develop therapies. Mice, because of their genetic and physiological resemblance to humans along with their relatively easy maintenance and propagation, have been used to study mitochondrial diseases[77]. Nevertheless, only a few models, mostly knockout, exist because of the resistance of animal mtDNA to transgenic manipulation. Another issue is that mice models usually display less severe phenotypes due to differences in metabolic demands and mechanism of mitochondrial biogenesis[78]. A summary of mouse MCM disease models is in **Table 13**. More specific models are desperately needed to understand patient-specific disease mechanisms and clinical pharmacotherapy.

With the generation of iPSCs and subsequent protocols to differentiate various cell types, new horizons are now possible. iPSC-CMs provide an infinite patient-specific models[79]. To date, a lot of cardiac disease iPSC models have been developed, such as long QT syndrome[8], catecholaminergic polymorphic ventricular tachycardia[80], DCM[81], and HCM[82]. For MCM, a few iPSC-CMs have been developed and they could recapitulate disease phenotype. A summary of these models in **Table 14**.

A few structural and functional differences exist between the mitochondria of adult cardiomyocytes and iPSC-CMs, thus, it is still challenging to fully recapture adult cardiac diseases[83,84,85]. Nevertheless, iPSC-CMs remain to be the most suitable method for MCM disease modeling as most MCM cases present in childhood. Moreover, protocols that produce more mature iPSC-CMs are emerging[42].

Table 13. Overview of some MCM mice models.

Abbreviations: ANT1, adenine nucleotide translocase 1; CHCHD, coiled-helix-coiled-helix; FXN, frataxin gene; MRPS34, mitochondrial ribosomal protein of the small subunit 34; OPA1, mitochondrial dynamin like GTPase; ROS, reactive oxygen species; TAZ, tafazzin; TFAM: mitochondrial transcription factor A.

Mutation	Cardiac manifestation	Reference
Ant1 Knock-out	Significant increase of mitochondrial proliferation, cardiac hypertrophy, defects of coupled respiration, metabolic acidosis, and exercise intolerance.	86
MRPS34 Knock-out	Increased fractional shortening of the heart, posterior wall hypertrophy, inhibition of mitochondrial translation, decreased oxygen consumption rates, and respiratory complex activity.	87
Ndufs6 Knock-out	Left ventricular systolic dysfunction, decreased cardiac output, reduced functional work capacity, decreased ATP synthesis, increased hydroxy acylcarnitine, increased risk of cardiac failure, and death after 4 months in males and 8 in females.	88
TFAM Knock-out	Decreased cardiomyocyte proliferation, elevated ROS production, and enhanced DNA damage response pathway.	89
TFAM Knock-out	Decreased expression of fatty acid oxidation enzymes, and increased expression of glycolytic enzymes.	90
CHCHD10-S55L Knock-in	Alteration of mitochondrial architecture and function in the heart, change of the metabolic pathways from oxidative to glycolytic.	91
CHCHD2/CHCHD10 Knock-out	Cardiomyopathy, disrupted mitochondrial cristae, cleavage of the l-OPA1 protein, activation of the mitochondrial integrated stress response.	92
FXN Knock-out	Cardiac hypertrophy, mitochondrial iron overload, and decreased activity of the mitochondrial respiratory chain (complexes I–III).	93
TAZ Knock-out	Cardiomyopathy, ventricular dilation, heart dysfunction, and mitochondrial structural abnormalities.	46 ,94

Table 14 . Summary of iPSC-CMs MCM disease models

Gene mutation	Protein	Disease	Phenotype
TAZ, c.517delG c.328T > C	Tafazzin	Barth syndrome	Abnormal mitochondrial and sarcomere structure and function[95,96,97,98].
FXN, Expanded GAA repeats	Frataxin	Friedreich ataxia	Mitochondrial dysfunction, disrupted Ca^{2+} handling, and iron homeostasis[99,100].
DNAJC19, (rs137854888)	Mitochondrial translocase TIM14	DCM with ataxia syndrome	Impaired mitochondria and conduction defects[101].
SCO2, E140K G193S	cytochrome coxidase (COX)	HCM	Ultrastructural abnormalities, impaired Ca^{2+} handling and delayed after depolarizations[102].
MT-RNR2, m.2336T > C	Mitochondrial encoded16S rRNA	HCM	Mitochondrial dysfunction and electrophysiological disturbance[82].

4.1.4) Current treatment options of MCM

Treating MCM or mitochondrial diseases is still challenging because of the genetic complexity, mitochondrial heteroplasmy, and heterogenous clinical presentation. Emerging therapeutic options are being studied, including pharmacological, genetic, and mitochondrial replacement therapy[76]. Nevertheless, there is no definitive cure till now.

There are a few compounds that are approved for treating mitochondrial disease. Namely; **Idebenone**, a CoQ_{10} analogue that is approved by the European Medicine Agency for treating Leber's hereditary optic neuropathy[103], **Taurine** is approved for treating MELAS (Mitochondrial myopathy, encephalopathy, lactic acidosis, stroke-like episodes) patients with MT-TL1 (m.3243A>G) mutation in Japan[104], and **Omaveloxolone**, the first FDA-approved treatment for mitochondrial disease (Friedreich's ataxia)[105,].

A few other compounds are under investigation for possible therapeutic effect on mitochondrial disease: (1) **Apomorphine** activates mitochondria and has protective effects against oxidative stress in the fibroblasts from Leigh syndrome[106].

(2) **Mitochonic acid 5 (MA-5)**, a derivative of the plant hormone indole-3-acetic acid, improves survival of fibroblasts from patients with mitochondrial diseases[107]. (3) **5-Aminolevulinic acid (5-ALA)**, an endogenous amino acid important for heme biosynthesis, improves ATP production. It is effective in fibroblasts derived from mitochondrial disease patients[108]. (4) **Niacin** supplementation increased muscle strength and mitochondrial biogenesis of adult-onset mitochondrial myopathy patients[109].

Along with mitochondrial disease treatment options, other compounds that improve the overall mitochondrial functions can be used to mitigate the pathological presentations of MCM. These include antioxidants[110], agents that enhance ETC function and mitochondrial biogenesis[111,112]. However, there is a lack of MCM-specific treatments which can be partially attributed to the lack of suitable MCM disease models for drug screening and development.

Besides pharmacological compounds, other mitochondrial disease treatment options include gene therapy and mitochondrial replacement therapy. Both of which are far from providing a definitive treatment for MCM[113,76].

4.2) Results

4.2.1) Production and quality check of iPSC cell lines from MCM patient-derived fibroblasts

The lack of robust and dependable models for mitochondrial diseases has impeded the unraveling of disease pathophysiology and the discovery of novel therapeutic options. One predominant cause is the genetic variability observed among afflicted individuals. Over the last decade, the vast development of iPSC technology allowed us to study human diseases by using patient-specific cells, thus bypassing that issue. Thus, I aimed to produce a patient-specific MCM-iPSC repository that can be differentiated for further studies.

To produce MCM-iPSCs, I used fibroblasts of 26 patients suffering from MCM and four healthy donors. Sendai virus-based SRV-iPSC-1 vector was used to reprogram the fibroblasts into iPSCs (**Figure 15A**). Due to the inability of stable maintenance and other reasons, iPSCs from patients #14, 20, and 23 were excluded for further assessment. Next, I examined if iPSC clones express pluripotency markers SOX2, OCT3/4, and NANOG. Compared to the control iPSCs (648A1), SOX2 and OCT3/4 were expressed at least 50%, while NANOG was expressed at more than 150%, which was a comparable expression level to another control iPSCs (TIP1-11) (**Figure 15B**).

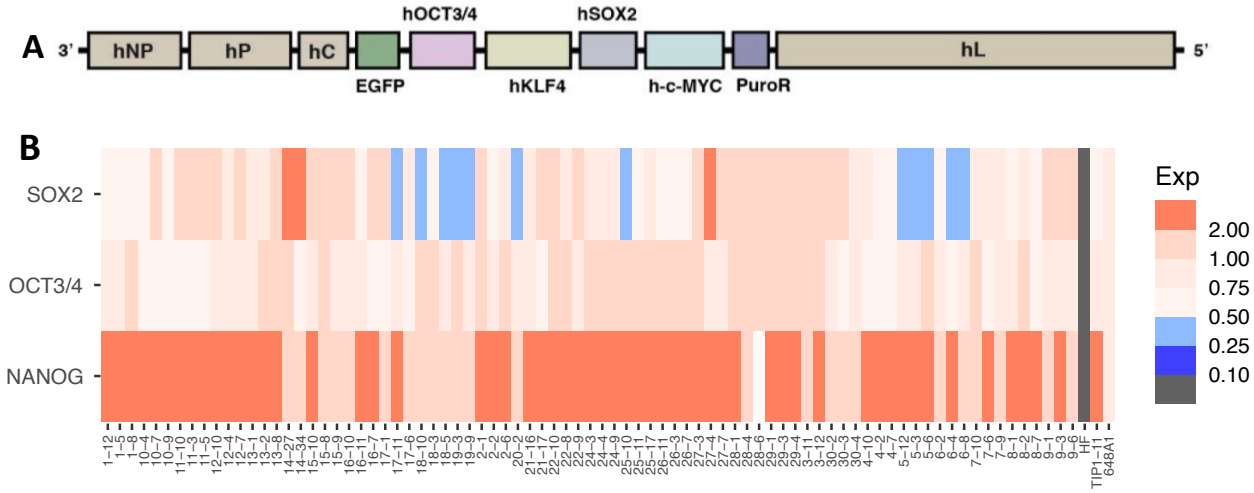

Figure 15. Pluripotency gene expression.

A. SRV-iPSC-1 vector map as provided by the manufacturing company.

B. Heat map showing pluripotency markers expression levels; SOX2 and OCT3/4 were expressed at least 50%, while NANOG was expressed more than 150% in iPSCs compared to the control 648A1.

4.2.2) MCM-iPSCs showed reduced proliferation

Mitochondrial diseases have a multifaceted impact on cell proliferation. Impaired oxidative phosphorylation in dysfunctional mitochondria leads to decreased ATP production, reducing the energy required for cell division. Moreover, increased production of reactive oxygen species (ROS) due to mitochondrial dysfunction contributes to oxidative stress, which can further interfere with normal cell cycle progression. The effects on cell proliferation vary depending on the specific genetic mutations and the tissues affected, with a more pronounced impact in tissues with high energy demands[114,115]. A comprehensive understanding of these complexities is not well established.

In this study, an important observation was the reduced cumulative cell number at day 14 in MCM-iPSCs in comparison to the control iPSCs (**Figure 16A**). This was accompanied by an increased production of the ROS; H_2O_2, indicating increased mitochondrial oxidative stress. H_2O_2 increase was significant in ATAD3 (2-1), TAZ (12-10, 26-3), MT-ND5 (15-10) and ACAD9 (18-5) gene mutations. (**Figure 16B**). These findings underscore the significance of intact mitochondrial function in maintaining the normal progression of the cell cycle and, consequently, cellular proliferation. However, MCM-iPSCs' ATP levels were not significantly different from those of control lines (**Figure 16C**). This can be explained by the decreased reliance of stem cells on mitochondria to produce energy. Instead, the mitochondria are probably reserved for other functions essential to maintain the pluripotent state of stem cells[116].

To gain further insight into the impact of reduced proliferation on gene expression in MCM-iPSCs, a detailed investigation was conducted on various gene markers. These markers included those associated with pluripotency (NANOG, SOX2, OCT4), differentiation (FOXA2, T, PAX6), proliferation (CCND1, CDK1, AURKA), and the response to ROS (HMOX1, NFE2L1, NFE2L2). The examination of these gene markers aimed to provide a comprehensive view of the quality of MCM-iPSCs and the molecular changes associated with the observed reduction in proliferative activity in MCM-iPSCs. However, there were no clear differences at the transcriptome levels in iPSCs (**Figure 16D**). These findings show that reduced proliferation of MCM-iPSCs did not negatively affect their gene expression of pluripotency, differentiation, proliferation, or ROS response markers.

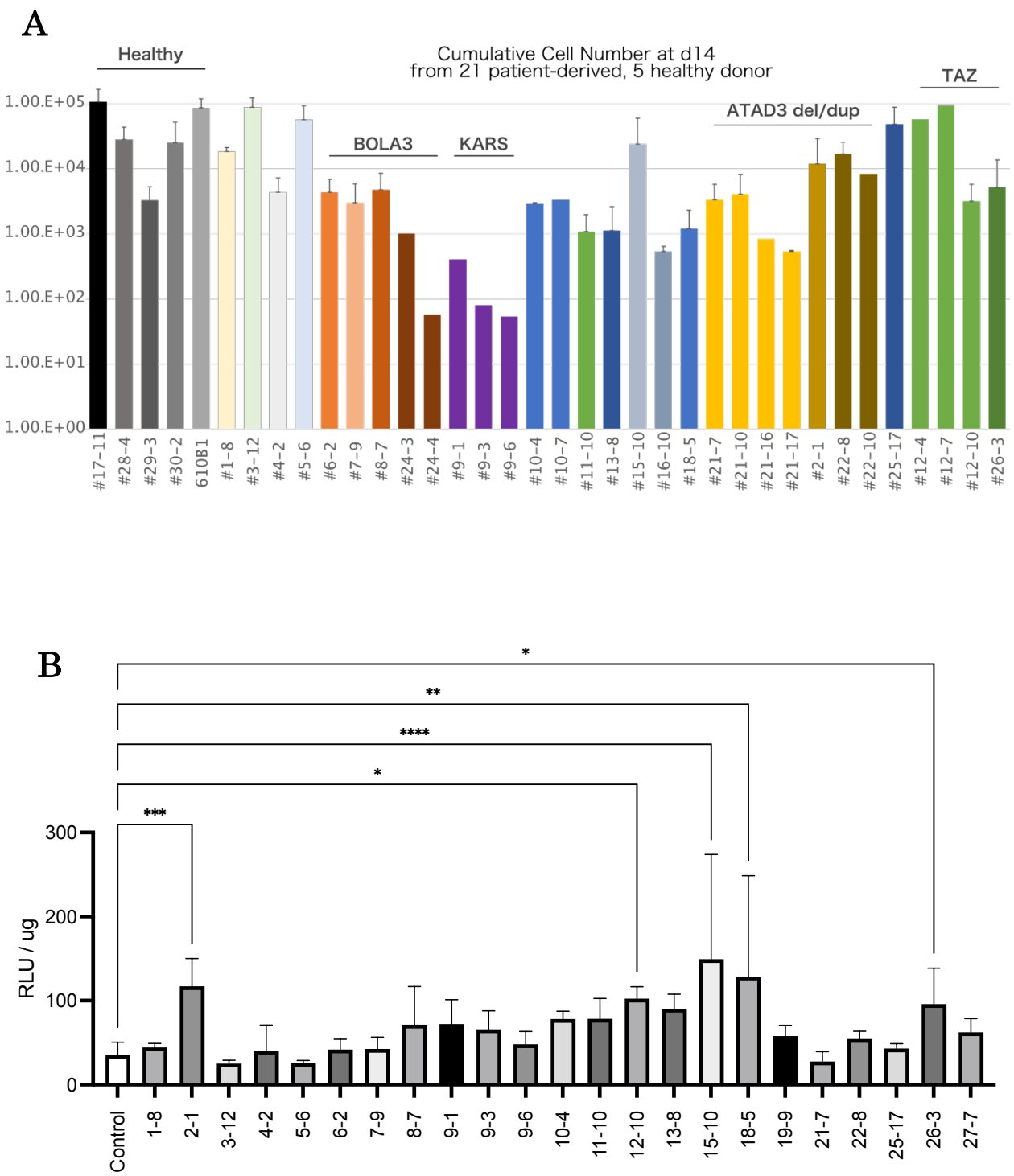
A
Healthy
Cumulative Cell Number at d14
from 21 patient-derived, 5 healthy donor
TAZ
ATAD3 del/dup
BOLA3
KARS
1.00.E+05
1.00.E+04
1.00.E+03
1.00.E+02
1.00.E+01
1.00.E+00
#17-11
#28-4
#29-3
#30-2
610B1
#1-8
#3-12
#4-2
#5-6
#6-2
#7-9
#8-7
#24-3
#24-4
#9-1
#9-3
#9-6
#10-4
#10-7
#11-10
#13-8
#15-10
#16-10
#18-5
#21-7
#21-10
#21-16
#21-17
#2-1
#22-8
#22-10
#25-17
#12-4
#12-7
#12-10
#26-3
B
*
**
****
*
***
RLU / ug
300
200
100
0
Control
1-8
2-1
3-12
4-2
5-6
6-2
7-9
8-7
9-1
9-3
9-6
10-4
11-10
12-10
13-8
15-10
18-5
19-9
21-7
22-8
25-17
26-3
27-7

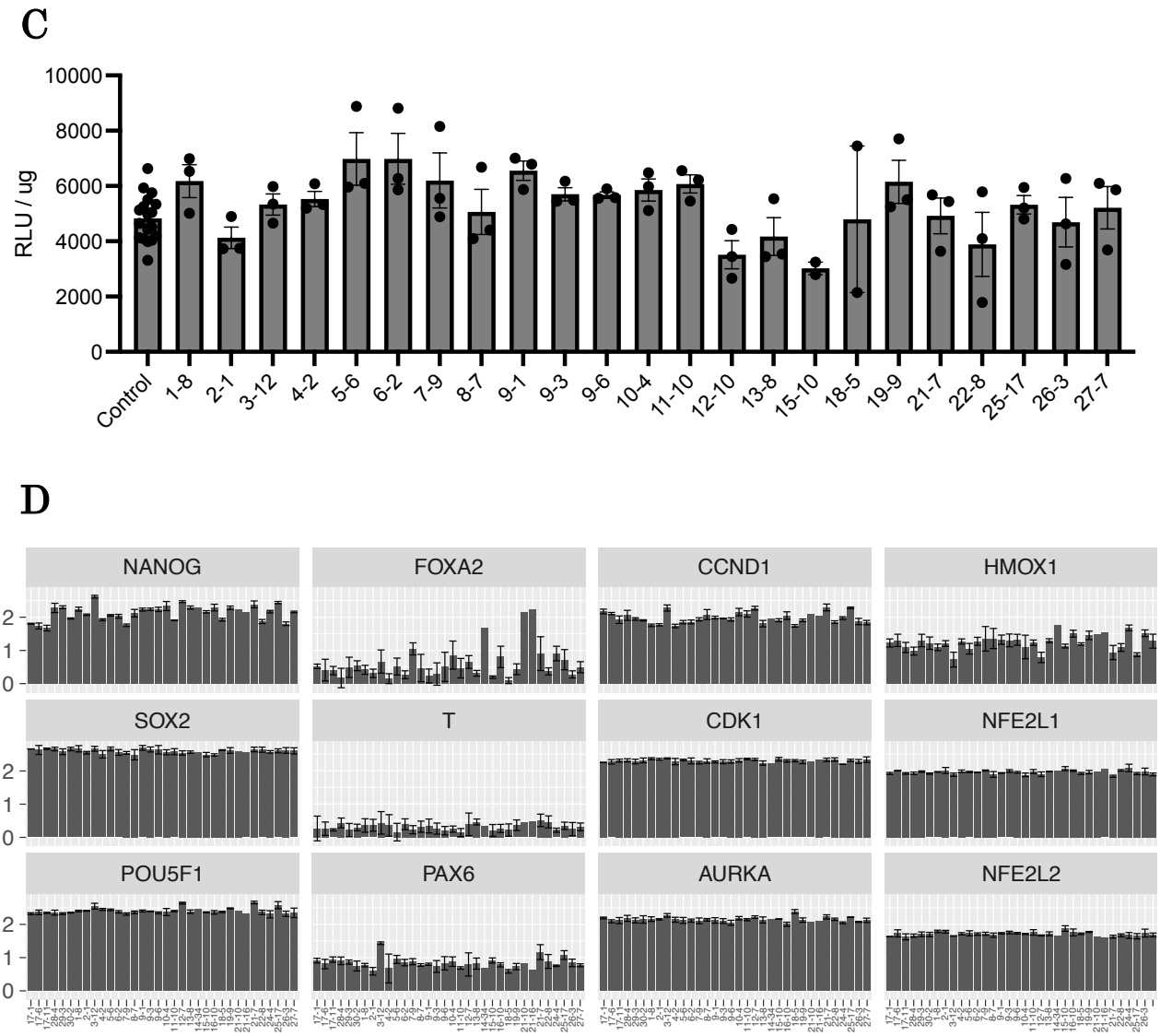

Figure 16. Cumulative cell number at day 14.

A. Compared to the 14-day cumulative cell number at 10^4 to 10^5 in healthy lines, many MCM-iPSC lines showed reduced number, suggesting the importance of mitochondrial function in iPSCs.

B. H_2O_2 levels in MCM-iPSCs compared to control lines. ANOVA Dunnett test was used to compare the difference between the control and disease iPSC-CMs. *P<0.01, **P<0.001, ***P<0.0001, ****P<0.00001. Data are from 3 different sets.

C. Despite the increased H_2O_2 production, ATP generation of MCM-iPSC was not significantly different from that of control lines.

D. Although the reduced proliferative activity, there was no difference in gene expression regarding pluripotency, differentiation, proliferation, or ROS response. Y-axis is Transcript per million (TPM).

4.2.3) MCM-iPSC differentiation capacity

The ability to differentiate iPSCs into functional cardiomyocytes is a pivotal point for understanding MCM. After the production and quality check of MCM-iPSCs (**Results 4.2.1**), I assessed whether MCM-iPSC lines exhibit any differentiation capacity differences compared to control iPSC lines. I conducted cardiac differentiation (as previously described in **Methods 2.4**) of more than 70 and 12 lines from 24 MCM patients and four healthy donors, respectively, following our standard differentiation method. Then, I conducted flow cytometry to examine the proportion of cTnT^{+} cells in each line (**Figure 17**). Notably, the results indicate that both control (23.7±20.4%) and MCM (37.2±25.5%) lines exhibited similar differentiation capacities albeit with a large variance. This essential finding suggests that the presence of mitochondrial dysfunction in MCM-derived iPSCs does not inherently impede their ability to differentiate into cardiomyocytes. To further assess their phenotypes, I selected at least one line per patient/donor.

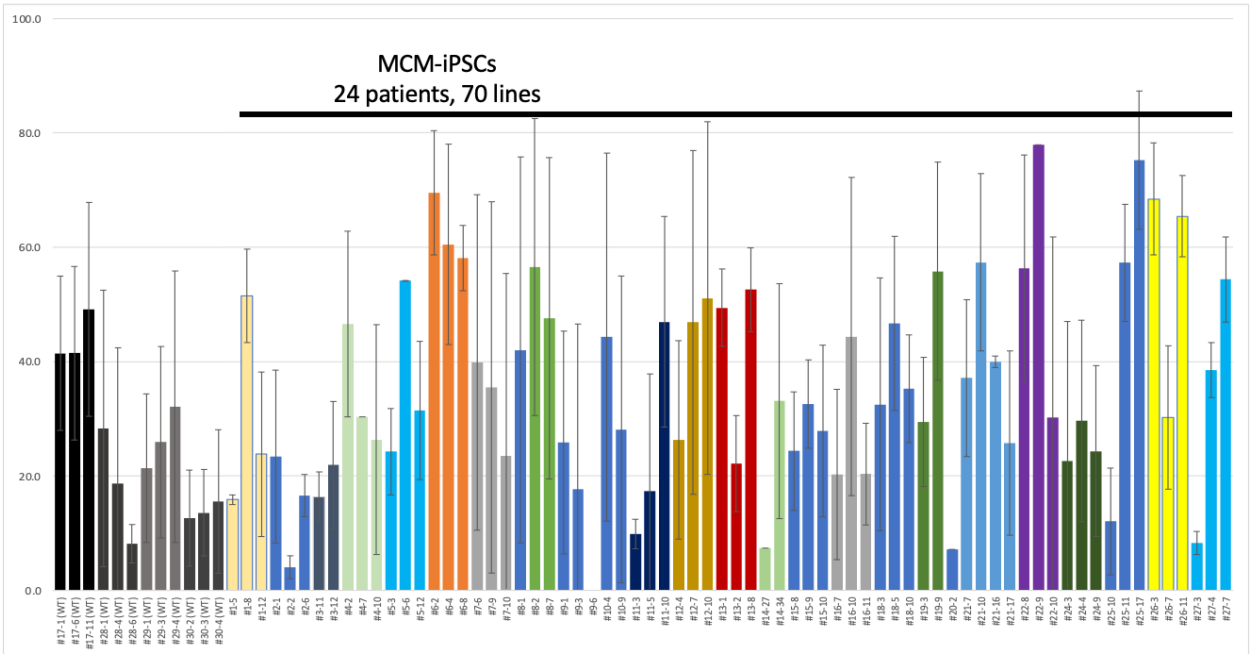

Figure 17. MCM-iPSC cardiac differentiation.

The percentage of cTnT^{+} cells in the healthy controls (gray) vs. MCM-iPSCs (in color) show that both display comparable differentiation capacities. Data are from 2-10 differentiation experiments except for #22-9 (N=1).

4.2.4) MCM-iPSC-CMs mitochondrial function

MCM is caused by various genetic mutations that disrupt the normal functioning of mitochondria. In this study, there is a diverse group of mutations affecting different aspects of mitochondrial structure and function. To investigate whether this is reflected in MCM-iPSC-CMs, I measured mitochondrial ATP and ROS generation. However, the number of samples is insufficient. For some mutations, I did not have enough experimental data for statistical analysis. Another important point to consider before examining the data, is that each gene in this MCM cohort has a unique age-related expression profile. It is expected that because of MCM-iPSC-CMs immaturity, they will not express enough mutant genes to compromise mitochondrial function. This is of significance specially with genes that have low expression levels in fetal and early childhood stages. For reference, gene expression levels are in **Figure 18,** data is from the application devised by Kaessmann lab, Evo-devo mammalian organs[117].

For ATP, the findings show that despite the lack of statistically significant differences from the control, overall trends are seen. Upward trend can be seen with QRSL1 (1-8), ATAD3 (2-1, 21-7, 21-10, 21-16), ECHS1 (5-6), BOLA3 (6-2), KARS(9-6), TMEM70 (10-4), TAZ (12-10), MT-ATP6/8 (13-8), and MT-TL1 (19-9) gene mutations. Downward trends, on the other hand, are observed in BOLA3 (7-9) and ACAD9 (25-17) gene mutations (**Figure 19A**).

In terms of ROS production, measured by H_2O_2 levels (**Figure 19B**), it is biased because of the huge amount of antioxidants in the culture medium. Therefore, I tried antioxidant-free medium, in which I observed more H_2O_2. Nevertheless, data are not enough to be presented here.

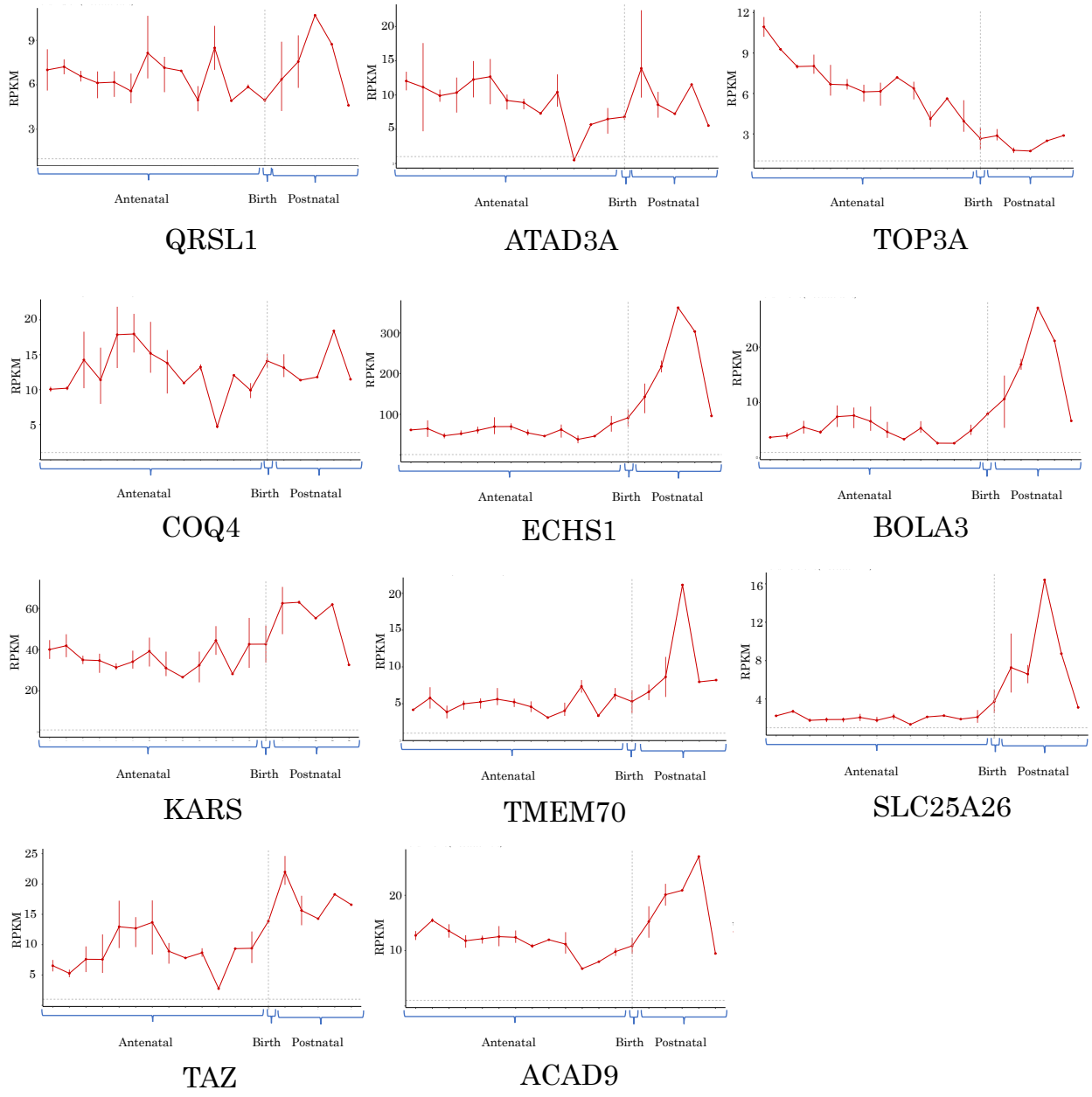

Figure 18. Gene expression of some MCM-related genes by age.

RPKM stands for Reads Per Kilobase of transcript per Million mapped reads. Data are from Evo-devo mammalian organs application[117].

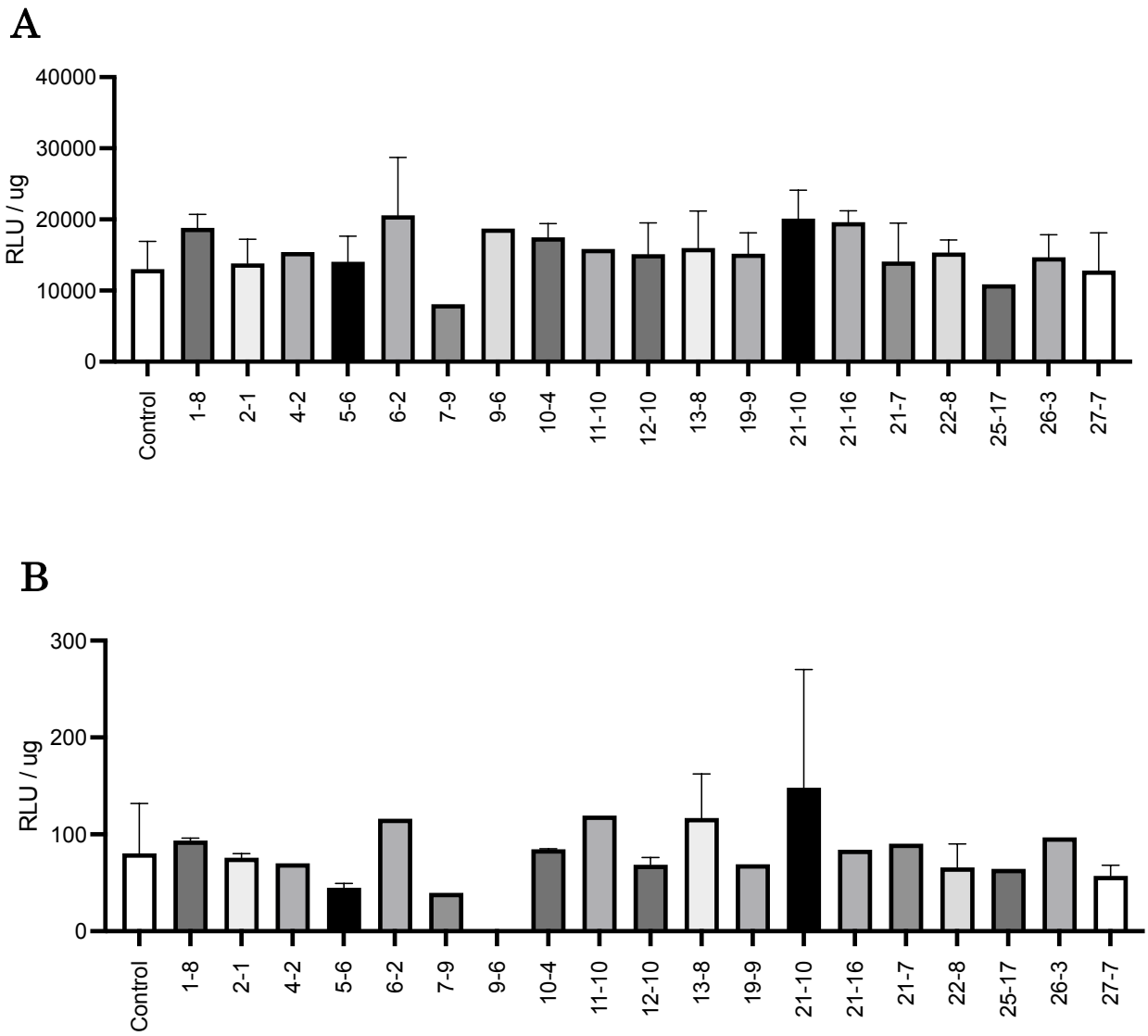

Figure 19. MCM-iPSC-CMs ATP and H_2O_2 levels.

A. ATP levels in MCM-iPSC-CMs compared to control lines.

B. H_2O_2 levels in MCM-iPSC-CMs compared to control lines.

No statistical significance was found in ATP and H_2O_2 production levels. ATP and H_2O_2 were measured in relative light units per micrograms (RLU/µg).

4.2.5) MCM-iPSC-CMs exhibited hypertrophy compared to control iPSC-CMs

MCM is a genetically heterogeneous disorder caused by various mitochondrial DNA mutations, each having unique effects on cardiomyocytes. It is expected for MCM-iPSC-CMs to exhibit morphological abnormalities similar to those seen in MCM cardiomyocytes. To gain insights into the specific consequences of MCM on iPSC-CM morphology, I investigated the phenotypic characteristics of MCM-iPSC-CMs, starting with hypertrophy. Many MCM patients develop cardiac hypertrophy as part of their disease phenotypes. Thus, MCM-iPSC-CMs were expected to show hypertrophic morphology. I differentiated MCM-iPSC-CMs using the protocol previously explained in **Method 2.4**. For purification, I transduced AAV to specifically express blasticidin in cardiomyocytes into MCM-iPSC-CMs (**Results 3.2.3**) on day 9 followed by blasticidin purification between day 11 to 15. Then, I replated MCM-iPSC-CMs on day 15 and analyzed them on day 21. The timeline of cardiomyocyte differentiation is in **Figure 20A**.

For immunofluorescent imaging, I used α-actinin and TOM20 antibodies to stain the sarcomere and mitochondria, respectively (**Methods 2.10**). Results depicted that MCM-iPSC-CMs exhibited marked hypertrophy compared to the control. This hypertrophy was significant in MCM-iPSC-CMs harboring mutations in QRSL1, ATAD3, ECHS1, BOLA3, KARS, TAZ, MT-ND5, and m.3243A>G (MT-TL1). A summary of the cell size data obtained from immunofluorescence imaging data is in **Figure 20B**, while representative images showing MCM-iPSC-CM hypertrophy are in **Figure 20C**. The observed hypertrophy in MCM-iPSC-CMs suggests that these mutations share common pathways or mechanisms leading to cellular hypertrophy which raises important questions about the role of mitochondrial dysfunction in initiating these molecular changes and the subsequent impact on cardiomyocyte health.

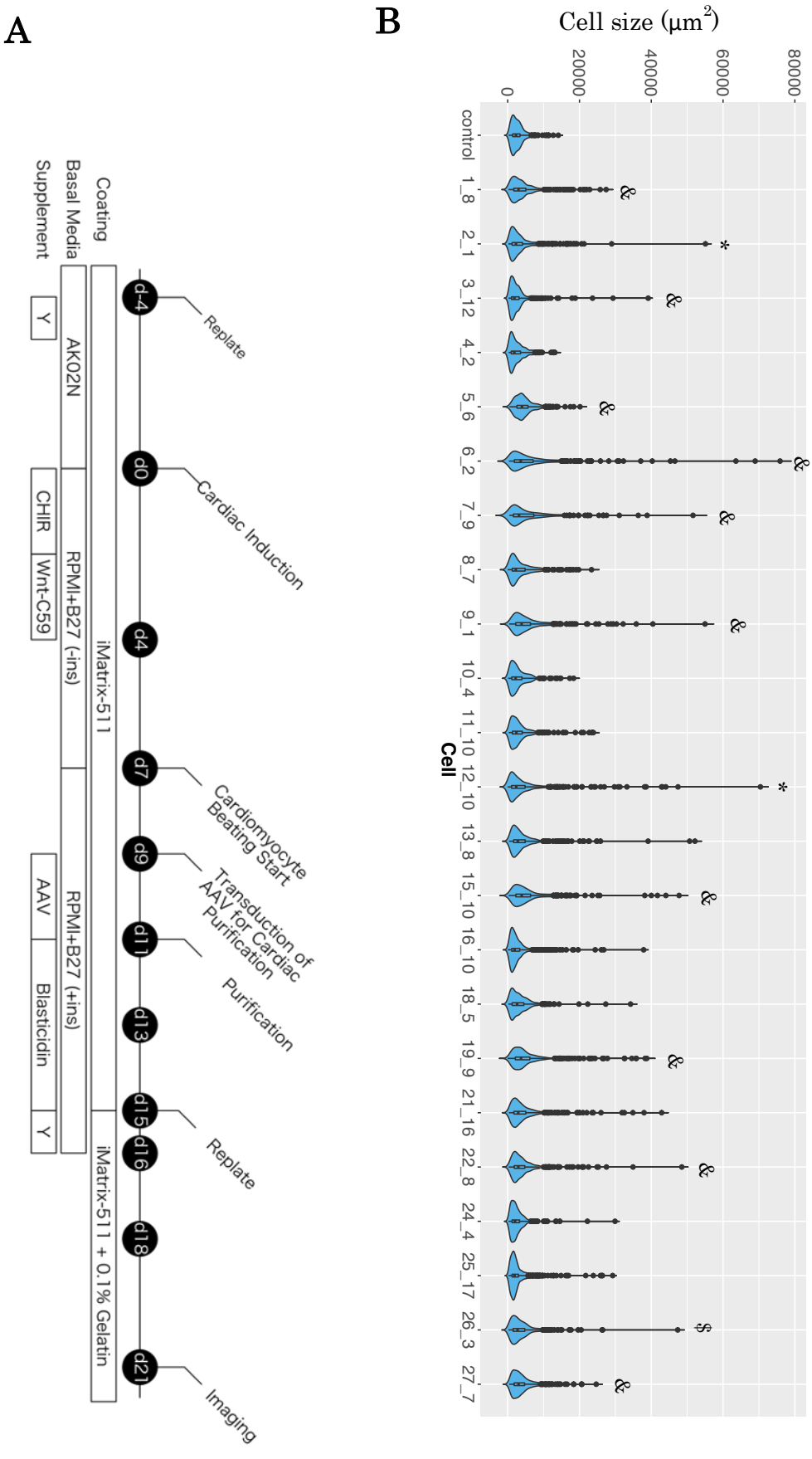
A
Coating
Basal Media
Supplement
iMatrix-511
AK02N
RPMI+B27 (-ins)
RPMI+B27 (+ins)
iMatrix-511 + 0.1% Gelatin
Y
CHIR
Wnt-C59
AAV
Blasticidin
Y
d-4
d0
d4
d7
d9
d11
d13
d15
d16
d18
d21
Replate
Cardiac Induction
Cardiomyocyte Beating Start
Transduction of AAV for Cardiac Purification
Purification
Replate
Imaging
B
Cell size (μm2)
0
20000
40000
60000
80000
Cell
control
1_8
2_1
3_12
4_2
5_6
6_2
7_9
8_7
9_1
10_4
11_10
12_10
13_8
15_10
16_10
18_5
19_9
21_16
22_8
24_4
25_17
26_3
27_7

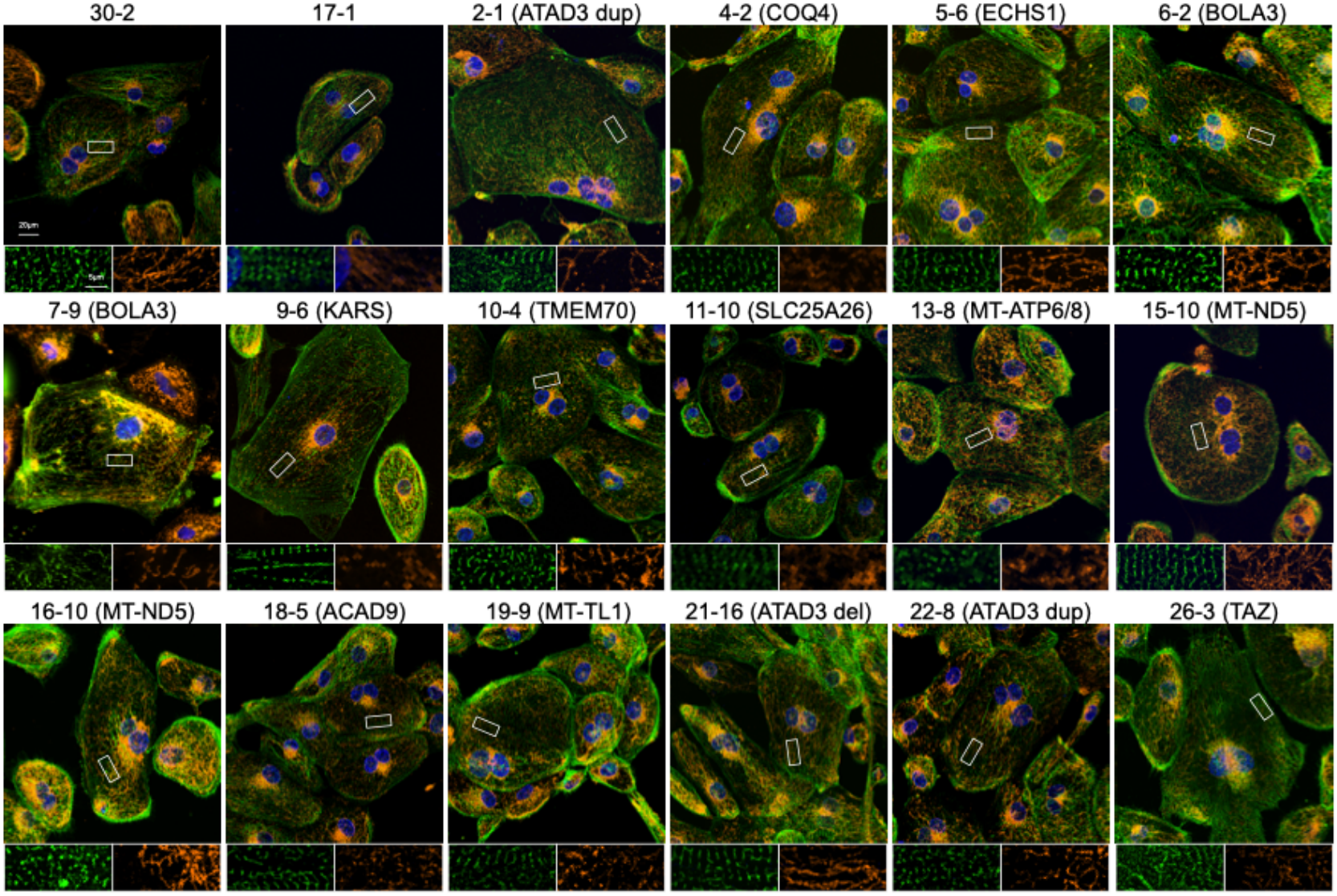
30-2
17-1
2-1 (ATAD3 dup)
4-2 (COQ4)
5-6 (ECHS1)
6-2 (BOLA3)
7-9 (BOLA3)
9-6 (KARS)
10-4 (TMEM70)
11-10 (SLC25A26)
13-8 (MT-ATP6/8)
15-10 (MT-ND5)
16-10 (MT-ND5)
18-5 (ACAD9)
19-9 (MT-TL1)
21-16 (ATAD3 del)
22-8 (ATAD3 dup)
26-3 (TAZ)
C
DAPI / TOM20 / alpha-actinin

Figure 20. MCM-iPSC-CMs exhibited significant hypertrophy.

A. Time-line of MCM-iPSC-CMs differentiation, purification, and imaging.

B. Cell morphology of MCM-iPSC-CMs vs. control (17_1). Wilcoxon rank sum test was used to compare the difference between the control and disease iPSC-CMs. *P<0.01, #P<0.001, $P<0.0001, &P<0.00001. n=315-574, from 3-4 different data sets. Lines 6-2 and 7-9 from 2 data sets.

C. Representative images of differentiated cardiomyocytes. Many of them displayed hypertrophic phenotypes compared to healthy control.

4.2.6) MCM-iPSC-CMs exhibited abnormal sarcomere formation

Mitochondria are distributed in lattice formation in between the sarcomeres to meet their high energy demands. Developmentally, mitochondria play an essential role in myofibrillogenesis, sarcomere assembly, and organization during cardiomyocyte maturation process[98]. That is evidenced by cardiac dysfunction and sarcomere disarray caused by decreased mitochondrial function. Moreover, mutations affecting the mitochondria such as Mfn1/2 (mitofusin 1 and 2) and Tfam (Transcription Factor A, Mitochondrial) have adverse effects on sarcomere organization[66]. In MCM patients, sarcomere abnormality is a known feature seen in histopathology[118,119]. As I showed in **Results 4.2.4**, MCM-iPSC-CMs displayed marked hypertrophy in accordance with MCM clinical presentation. Consequently, sarcomeres were expected to be abnormally structured as well.

Immunostaining of the sarcomeres (using α-actinin antibody, **Methods 2.10**) showed that MCM-iPSC-CMs exhibited marked sarcomere structural abnormalities when compared to control iPSC-CMs (**Figure 21A**). The sarcomere structure was subjectively analyzed by a colleague who did not have direct knowledge about the samples to avoid any bias (**Figure 21B**). MCM-iPSC-CMs cell lines that showed marked sarcomere disruption (disformed sarcomeres > 50%) were QRSL1 (1-8), ATAD3 (2-1), COQ4 (4-2), KARS (9-1, 9-3), TMEM70 (10-4), SLC25A26 (11-10), and TAZ (12-10, 26-3) mutations.

It was notable that hypertrophic cells showed marked sarcomere disruption, suggesting that treating the hypertrophy might have a positive impact on the sarcomere structure and hence the cell contractile function.

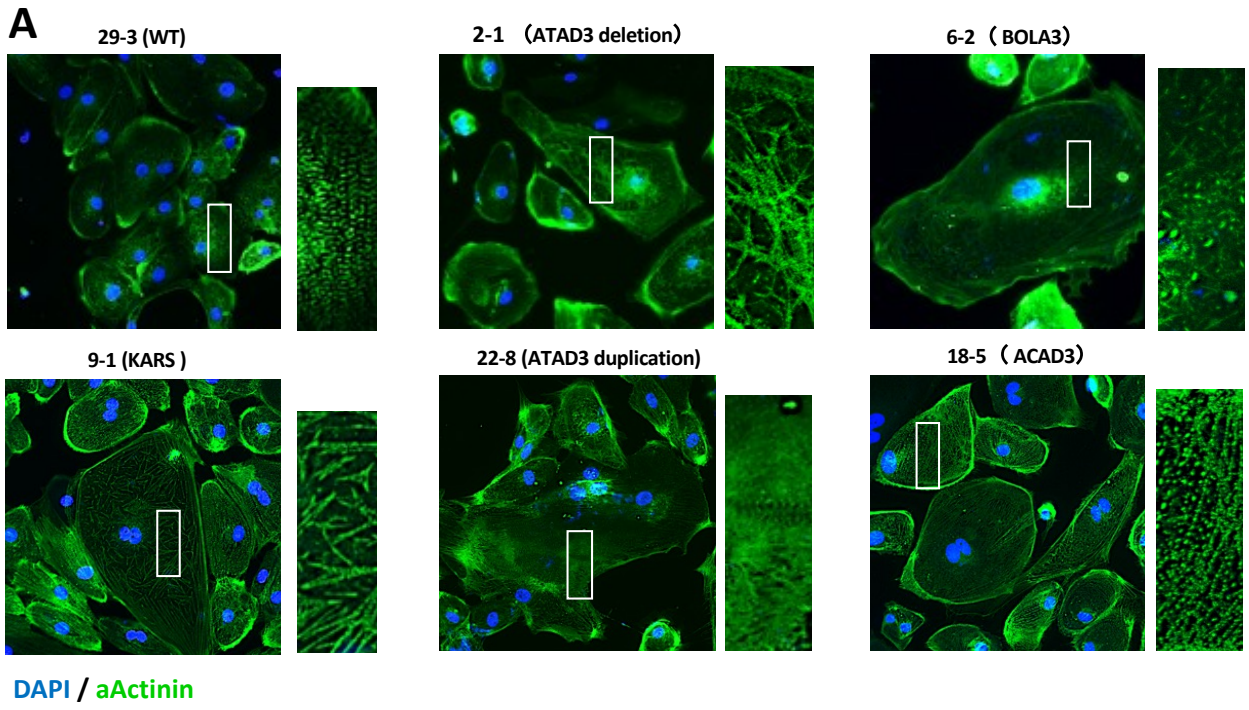

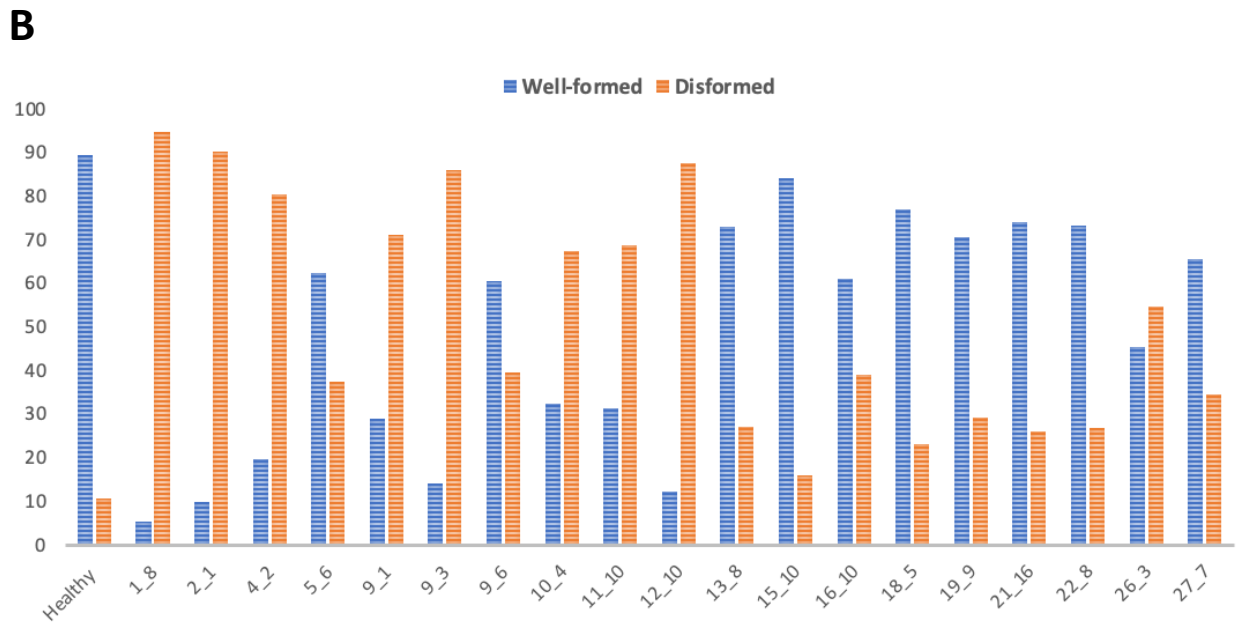

Figure 21. MCM-iPSC-CMs exhibited disrupted sarcomere structure.

A. Representative images of the abnormally shaped sarcomeres of hypertrophic MCM-iPSC-CMs

B. Percentage of well- and disformed sarcomeres in MCM-iPSC-CMs vs. healthy control. Data are from 3 data sets. Lines 3-12, 6-2, 7-9, 8-7, 24-4, 25-17, 26-3 are incomplete.

4.2.7) MCM-iPSC-CMs showed abnormal mitochondrial morphology

The dynamic change of mitochondrial morphology occurs as a response to various physiological and pathological stimuli. They are regulated by the mitochondrial fusion proteins (MFN1/2 and optic atrophy 1) and the mitochondrial fission proteins (dynamin-related peptide 1 and mitochondrial fission protein 1)[120]. Structural abnormalities in mitochondria are indicative of impaired mitochondrial dynamics (fusion and fission processes) and have been implicated in various biological processes in relation to the heart including cardiac development, the response to ischemia-reperfusion injury, heart failure, apoptosis, and autophagy.

Abnormally shaped mitochondria are a distinctive hallmark of MCM. In which mitochondrial structural abnormalities disrupt their normal functions such as energy production and Ca^{2+} handling within cardiac cells, ultimately compromising the heart's contractile function[121,3,7].

Representative mitochondrial structure images of MCM-iPSC-CMs are in **Figure 22**. Various abnormalities in mitochondrial morphology were seen, such as thickened, thinned, and peripheral mitochondrial location. However, I am working to devise a more comprehensive method to evaluate the degree of mitochondrial structural disturbance.

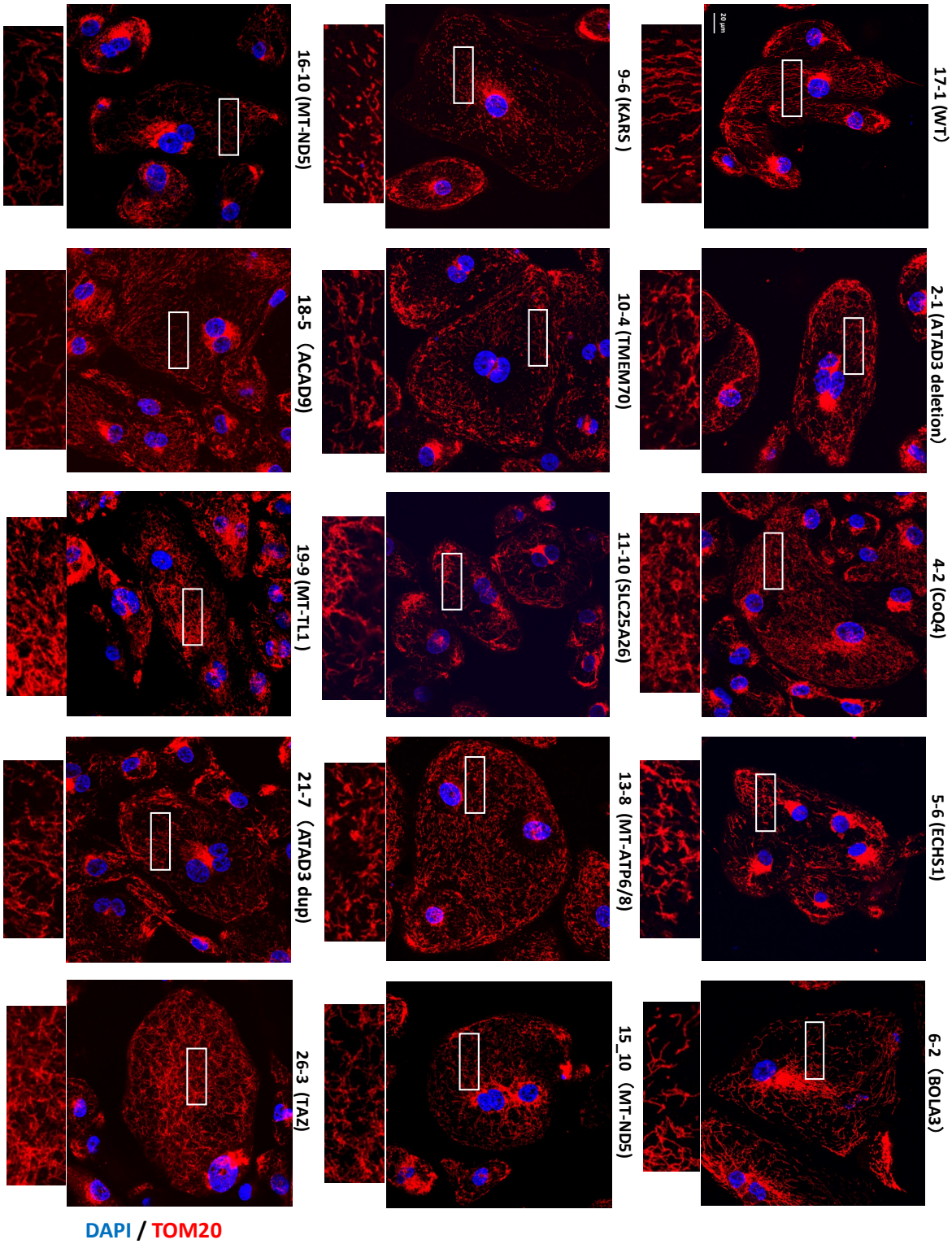

Figure 22. Representative images of MCM-iPSC-CMs mitochondrial structure.

Various abnormal mitochondrial morphological characteristics and location are seen.

4.2.8) MCM-iPSC-CMs showed abnormal Ca^{2+} handling

The cardiac muscle contractile function heavily relies on the normal Ca^{2+} handling function of the cell, which in turn depends on normal mitochondrial function. SERCA, sarcoplasmic/endoplasmic reticulum Ca^{2+}-ATPase, which regulates intracellular Ca^{2+} levels by uptalking cytosolic Ca^{2+} back into the SR lumen, is one of the major ATP consumers in the body[122]. Intracellular Ca^{2+} is the main regulator of the excitation-contraction coupling, the process by which action potential evokes cardiomyocyte contraction[123]. Clinically, MCM patients present with compromised contractile and conductive functions. Thus, MCM-related gene mutations are expected to exert similar effects *in vitro*[124].

In this study, I explored the impact of specific mitochondrial mutations associated with MCM-iPSC-CMs. To assess Ca^{2+} handling in MCM-iPSC-CMs, I used the intracellular Ca^{2+} -sensitive dye, Calbryte 520-AM, to visualize the intracellular Ca^{2+} transients of electrically stimulated cells (detailed steps in **Methods 3.12**).

Ca^{2+} imaging results showed various Ca^{2+} transients in response to electrical stimulation of MCM-iPSC-CMs. Cell lines that had synchronized responses comparable to control lines, at least in some cells, were ATAD3 (2-1, 21-7, 22-8), TOP3A (3-12), ECHS1 (5-6), TMEM70 (10-4), SLC25A26 (11-10), TAZ (12-7, 26-3), MT-ND5 (15-10), ACAD9 (18-5, 25-17), and MT-TL1 (19-9, 27-7) mutations. Representative Ca^{2+} transients are in **Figure 23**.

The remaining lines displayed an abnormal, desynchronized, or complete absence of intracellular Ca^{2+} transients in response to electrical stimulation. It is of note that hypertrophic cells had weaker and/or absent Ca^{2+} transients.

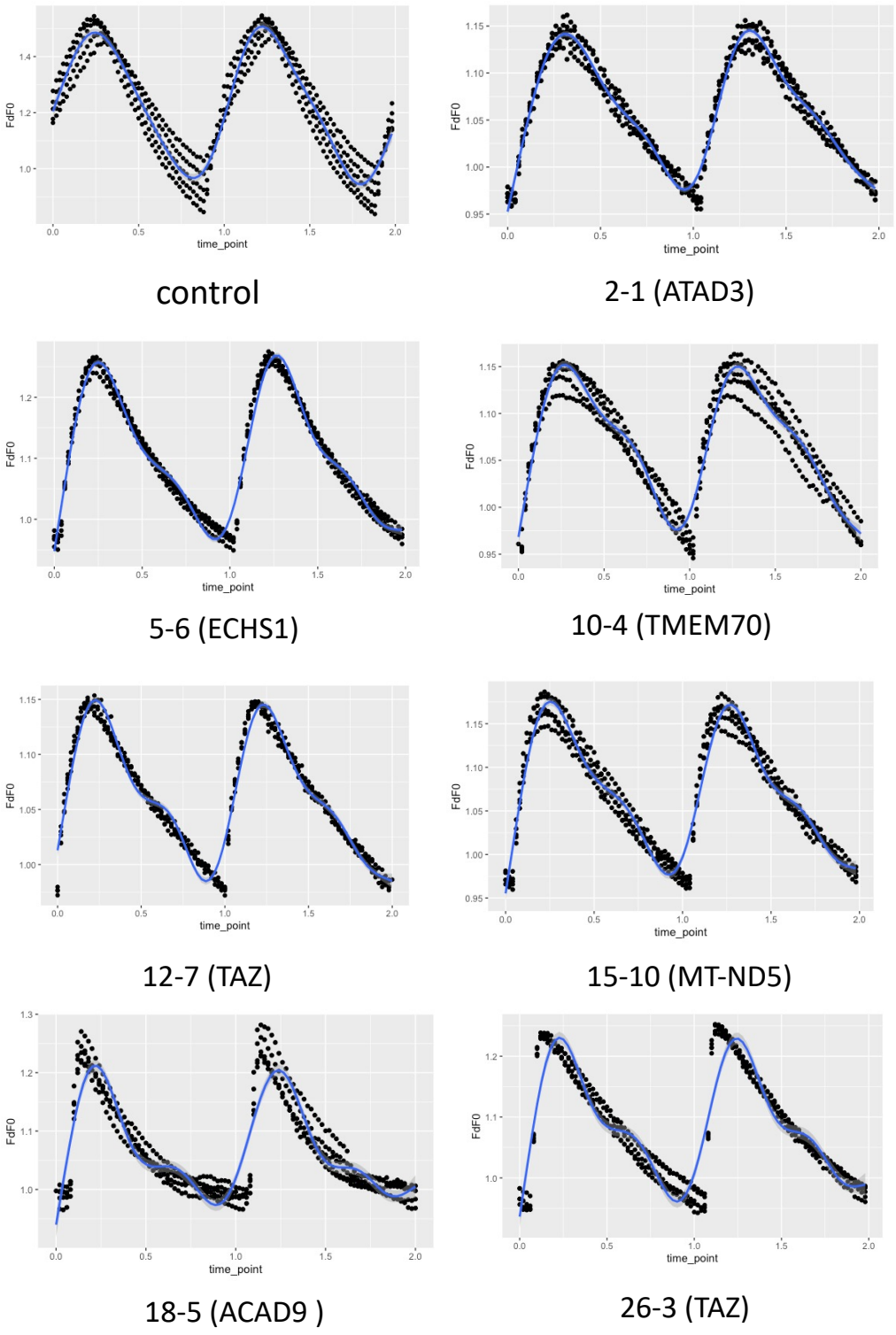

Figure 23. Representative averaged profiles of cytosolic Ca^{2+} transients of MCM-iPSC-CMs.

Cells were evoked by electrical field stimulation at 1 Hz.

4.3) Discussion

MCM is a dangerous component of mitochondrial diseases, raising the fatality by 40%. With the rise of iPSC technology, individualized platforms to study and treat MCM are available. In this research, I established the largest MCM-iPSC library reflecting various gene mutations that cause MCM. Differentiated MCM-iPSC-CMs exhibit a variety of morphological and functional disturbances, as seen in MCM.

First, I established patient-specific MCM-iPSC lines. However, there was a significant observation of reduced cell growth along with increased production of ROS in MCM-iPSCs compared to control iPSCs. These findings suggested a crucial role of healthy mitochondrial function for iPSC maintenance and cell cycle progression, which goes along with the previous reports about the importance of mitochondria for stem cell self-renewal[125,126]. Mitochondria exist as an elongated and filamentous network, densely packed with cristae. However, in stem cells, mitochondria are small and rounded, with low numbers of swollen cristae. Therefore, stem cell mitochondria have a lower respiratory capacity and low ROS levels[127]. ROS levels have a marked impact on stem cell proliferation capacity[128]. Low ROS levels are found in self-renewing stem cells[129]. There is a negative correlation between the ROS concentration and pluripotency markers' expression levels. Further, a high concentration of ROS (>150 μM) stimulated apoptotic changes in ESCs[130]. Despite that, further exploration of gene markers associated with pluripotency, differentiation, proliferation, and ROS response in my MCM-iPSCs revealed that reduced proliferation did not significantly impact marker expression.

Next, I proceeded to differentiate these MCM-iPSCs into cardiomyocytes, and the results indicated that MCM-iPSCs can differentiate into cardiomyocytes comparable to control iPSCs. This finding is crucial as it shows that the expected mitochondrial dysfunction of MCM-iPSCs did not inherently impede their differentiation into functional cardiomyocytes. Thus, MCM-iPSC-CMs can be used for *in vitro* studies of MCM disease.

To examine whether MCM-iPSC-CMs reflect the disease state of MCM, I first examined mitochondrial ATP and ROS generation. There was a marked variation of results among different MCM-iPSC-CM lines. This can be explained by the low maturation stage of MCM-iPSC-CMs, at which not all MCM-related genes are expressed in levels enough to compromise the mitochondrial function. Similar variation was observed regarding cell size, sarcomere structure, and Ca^{2+} transients. A summary of the observed phenotypes is in **Table 15**.

Table 15. Summary of the observed morphological and functional changes of MCM-iPSC-CMs

Abbreviations: sync, synchronized; N/C, no change.

Pt	Gene	Pt phenotype	Hypertrophy	Sarcomere	Ca^{2+} Transients
1	QRSL1	nuclear	hypertrophic	disformed	Not sync
2, 21, 22	ATAD3	nuclear	2 and 22 are hypertrophic	2 is disformed	Sync
3	TOP3A	nuclear	small	incomplete	Not sync
4	COQ4	nuclear	N/C	well-formed	Not sync
5	ECHS1	nuclear	hypertrophic	well-formed	Sync
6, 7, 8, 24	BOLA3	nuclear	6 and 7 are hypertrophic	Not complete	Not sync
9	KARS	nuclear	hypertrophic	disformed	Not sync
10	TMEM70	nuclear	N/C	disformed	Sync
11	SLC25A 26	nuclear	N/C	disformed	Sync
12, 26	TAZ	nuclear	hypertrophic	disformed	Sync
13	MT-ATP6/8	mitochondrial	N/C	well-formed	Not sync
15, 16	MT-ND5	mitochondrial	15 is hypertrophic	well-formed	Sync
18, 25	ACAD9	nuclear	N/C	18 is well-formed	Sync
19, 27	MT-TL1	mitochondrial	hypertrophic	well-formed	Sync

Overall, many lines exhibited hypertrophy sarcomere structural abnormalities. Functionally, a few had abnormal Ca^{2+} handling properties. These findings align with the clinical presentation of MCM patients and highlight the crucial role of mitochondria in maintaining cardiac sarcomere integrity and contractile functions. Mitochondrial dysfunction decreases the high energy levels required to fuel the sarcomere contraction process. Moreover, it often leads to increased production of ROS, causing oxidative stress, which can directly damage sarcomeric proteins, including actin and myosin, leading to structural abnormalities and contractile dysfunction within the sarcomere[131,132,133]. Another crucial role of mitochondria is to regulate intracellular Ca^{2+} levels, which is crucial for sarcomere contraction and relaxation[134]. Dysfunctional mitochondria can disrupt Ca^{2+} homeostasis, leading to abnormal Ca^{2+} handling within the sarcomere. It is reported that increased oxidative stress decreases the activity of SERCA[122]. This alteration of Ca^{2+} dynamics results in impaired contractility and develop cardiomyopathies[134], including cardiac hypertrophy.

When examining different gene mutations represented in this MCM-iPSC-CMs cohort, mutation-related phenotype differences arise. However, the immaturity of MCM-iPSC-CMs, along with the large amounts of antioxidants present in the culture medium, may be the reason why some lines did not recapture MCM disease phenotype. I will attempt to optimize both aspects by increasing the maturity of MCM-iPSC-CMs and eliminating antioxidants from the culture medium, respectively.

In QRSL1, BOLA3, and KARS mutations, cell hypertrophy was accompanied by disturbed Ca^{2+} handling in a state similar to the disease phenotype[135,136,137,138,139]. Hypertrophy with reserved Ca^{2+} handling was exhibited by ATAD3, TAZ, MT-ND5, and MT-TL1 mutations. TOP3A mutated cells showed a unique finding of cells smaller than the control. Compromised Ca^{2+} handling without hypertrophy was seen in COQ4 and MT-ATP6/8 mutations.

In conclusion, this study generated the largest cohort of MCM-iPSC-CMs. Results show that mitochondrial dysfunction of MCM-iPSC-CMs affected cell size, sarcomere integrity, mitochondrial morphology, and calcium handling properties. Therefore, I established MCM-iPSC-CMs disease models that reflect MCM disease phenotype to some extent. Improvements in cell maturation state and culture medium are expected to enhance MCM disease modeling. These models will provide a platform to study each mutation in depth to better understand its pathophysiology and develop more targeted treatment options. Further, they will be more sensitive tools for drug screening and toxicity assessment.

Chapter 5
Overall Discussion and Conclusion

Discussion

Cardiac involvement of mitochondrial disease, MCM, is a serious condition that significantly increases the death rate. So far, there is no treatment for MCM. With the rapid progression of cardiac differentiation techniques, iPSC-CMs became appealing, patient-specific platforms for disease modeling, drug development, and toxicity screening of diseases like MCM. Here, I aimed to establish MCM-iPSC-CM disease models using fibroblasts from MCM patients.

The use of iPSC-CMs, however, is hindered by the lack of suitable methods for purification and contractile function analysis. For purification, conventional methods that require knock-in are time-consuming when used for many cell lines. The same applies to knock-in fluorescent sarcomere reporter lines. With the rapidly developing AAV vectors, an alternative method to deliver antibiotic resistance and fluorescent sarcomere proteins is possible. An AAV serotype is chosen to better suit cardiomyocytes in vitro (usually AAV6) and a cardiac-specific promoter is inserted to ensure selective expression.

Thus, I developed an AAV-based antibiotic selection method. I was able to successfully enrich PSC-CMs up to 92%, which is high enough for disease modeling studies. For sarcomere shortening measurement, I established AAV-based fluorescent-tagged Z-line proteins that can be used for live-imaging and sarcomere shortening analysis (TCAP-GFP, TCAP1-80-GFP, and PDLIM3-GFP).

The AAV-based purification and sarcomere function evaluation techniques generated in this study present innovative tools for advancing research using PSC-CMs. These tools can be refined to study more cardiac functions, bringing us closer to realizing the full potential of PSC-CMs in both research and clinical contexts. Further, these adaptable techniques could also be modified and extended to other PSC models, promising broader insights across diverse fields of research.

After generating methods suitable for PSC-CM purification and contractile function analysis, I moved to produce patient-specific MCM-iPSC. MCM-iPSCs lines had reduced proliferation along with increased ROS levels compared to control iPSCs, which can be explained by the importance of healthy mitochondrial function in maintaining the cell cycle and self-renewal of iPSCs. However, the expression of gene markers associated with pluripotency, differentiation, proliferation, and ROS response was not significantly affected. The decrease in MCM-iPSCs cell number can

be utilized in the context of drug screening. Drugs that recover the cell number may have beneficial effects on mitochondrial function and vice versa.

Next, I differentiated MCM-iPSCs into MCM-iPSC-CMs. To examine whether the latter reflects MCM disease phenotype, I examined mitochondrial ATP and ROS generation, cell size, sarcomere structure, and Ca2+ transients. There was a marked variation of results among different MCM-iPSC-CM lines. This can be explained by the low maturation stage of MCM-iPSC-CMs, at which not all MCM-related genes are expressed in levels enough to compromise the mitochondrial function and cause the specific phenotype.

When analyzing mutation-specific phenotypes, commonalities arise. Cell hypertrophy, alone or accompanied by Ca2+ handling disturbance, is the major phenotype observed. Hypertrophic cells usually have disrupted sarcomere structure, hence impairing their contractile functions. Thus, investigating and targeting the pathways by which mitochondrial dysfunction affects sarcomere integrity may be of use for MCM patients.

An increased cell size may occur in cases of cellular senescence, which mitochondrial dysfunction may result in. As we have not examined the possible senescence markers, such as ß-galactosidase activity and expressions of cyclin-dependent kinase inhibitors, there is no definitive answer as to whether it was hypertrophy or senescence. However, the morphological study performed at the early stage (day 21) and sarcomere disarray in the MCM-iPSC-CMs decreases the possibility of cellular senescence but implicates the MCM-iPSC-CMs displayed hypertrophy.

Mitochondrial heteroplasmy level is the percentage of mitochondria that harbors the mutation. A certain threshold value must be reached to cause disease, the severity of which is determined by the heteroplasmy level. Among the MCM-iPSC cohort in this study, only five lines have mutations in the mitochondrial DNA (#13, 15, 16, 19, 27). #13 was homoplasmy (100% mutation), and others were heteroplasmy. Among the lines we established, we primarily used the highest heteroplasmy lines (#15-10, 81.3%; #16-10, 82.0%; #19-9, 92.6%; #27-7, 91.7%) for phenotype studies. To further validate the findings are due to mitochondrial dysfunction, I plan to examine their heteroplasmy rates in MCM-iPSC-CMs.

Nevertheless, better outcomes may result from elaborating the mechanisms by which MCM-related genes disturb mitochondrial function and directly addressing them. This approach, however, requires MCM-iPSC-CMs that reflect the mitochondrial functional disturbance as seen in MCM patients. To acheive that, more mature MCM-iPSC-CMs are needed. Another option is via gene therapy to deliver functional genes into cardiomyocytes. However, it comes with a few setbacks, among which heteroplasmy and intramitochondrial delivery in the case of mDNA gene

mutation are major concerns.

Conclusion

In this study, I established the largest cohort of MCM-iPSC-CMs with various genetic mutations. Some of the MCM-iPSC-CMs recapitulated the disease phenotype of mitochondrial dysfunction, cell hypertrophy, sarcomere structural abnormality, and Ca^{2+} handling disruption. These MCM-iPSC-CMs disease models enhance our understanding of the specific cellular consequences of MCM, laying the groundwork for future research and potential therapeutic strategies. Further, it provides a much-needed platform for drug screening and development. However, further improvement to better recapitulate disease phenotype are required.

Moreover, to achieve rapid and efficient purification and sarcomere function analysis with the large cohort of MCM-iPSC-CMs, I developed AAV-based modifications of PSC-CMs to acquire drug resistance or sarcomere visualization.

Acknowledgments

To Allah, first and foremost. To my husband, my cornerstone, journey partner, and support system. To my boys, the greatest gifts from Allah. To my mom, my first teacher and role model. To my dad, my greatest supporter. To my sisters, my beautiful cheering squad.

I also gratefully acknowledge Guidance, technical support, and helpful discussions from all members in Regenerative Medicine including Prof. Yutaka Hanazono, Prof. Hideki Uosaki, Takeshi Tokuyama, Nawin Chanthra, Fuad Gandhi-Torizal, Tatsuya Anzai, Kumiko A Iwabuchi, Tomoyuki Abe, Hiromasa Hara, Rie Ishihara.

Funding support

This work was supported by Tokyo Biomedical Research Foundation, Scholarship Grant for Living Expenses of Foreign Nationals in Japan from the Ichiro Kanehara Foundation and the Otsuka Toshimi Foundation Scholarship.

References

1. Mazzaccara C, Mirra B, Barretta F, et al. Molecular Epidemiology of Mitochondrial Cardiomyopathy: A Search Among Mitochondrial and Nuclear Genes. *IJMS*. 2021;22(11):5742. doi:10.3390/ijms22115742

2. Stefano GB, Kream RM. Mitochondrial DNA heteroplasmy in human health and disease. *Biomed Rep*. 2016;4(3):259-262. doi:10.3892/br.2016.590

3. Meyers DE, Basha HI, Koenig MK. Mitochondrial cardiomyopathy: pathophysiology, diagnosis, and management. *Tex Heart Inst J*. 2013;40(4):385-394.

4. Tokuyama T, Ahmed RE, Chanthra N, Anzai T, Uosaki H. Disease Modeling of Mitochondrial Cardiomyopathy Using Patient-Specific Induced Pluripotent Stem Cells. *Biology*. 2021;10(10):981. doi:10.3390/biology10100981

5. Wahbi K, Bougouin W, Béhin A, et al. Long-term cardiac prognosis and risk stratification in 260 adults presenting with mitochondrial diseases. *Eur Heart J*. 2015;36(42):2886-2893. doi:10.1093/eurheartj/ehv307

6. Scaglia F, Towbin JA, Craigen WJ, et al. Clinical Spectrum, Morbidity, and Mortality in 113 Pediatric Patients With Mitochondrial Disease. *Pediatrics*. 2004;114(4):925-931. doi:10.1542/peds.2004-0718

7. El-Hattab AW, Scaglia F. Mitochondrial Cardiomyopathies. *Front Cardiovasc Med*. 2016;3. doi:10.3389/fcvm.2016.00025

8. Sala L, Gnecchi M, Schwartz PJ. Long QT Syndrome Modelling with Cardiomyocytes Derived from Human-induced Pluripotent Stem Cells. *Arrhythm Electrophysiol Rev*. 2019;8(2):105-110. doi:10.15420/aer.2019.1.1

9. Ma D, Wei H, Lu J, et al. Generation of patient-specific induced pluripotent stem cell-derived cardiomyocytes as a cellular model of arrhythmogenic right ventricular cardiomyopathy. *European Heart Journal*. 2013;34(15):1122-1133. doi:10.1093/eurheartj/ehs226

10. Lan F, Lee AS, Liang P, et al. Abnormal Calcium Handling Properties Underlie Familial Hypertrophic Cardiomyopathy Pathology in Patient-Specific Induced

Pluripotent Stem Cells. *Cell Stem Cell*. 2013;12(1):101-113. doi:10.1016/j.stem.2012.10.010

11. Sun N, Yazawa M, Liu J, et al. Patient-Specific Induced Pluripotent Stem Cells as a Model for Familial Dilated Cardiomyopathy. *Sci Transl Med*. 2012;4(130). doi:10.1126/scitranslmed.3003552

12. Grandi E, Dobrev D. Atrial fibrillation in a dish: insights into atrial arrhythmogenesis from induced pluripotent stem cell-derived cardiomyocytes. *Cardiovasc Res*. 2020;116(6):1089-1091. doi:10.1093/cvr/cvz342

13. Ban K, Bae S, Yoon YS. Current Strategies and Challenges for Purification of Cardiomyocytes Derived from Human Pluripotent Stem Cells. *Theranostics*. 2017;7(7):2067-2077. doi:10.7150/thno.19427

14. Chanthra N, Abe T, Miyamoto M, et al. A Novel Fluorescent Reporter System Identifies Laminin-511/521 as Potent Regulators of Cardiomyocyte Maturation. *Sci Rep*. 2020;10(1):4249. doi:10.1038/s41598-020-61163-3

15. Ahmed RE, Chanthra N, Anzai T, et al. Sarcomere Shortening of Pluripotent Stem Cell-Derived Cardiomyocytes using Fluorescent-Tagged Sarcomere Proteins. *JoVE*. 2021;(169):62129. doi:10.3791/62129

16. Muto A, Ohkura M, Abe G, Nakai J, Kawakami K. Real-Time Visualization of Neuronal Activity during Perception. *Current Biology*. 2013;23(4):307-311. doi:10.1016/j.cub.2012.12.040

17. Evans MJ, Kaufman MH. Establishment in culture of pluripotential cells from mouse embryos. *Nature*. 1981;292(5819):154-156. doi:10.1038/292154a0

18. Charitos IA, Ballini A, Cantore S, et al. Stem Cells: A Historical Review about Biological, Religious, and Ethical Issues. *Stem Cells Int*. 2021;2021:9978837. doi:10.1155/2021/9978837

19. Takahashi K, Yamanaka S. Induction of Pluripotent Stem Cells from Mouse Embryonic and Adult Fibroblast Cultures by Defined Factors. *Cell*. 2006;126(4):663-676. doi:10.1016/j.cell.2006.07.024

20. Takahashi K, Tanabe K, Ohnuki M, et al. Induction of Pluripotent Stem Cells from Adult Human Fibroblasts by Defined Factors. *Cell*. 2007;131(5):861-872. doi:10.1016/j.cell.2007.11.019

21. Yu J, Vodyanik MA, Smuga-Otto K, et al. Induced Pluripotent Stem Cell Lines Derived from Human Somatic Cells. *Science*. 2007;318(5858):1917-1920. doi:10.1126/science.1151526

22. Ye L, Swingen C, Zhang J. Induced pluripotent stem cells and their potential for basic and clinical sciences. *Curr Cardiol Rev*. 2013;9(1):63-72. doi:10.2174/157340313805076278

23. Romito A, Cobellis G. Pluripotent Stem Cells: Current Understanding and Future Directions. *Stem Cells Int*. 2016;2016:9451492. doi:10.1155/2016/9451492

24. Yamanaka S, Li J, Kania G, et al. Pluripotency of embryonic stem cells. *Cell Tissue Res*. 2008;331(1):5-22. doi:10.1007/s00441-007-0520-5

25. Mensah GA, Roth GA, Fuster V. The Global Burden of Cardiovascular Diseases and Risk Factors. *Journal of the American College of Cardiology*. 2019;74(20):2529-2532. doi:10.1016/j.jacc.2019.10.009

26. Mummery CL, Zhang J, Ng ES, Elliott DA, Elefanty AG, Kamp TJ. Differentiation of human embryonic stem cells and induced pluripotent stem cells to cardiomyocytes: a methods overview. *Circ Res*. 2012;111(3):344-358. doi:10.1161/CIRCRESAHA.110.227512

27. Rajala K, Pekkanen-Mattila M, Aalto-Setälä K. Cardiac Differentiation of Pluripotent Stem Cells. *Stem Cells International*. 2011;2011:1-12. doi:10.4061/2011/383709

28. Lyra-Leite DM, Gutiérrez-Gutiérrez Ó, Wang M, Zhou Y, Cyganek L, Burridge PW. A review of protocols for human iPSC culture, cardiac differentiation, subtype-specification, maturation, and direct reprogramming. *STAR Protoc*. 2022;3(3):101560. doi:10.1016/j.xpro.2022.101560

29. Batalov I, Feinberg AW. Differentiation of Cardiomyocytes from Human Pluripotent Stem Cells Using Monolayer Culture. *Biomark Insights*. 2015;10(Suppl 1):71-76. doi:10.4137/BMI.S20050

30. Gao Y, Pu J. Differentiation and Application of Human Pluripotent Stem Cells Derived Cardiovascular Cells for Treatment of Heart Diseases: Promises and Challenges. *Front Cell Dev Biol*. 2021;9:658088. doi:10.3389/fcell.2021.658088

31. Ma J, Guo L, Fiene SJ, et al. High purity human-induced pluripotent stem cell-derived cardiomyocytes: electrophysiological properties of action potentials and ionic currents. *Am J Physiol Heart Circ Physiol*. 2011;301(5):H2006-2017. doi:10.1152/ajpheart.00694.2011

32. Dubois NC, Craft AM, Sharma P, et al. SIRPA is a specific cell-surface marker for isolating cardiomyocytes derived from human pluripotent stem cells. *Nat Biotechnol*. 2011;29(11):1011-1018. doi:10.1038/nbt.2005

33. Uosaki H, Fukushima H, Takeuchi A, et al. Efficient and scalable purification of cardiomyocytes from human embryonic and induced pluripotent stem cells by VCAM1 surface expression. *PLoS One*. 2011;6(8):e23657. doi:10.1371/journal.pone.0023657

34. Lin B, Kim J, Li Y, et al. High-purity enrichment of functional cardiovascular cells from human iPS cells. *Cardiovasc Res*. 2012;95(3):327-335. doi:10.1093/cvr/cvs185

35. Hattori F, Chen H, Yamashita H, et al. Nongenetic method for purifying stem cell–derived cardiomyocytes. *Nat Methods*. 2010;7(1):61-66. doi:10.1038/nmeth.1403

36. Tohyama S, Hattori F, Sano M, et al. Distinct Metabolic Flow Enables Large-Scale Purification of Mouse and Human Pluripotent Stem Cell-Derived Cardiomyocytes. *Cell Stem Cell*. 2013;12(1):127-137. doi:10.1016/j.stem.2012.09.013

37. Tohyama S, Fujita J, Hishiki T, et al. Glutamine Oxidation Is Indispensable for Survival of Human Pluripotent Stem Cells. *Cell Metabolism*. 2016;23(4):663-674. doi:10.1016/j.cmet.2016.03.001

38. Ban K, Wile B, Kim S, et al. Purification of cardiomyocytes from differentiating pluripotent stem cells using molecular beacons that target cardiomyocyte-specific mRNA. *Circulation*. 2013;128(17):1897-1909. doi:10.1161/CIRCULATIONAHA.113.004228

39. Miki K, Endo K, Takahashi S, et al. Efficient Detection and Purification of Cell Populations Using Synthetic MicroRNA Switches. *Cell Stem Cell*. 2015;16(6):699-711. doi:10.1016/j.stem.2015.04.005

40. Laflamme MA, Chen KY, Naumova AV, et al. Cardiomyocytes derived from human embryonic stem cells in pro-survival factors enhance function of infarcted rat hearts. *Nat Biotechnol*. 2007;25(9):1015-1024. doi:10.1038/nbt1327

41. Li X, Yu L, Li J, et al. On chip purification of hiPSC-derived cardiomyocytes using a fishnet-like microstructure. *Biofabrication*. 2016;8(3):035017. doi:10.1088/1758-5090/8/3/035017

42. Ahmed RE, Anzai T, Chanthra N, Uosaki H. A Brief Review of Current Maturation Methods for Human Induced Pluripotent Stem Cells-Derived Cardiomyocytes. *Front Cell Dev Biol*. 2020;8:178. doi:10.3389/fcell.2020.00178

43. Karbassi E, Fenix A, Marchiano S, et al. Cardiomyocyte maturation: advances in knowledge and implications for regenerative medicine. *Nat Rev Cardiol*. 2020;17(6):341-359. doi:10.1038/s41569-019-0331-x

44. Kamakura T, Makiyama T, Sasaki K, et al. Ultrastructural Maturation of Human-Induced Pluripotent Stem Cell-Derived Cardiomyocytes in a Long-Term Culture. *Circ J*. 2013;77(5):1307-1314. doi:10.1253/circj.CJ-12-0987

45. Chong JJH, Yang X, Don CW, et al. Human embryonic-stem-cell-derived cardiomyocytes regenerate non-human primate hearts. *Nature*. 2014;510(7504):273-277. doi:10.1038/nature13233

46. Shiba Y, Gomibuchi T, Seto T, et al. Allogeneic transplantation of iPS cell-derived cardiomyocytes regenerates primate hearts. *Nature*. 2016;538(7625):388-391. doi:10.1038/nature19815

47. Yamanaka S. Pluripotent Stem Cell-Based Cell Therapy—Promise and Challenges. *Cell Stem Cell*. 2020;27(4):523-531. doi:10.1016/j.stem.2020.09.014

48. Volpato V, Webber C. Addressing variability in iPSC-derived models of human disease: guidelines to promote reproducibility. *Dis Model Mech*. 2020;13(1):dmm042317. doi:10.1242/dmm.042317

49. McCarty DM. Self-complementary AAV Vectors; Advances and Applications. *Molecular Therapy*. 2008;16(10):1648-1656. doi:10.1038/mt.2008.171

50. Issa SS, Shaimardanova AA, Solovyeva VV, Rizvanov AA. Various AAV Serotypes and Their Applications in Gene Therapy: An Overview. *Cells*. 2023;12(5):785. doi:10.3390/cells12050785

51. Boutin S, Monteilhet V, Veron P, et al. Prevalence of Serum IgG and Neutralizing Factors Against Adeno-Associated Virus (AAV) Types 1, 2, 5, 6, 8, and 9 in the Healthy Population: Implications for Gene Therapy Using AAV Vectors. *Human Gene Therapy*. 2010;21(6):704-712. doi:10.1089/hum.2009.182

52. Colella P, Ronzitti G, Mingozzi F. Emerging Issues in AAV-Mediated In Vivo Gene Therapy. *Molecular Therapy - Methods & Clinical Development*. 2018;8:87-104. doi:10.1016/j.omtm.2017.11.007

53. Brown N, Song L, Kollu NR, Hirsch ML. Adeno-Associated Virus Vectors and Stem Cells: Friends or Foes? *Hum Gene Ther*. 2017;28(6):450-463. doi:10.1089/hum.2017.038

54. Grieger JC, Samulski RJ. Adeno-Associated Virus Vectorology, Manufacturing, and Clinical Applications. In: *Methods in Enzymology*. Vol 507. Elsevier; 2012:229-254. doi:10.1016/B978-0-12-386509-0.00012-0

55. Au HKE, Isalan M, Mielcarek M. Gene Therapy Advances: A Meta-Analysis of AAV Usage in Clinical Settings. *Front Med*. 2022;8:809118. doi:10.3389/fmed.2021.809118

56. Kuzmin DA, Shutova MV, Johnston NR, et al. The clinical landscape for AAV gene therapies. *Nat Rev Drug Discov*. 2021;20(3):173-174. doi:10.1038/d41573-021-00017-7

57. Haery L, Deverman BE, Matho KS, et al. Adeno-Associated Virus Technologies and Methods for Targeted Neuronal Manipulation. *Front Neuroanat*. 2019;13:93. doi:10.3389/fnana.2019.00093

58. Zingg B, Chou X lin, Zhang Z gang, et al. AAV-Mediated Anterograde Transsynaptic Tagging: Mapping Corticocollicular Input-Defined Neural Pathways for Defense Behaviors. *Neuron*. 2017;93(1):33-47. doi:10.1016/j.neuron.2016.11.045

59. Ambrosi CM, Sadananda G, Han JL, Entcheva E. Adeno-Associated Virus Mediated Gene Delivery: Implications for Scalable in vitro and in vivo Cardiac Optogenetic Models. *Front Physiol*. 2019;10:168. doi:10.3389/fphys.2019.00168

60. Kannan S, Kwon C. Regulation of cardiomyocyte maturation during critical perinatal window. *The Journal of Physiology*. 2020;598(14):2941-2956. doi:10.1113/JP276754

61. Lodola F, Morone D, Denegri M, et al. Adeno-associated virus-mediated CASQ2 delivery rescues phenotypic alterations in a patient-specific model of recessive catecholaminergic polymorphic ventricular tachycardia. *Cell Death Dis*. 2016;7(10):e2393-e2393. doi:10.1038/cddis.2016.304

62. Katz MG, Fargnoli AS, Weber T, Hajjar RJ, Bridges CR. Use of Adeno-Associated Virus Vector for Cardiac Gene Delivery in Large-Animal Surgical Models of Heart Failure. *Human Gene Therapy Clinical Development*. 2017;28(3):157-164. doi:10.1089/humc.2017.070

63. Pacak CA, Byrne BJ. AAV Vectors for Cardiac Gene Transfer: Experimental Tools and Clinical Opportunities. *Molecular Therapy*. 2011;19(9):1582-1590. doi:10.1038/mt.2011.124

64. Riedl J, Crevenna AH, Kessenbrock K, et al. Lifeact: a versatile marker to visualize F-actin. *Nat Methods*. 2008;5(7):605-607. doi:10.1038/nmeth.1220

65. Ribeiro AJS, Ang YS, Fu JD, et al. Contractility of single cardiomyocytes differentiated from pluripotent stem cells depends on physiological shape and substrate stiffness. *Proc Natl Acad Sci USA*. 2015;112(41):12705-12710. doi:10.1073/pnas.1508073112

66. Ahmed RE, Tokuyama T, Anzai T, Chanthra N, Uosaki H. Sarcomere maturation: function acquisition, molecular mechanism, and interplay with other organelles. *Phil Trans R Soc B*. 2022;377(1864):20210325. doi:10.1098/rstb.2021.0325

67. Pyle WG, Solaro RJ. At the Crossroads of Myocardial Signaling: The Role of Z-Discs in Intracellular Signaling and Cardiac Function. *Circulation Research*. 2004;94(3):296-305. doi:10.1161/01.RES.0000116143.74830.A9

68. Tan Y, Xia F, Li L, et al. Novel Insights into the Molecular Features and Regulatory Mechanisms of Mitochondrial Dynamic Disorder in the Pathogenesis of Cardiovascular Disease. Cipak Gasparovic A, ed. *Oxidative Medicine and Cellular Longevity*. 2021;2021:1-11. doi:10.1155/2021/6669075

69. Poburko D, Santo-Domingo J, Demaurex N. Dynamic Regulation of the Mitochondrial Proton Gradient during Cytosolic Calcium Elevations. *Journal of Biological Chemistry*. 2011;286(13):11672-11684. doi:10.1074/jbc.M110.159962

70. Dunn J, Grider MH. Physiology, Adenosine Triphosphate. In: *StatPearls*. StatPearls Publishing; 2023. Accessed January 8, 2024. http://www.ncbi.nlm.nih.gov/books/NBK553175/

71. Kühlbrandt W. Structure and function of mitochondrial membrane protein complexes. *BMC Biol*. 2015;13(1):89. doi:10.1186/s12915-015-0201-x

72. DiMauro S, Schon EA. Mitochondrial Respiratory-Chain Diseases. *N Engl J Med*. 2003;348(26):2656-2668. doi:10.1056/NEJMra022567

73. Gorman GS, Chinnery PF, DiMauro S, et al. Mitochondrial diseases. *Nat Rev Dis Primers*. 2016;2(1):16080. doi:10.1038/nrdp.2016.80

74. Goldstein AC, Bhatia P, Vento JM. Mitochondrial disease in childhood: nuclear encoded. *Neurotherapeutics*. 2013;10(2):212-226. doi:10.1007/s13311-013-0185-6

75. Yang J, Zhang X, Kou M, et al. Mitochondrial cardiomyopathy and emerging therapeutics. *Translational Medicine of Aging*. 2023;7:98-108. doi:10.1016/j.tma.2023.10.002

76. Yang J, Chen S, Duan F, et al. Mitochondrial Cardiomyopathy: Molecular Epidemiology, Diagnosis, Models, and Therapeutic Management. *Cells*. 2022;11(21):3511. doi:10.3390/cells11213511

77. Russell L, Finck B, Kelly D. Mouse models of mitochondrial dysfunction and heart failure. *Journal of Molecular and Cellular Cardiology*. 2005;38(1):81-91. doi:10.1016/j.yjmcc.2004.10.010

78. Stewart JB. Current progress with mammalian models of mitochondrial DNA disease. *J of Inher Metab Disea*. 2021;44(2):325-342. doi:10.1002/jimd.12324

79. Denning C, Borgdorff V, Crutchley J, et al. Cardiomyocytes from human pluripotent stem cells: From laboratory curiosity to industrial biomedical platform. *Biochim Biophys Acta*. 2016;1863(7 Pt B):1728-1748. doi:10.1016/j.bbamcr.2015.10.014

80. Itzhaki I, Maizels L, Huber I, et al. Modeling of Catecholaminergic Polymorphic Ventricular Tachycardia With Patient-Specific Human-Induced Pluripotent Stem Cells. *Journal of the American College of Cardiology*. 2012;60(11):990-1000. doi:10.1016/j.jacc.2012.02.066

81. Shah D, Virtanen L, Prajapati C, et al. Modeling of LMNA-Related Dilated Cardiomyopathy Using Human Induced Pluripotent Stem Cells. *Cells*. 2019;8(6):594. doi:10.3390/cells8060594

82. Li S, Pan H, Tan C, et al. Mitochondrial Dysfunctions Contribute to Hypertrophic Cardiomyopathy in Patient iPSC-Derived Cardiomyocytes with MT-RNR2 Mutation. *Stem Cell Reports*. 2018;10(3):808-821. doi:10.1016/j.stemcr.2018.01.013

83. Sayed N, Liu C, Wu JC. Translation of Human-Induced Pluripotent Stem Cells: From Clinical Trial in a Dish to Precision Medicine. *J Am Coll Cardiol*. 2016;67(18):2161-2176. doi:10.1016/j.jacc.2016.01.083

84. Wu JC, Garg P, Yoshida Y, et al. Towards Precision Medicine With Human iPSCs for Cardiac Channelopathies. *Circ Res*. 2019;125(6):653-658. doi:10.1161/CIRCRESAHA.119.315209

85. Hoppel CL, Tandler B, Fujioka H, Riva A. Dynamic organization of mitochondria in human heart and in myocardial disease. *Int J Biochem Cell Biol*. 2009;41(10):1949-1956. doi:10.1016/j.biocel.2009.05.004

86. Graham BH, Waymire KG, Cottrell B, Trounce IA, MacGregor GR, Wallace DC. A mouse model for mitochondrial myopathy and cardiomyopathy resulting from a deficiency in the heart/muscle isoform of the adenine nucleotide translocator. *Nat Genet*. 1997;16(3):226-234. doi:10.1038/ng0797-226

87. Richman TR, Ermer JA, Davies SMK, et al. Mutation in MRPS34 compromises protein synthesis and causes mitochondrial dysfunction. *PLoS Genet*. 2015;11(3):e1005089. doi:10.1371/journal.pgen.1005089

88. Ke BX, Pepe S, Grubb DR, et al. Tissue-specific splicing of an *Ndufs6* gene-trap insertion generates a mitochondrial complex I deficiency-specific cardiomyopathy. *Proc Natl Acad Sci USA*. 2012;109(16):6165-6170. doi:10.1073/pnas.1113987109

89. Zhang D, Li Y, Heims-Waldron D, et al. Mitochondrial Cardiomyopathy Caused by Elevated Reactive Oxygen Species and Impaired Cardiomyocyte Proliferation. *Circ Res*. 2018;122(1):74-87. doi:10.1161/CIRCRESAHA.117.311349

90. Hansson A, Hance N, Dufour E, et al. A switch in metabolism precedes increased mitochondrial biogenesis in respiratory chain-deficient mouse hearts. *Proc Natl Acad Sci USA*. 2004;101(9):3136-3141. doi:10.1073/pnas.0308710100

91. Sayles NM, Southwell N, McAvoy K, et al. Mutant CHCHD10 causes an extensive metabolic rewiring that precedes OXPHOS dysfunction in a murine model of mitochondrial cardiomyopathy. *Cell Reports*. 2022;38(10):110475. doi:10.1016/j.celrep.2022.110475

92. Liu YT, Huang X, Nguyen D, et al. Loss of CHCHD2 and CHCHD10 activates OMA1 peptidase to disrupt mitochondrial cristae phenocopying patient mutations. *Human Molecular Genetics*. 2020;29(9):1547-1567. doi:10.1093/hmg/ddaa077

93. Puccio H, Simon D, Cossée M, et al. Mouse models for Friedreich ataxia exhibit cardiomyopathy, sensory nerve defect and Fe-S enzyme deficiency followed by intramitochondrial iron deposits. *Nat Genet*. 2001;27(2):181-186. doi:10.1038/84818

94. Phoon CKL, Acehan D, Schlame M, et al. Tafazzin Knockdown in Mice Leads to a Developmental Cardiomyopathy With Early Diastolic Dysfunction Preceding Myocardial Noncompaction. *JAHA*. 2012;1(2):e000455. doi:10.1161/JAHA.111.000455

95. Fatica EM, DeLeonibus GA, House A, et al. Barth Syndrome: Exploring Cardiac Metabolism with Induced Pluripotent Stem Cell-Derived Cardiomyocytes. *Metabolites*. 2019;9(12):306. doi:10.3390/metabo9120306

96. Liu X, Wang S, Guo X, et al. Increased Reactive Oxygen Species-Mediated Ca^{2+}/Calmodulin-Dependent Protein Kinase II Activation Contributes to Calcium Handling Abnormalities and Impaired Contraction in Barth Syndrome. *Circulation*. 2021;143(19):1894-1911. doi:10.1161/CIRCULATIONAHA.120.048698

97. Chowdhury A, Aich A, Jain G, et al. Defective Mitochondrial Cardiolipin Remodeling Dampens HIF-1α Expression in Hypoxia. *Cell Rep*. 2018;25(3):561-570.e6. doi:10.1016/j.celrep.2018.09.057

98. Wang G, McCain ML, Yang L, et al. Modeling the mitochondrial cardiomyopathy of Barth syndrome with induced pluripotent stem cell and heart-on-chip technologies. *Nat Med*. 2014;20(6):616-623. doi:10.1038/nm.3545

99. Lee YK, Ho PWL, Schick R, et al. Modeling of Friedreich ataxia-related iron overloading cardiomyopathy using patient-specific-induced pluripotent stem cells. *Pflugers Arch - Eur J Physiol*. 2014;466(9):1831-1844. doi:10.1007/s00424-013-1414-x

100. Hick A, Wattenhofer-Donzé M, Chintawar S, et al. Neurons and cardiomyocytes derived from induced pluripotent stem cells as a model for mitochondrial defects in Friedreich's ataxia. *Dis Model Mech*. 2013;6(3):608-621. doi:10.1242/dmm.010900

101. Rohani L, Meng G, Machiraju P, et al. MODELING THE DILATED CARDIOMYOPATHY WITH ATAXIA SYNDROME (DCMA), A PEDIATRIC MITOCHONDRIAL CARDIOMYOPATHY, USING CARDIOMYOCYTES DERIVED FROM INDUCED PLURIPOTENT STEM CELLS. *Canadian Journal of Cardiology*. 2017;33(10):S163-S164. doi:10.1016/j.cjca.2017.07.319

102. Hallas T, Eisen B, Shemer Y, et al. Investigating the cardiac pathology of SCO2-mediated hypertrophic cardiomyopathy using patients induced pluripotent stem cell-derived cardiomyocytes. *J Cell Mol Med*. 2018;22(2):913-925. doi:10.1111/jcmm.13392

103. Meng L, Wu G. Recent advances in small molecules for improving mitochondrial disorders. *RSC Adv*. 2023;13(30):20476-20485. doi:10.1039/d3ra03313a

104. Ohsawa Y, Hagiwara H, Nishimatsu S ichiro, et al. Taurine supplementation for prevention of stroke-like episodes in MELAS: a multicentre, open-label, 52-week phase III trial. *J Neurol Neurosurg Psychiatry*. 2019;90(5):529-536. doi:10.1136/jnnp-2018-317964

105. Hong S, Kim S, Kim K, Lee H. Clinical Approaches for Mitochondrial Diseases. *Cells*. 2023;12(20):2494. doi:10.3390/cells12202494

106. Miyauchi A, Kouga T, Jimbo EF, et al. Apomorphine rescues reactive oxygen species-induced apoptosis of fibroblasts with mitochondrial disease. *Mitochondrion*. 2019;49:111-120. doi:10.1016/j.mito.2019.07.006

107. Suzuki T, Yamaguchi H, Kikusato M, et al. Mitochonic Acid 5 (MA-5), a Derivative of the Plant Hormone Indole-3-Acetic Acid, Improves Survival of Fibroblasts from Patients with Mitochondrial Diseases. *Tohoku J Exp Med*. 2015;236(3):225-232. doi:10.1620/tjem.236.225

108. Shimura M, Nozawa N, Ogawa-Tominaga M, et al. Effects of 5-aminolevulinic acid and sodium ferrous citrate on fibroblasts from individuals with mitochondrial diseases. *Sci Rep*. 2019;9(1):10549. doi:10.1038/s41598-019-46772-x

109. Pirinen E, Auranen M, Khan NA, et al. Niacin Cures Systemic NAD+ Deficiency and Improves Muscle Performance in Adult-Onset Mitochondrial Myopathy. *Cell Metabolism*. 2020;31(6):1078-1090.e5. doi:10.1016/j.cmet.2020.04.008

110. Jiang Q, Yin J, Chen J, et al. Mitochondria-Targeted Antioxidants: A Step towards Disease Treatment. *Oxid Med Cell Longev*. 2020;2020:8837893. doi:10.1155/2020/8837893

111. Brown DA, Perry JB, Allen ME, et al. Mitochondrial function as a therapeutic target in heart failure. *Nat Rev Cardiol*. 2017;14(4):238-250. doi:10.1038/nrcardio.2016.203

112. Hu Y, Xu Y, Chen W, Qiu Z. Stomatin-Like Protein-2: A Potential Target to Treat Mitochondrial Cardiomyopathy. *Heart, Lung and Circulation*. 2021;30(10):1449-1455. doi:10.1016/j.hlc.2021.05.074

113. Di Donfrancesco A, Massaro G, Di Meo I, Tiranti V, Bottani E, Brunetti D. Gene Therapy for Mitochondrial Diseases: Current Status and Future Perspective. *Pharmaceutics*. 2022;14(6):1287. doi:10.3390/pharmaceutics14061287

114. Verbon EH, Post JA, Boonstra J. The influence of reactive oxygen species on cell cycle progression in mammalian cells. *Gene*. 2012;511(1):1-6. doi:10.1016/j.gene.2012.08.038

115. Antico Arciuch VG, Elguero ME, Poderoso JJ, Carreras MC. Mitochondrial regulation of cell cycle and proliferation. *Antioxid Redox Signal*. 2012;16(10):1150-1180. doi:10.1089/ars.2011.4085

116. Tsogtbaatar E, Landin C, Minter-Dykhouse K, Folmes CDL. Energy Metabolism Regulates Stem Cell Pluripotency. *Front Cell Dev Biol*. 2020;8:87. doi:10.3389/fcell.2020.00087

117. Cardoso-Moreira M, Halbert J, Valloton D, et al. Gene expression across mammalian organ development. *Nature*. 2019;571(7766):505-509. doi:10.1038/s41586-019-1338-5

118. Vallance HD, Jeven G, Wallace DC, Brown MD. A Case of Sporadic Infantile Histiocytoid Cardiomyopathy Caused by the A8344G (MERRF) Mitochondrial DNA Mutation. *Pediatr Cardiol*. 2004;25(5):538-540. doi:10.1007/s00246-003-0446-y

119. Yokoyama U, Shibata T, Yasui K, Iwamoto M, Takigiku K, Yokota S. A Case of Fatal Mitochondrial Cardiomyopathy. *Jpn Heart J*. 2002;43(1):61-67. doi:10.1536/jhj.43.61

120. Hall AR, Burke N, Dongworth RK, Hausenloy DJ. Mitochondrial fusion and fission proteins: novel therapeutic targets for combating cardiovascular disease. *Br J Pharmacol*. 2014;171(8):1890-1906. doi:10.1111/bph.12516

121. Ong SB, Hausenloy DJ. Mitochondrial morphology and cardiovascular disease. *Cardiovasc Res*. 2010;88(1):16-29. doi:10.1093/cvr/cvq237

122. Michelucci A, Liang C, Protasi F, Dirksen RT. Altered Ca^{2+} Handling and Oxidative Stress Underlie Mitochondrial Damage and Skeletal Muscle Dysfunction in Aging and Disease. *Metabolites*. 2021;11(7):424. doi:10.3390/metabo11070424

123. Eisner DA, Caldwell JL, Kistamás K, Trafford AW. Calcium and Excitation-Contraction Coupling in the Heart. *Circ Res*. 2017;121(2):181-195. doi:10.1161/CIRCRESAHA.117.310230

124. Bates MGD, Bourke JP, Giordano C, d'Amati G, Turnbull DM, Taylor RW. Cardiac involvement in mitochondrial DNA disease: clinical spectrum, diagnosis, and management. *Eur Heart J*. 2012;33(24):3023-3033. doi:10.1093/eurheartj/ehs275

125. Zhang H, Menzies KJ, Auwerx J. The role of mitochondria in stem cell fate and aging. *Development*. 2018;145(8):dev143420. doi:10.1242/dev.143420

126. Jang YY, Sharkis SJ. A low level of reactive oxygen species selects for primitive hematopoietic stem cells that may reside in the low-oxygenic niche. *Blood*. 2007;110(8):3056-3063. doi:10.1182/blood-2007-05-087759

127. Bigarella CL, Liang R, Ghaffari S. Stem cells and the impact of ROS signaling. *Development*. 2014;141(22):4206-4218. doi:10.1242/dev.107086

128. Abdal Dayem AM, Saadeldin IM, Zhang S. Editorial: Crosslinking ROS signaling and stem cells. *Front Cell Dev Biol*. 2022;10:1101802. doi:10.3389/fcell.2022.1101802

129. Khacho M, Slack RS. Mitochondrial activity in the regulation of stem cell self-renewal and differentiation. *Current Opinion in Cell Biology*. 2017;49:1-8. doi:10.1016/j.ceb.2017.11.003

130. Guo YL, Chakraborty S, Rajan SS, Wang R, Huang F. Effects of Oxidative Stress on Mouse Embryonic Stem Cell Proliferation, Apoptosis, Senescence, and Self-Renewal. *Stem Cells and Development*. 2010;19(9):1321-1331. doi:10.1089/scd.2009.0313

131. Bayeva M, Ardehali H. Mitochondrial Dysfunction and Oxidative Damage to Sarcomeric Proteins. *Curr Hypertens Rep*. 2010;12(6):426-432. doi:10.1007/s11906-010-0149-8

132. Steinberg SF. Oxidative stress and sarcomeric proteins. *Circ Res*. 2013;112(2):393-405. doi:10.1161/CIRCRESAHA.111.300496

133. Sumandea MP, Steinberg SF. Redox Signaling and Cardiac Sarcomeres. *Journal of Biological Chemistry*. 2011;286(12):9921-9927. doi:10.1074/jbc.R110.175489

134. Ramaccini D, Montoya-Uribe V, Aan FJ, et al. Mitochondrial Function and Dysfunction in Dilated Cardiomyopathy. *Front Cell Dev Biol*. 2021;8:624216. doi:10.3389/fcell.2020.624216

135. Kohda M, Tokuzawa Y, Kishita Y, et al. A Comprehensive Genomic Analysis Reveals the Genetic Landscape of Mitochondrial Respiratory Chain Complex Deficiencies. *PLoS Genet*. 2016;12(1):e1005679. doi:10.1371/journal.pgen.1005679

136. Kamps R, Szklarczyk R, Theunissen TE, et al. Genetic defects in mtDNA-encoded protein translation cause pediatric, mitochondrial cardiomyopathy with early-onset brain disease. *Eur J Hum Genet*. 2018;26(4):537-551. doi:10.1038/s41431-017-0058-2

137. Nishioka M, Inaba Y, Motobayashi M, et al. An infant case of diffuse cerebrospinal lesions and cardiomyopathy caused by a BOLA3 mutation. *Brain and Development*. 2018;40(6):484-488. doi:10.1016/j.braindev.2018.02.004

138. Yu Q, Tai YY, Tang Y, et al. BOLA (BolA Family Member 3) Deficiency Controls Endothelial Metabolism and Glycine Homeostasis in Pulmonary Hypertension. *Circulation*. 2019;139(19):2238-2255. doi:10.1161/CIRCULATIONAHA.118.035889

139. Verrigni D, Diodato D, Di Nottia M, et al. Novel mutations in *KARS* cause hypertrophic cardiomyopathy and combined mitochondrial respiratory chain defect. *Clinical Genetics*. 2017;91(6):918-923. doi:10.1111/cge.12931